UNIVERSIDAD EUROPEA DE MADRID

ESCUELA DE INGENIERÍA Y DE ARQUITECTURA

MÁSTER UNIVERSITARIO EN INGENIERÍA AERONÁUTICA

TRABAJO FIN DE MÁSTER

Determinación mediante modelo de elementos finitos de la velocidad balística en borde de ataque metálico

Autor: Rafael POZUELO de FRUTOS
Tutor: Alan DOMÍNGUEZ MONTERO

Abril 2023

to obtain the degree of Master of Science in Aerospace Engineering at the Universidad Europea de Madrid to be defended publicly on April of 2023.

"Manners maketh man" - William Horman / Harry Hart (Kingsman)

En primer lugar me gustaría agradecer a mi tutor Alan Dominguez por la cantidad de tiempo y de tutorías dedicadas a ayudarme con los problemas que iban surgiendo por el camino.

A mis padres, Raúl y Yolanda, por facilitarme las cosas día a día y presionarme para que mejore.

A Esther por ayudarme e insistirme que trabajara y que no lo dejara todo para el último dia y a Cris por aguantarme cuando no me salían las cosas.

Resumen

Dado que la comprobación de las propiedades balísticas de estructuras aeronáuticas solo se pueden estudiar mediante ensayos destructivos que son caros y complejos, se pretende desarrollar un método analítico que permita reducir el número de iteraciones de ensayo necesarias para obtener un diseño capaz de soportar los requerimientos de energías de impacto.

Se ha realizado una investigación mediante análisis por elementos finitos (usando el software Simulia Abaqus Explicit Solver), de la influencia de los distintos parámetros involucrados en el impacto de diversos proyectiles sobre un borde de ataque de avión fabricado en aluminio. El objetivo es obtener la velocidad de límite balístico y analizar como varía ésta según la influencia de los mencionados parámetros.

Para realizar esta investigación, previamente se ha llevado a cabo un proceso de convergencia de malla para analizar la ifluencia de ésta en los resutados finales. En términos generales, cuanto más fina es la malla, más precisos serán los resultados finales, pero esto acarrea un incremento en el tiempo de cómputo. Este puede llegar a ser tan grande que impida la finalización del proceso por falta de recursos del ordenador. Por lo tanto, se pretende encontrar un punto de equilibrio que maximice la precisión manteniendo un tiempo de cómputo razonable.

La optimización del mallado se ha realizado en dos pasos sucesivos, primero se ha optimizado el mallado del impactador y a continuación, manteniendo éste fijo, se ha procedido de igual manera con el mallado del borde de ataque.

Una vez definido el mallado óptimo, se ha hecho un studio del efecto del self-contact en los elemetos del borde de ataque. El self-contact es un parámetro que impide la interpenetración de unos elementos en otros. Tras realizar simulaciones con y sin interpenetración, la diferencia entre los resultados es despreciable, sin embargo el tiempo de cómputo aumenta considerablemente al utilizar el parámetro de self-contact.

Una vez fijados todos los parámetros del modelo de partida, se realiza el estudio de la variación de la velocidad balistica para los cuatro proyectiles escogidos. Los resultados y las tendencias de los mismos se han comparado con la ecuación experimental de Thor.

Tras realizar las simulaciones previstas y su análisis, se ha observado que para una misma energía de impacto, la velocidad balística disminuye significativamente cuando se reduce el tamaño del proyectil o éste tiene una forma balística. Así mismo, en el caso de proyectiles romos (como pueden ser un proyectil esférico o cilíndrico) el modo de fallo del borde de ataque se produce más por desgarro del material mientras que en el caso balístico (proyectil cónico) hay una pequeña rotura inicial que se va agrandando a medida que el proyetil penetra en el borde de ataque.

Comparando los resultados obtenidos en las simulaciones con los resultados experimentales del proyecto Thor, limitado a placas planas siendo impactadas por la cara plana de un proyectil cúbico, se puede observar que las tendencias de los resultados son similares.

El método parece prometedor, sin embargo, para explorar todo su potencial, se debería trabajar con máquinas más potentes que fueran capaces de simular estructuras más complejas y similares a las reales.

Abstract

Since the verification of the ballistic properties of aeronautical structures can only be studied through destructive tests that are expensive and complex, it is intended to develop an analytical method that allows reducing the number of iterations required to obtain a design able to withstand the impact energy requirements.

An investigation has been carried out through finite element analysis (using the Simulia Abaqus Explicit Solver), about the influence of the different parameters involved in the impact of several projectiles on an aircraft leading edge made of aluminum. The objective is to obtain the corresponding ballistic limit speed and analyze how it varies according to the influence of the mentioned parameters.

To perform this research, a mesh convergence process has previously been carried out to analyze its influence on the final results. In general terms, the finer the mesh, the more precise the final results will be, but this entails an increase in computation time. This can become so large that it prevents the completion of the process due to lack of computer resources. Therefore, it is intended to find a balance point that maximizes precision while maintaining a reasonable computation time.

The optimization of the mesh has been carried out in two successive steps, first the mesh of the impactor has been optimized and then, keeping it fixed, we have proceeded in the same way with the mesh of the leading edge.

Once the optimized mesh has been defined, a study of the effect of self-contact on the elements of the leading edge has been made. The self-contact is a parameter that prevents the interpenetration of some elements in others. After performing simulations with and without interpenetration, the difference between the results is negligible, however the computation time increases considerably when using the self-contact parameter.

Once all the parameters of the starting model have been set, the study of the variation of the ballistic velocity for the four chosen projectiles is carried out. The results and their trends have been compared with Thor's experimental equation.

After carrying out the planned simulations and their analysis, it has been observed that for the same impact energy, the ballistic velocity decreases significantly when the size of the projectile is reduced or it has a ballistic shape. Likewise, in the case of blunt projectiles (such as a spherical or cylindrical ones) the leading edge failure mode occurs more by tearing the material while in the ballistic case (conical projectile) there is a small initial break that grows as the bullet penetrates the leading edge.

Comparing the results obtained in the simulations with the experimental results of the Thor project, limited to flat plates being impacted by the flat face of a cubic projectile, it can be observed that the trends of the results are similar.

The method seems promising, however, to explore its full potential, more powerful machines should be used that are able of simulating more complex structures closer to the real ones.

Contents

List of Figures

List of Tables

1

Introduction

During their lifecycles, aircraft are exposed to the impact of objects on the wings and the fuselage throughout the flight, especially during approximation, takeoff and landing phases. These impacts can be from small objects such as hail or particles that impact during taxiing or takeoff to bird strikes.

In the case of civil aircraft, these situations become requirements and a complete certification process is fulfilled to ensure their safety.

On the other hand, military aircraft, in addition to what has been mentioned above, are exposed to being hit by enemy fire, either artillery projectiles or high speed fragments coming from warheads bursts.

The impact of these projectiles is very demanding and must be considered from the initial design phases because it can damage critical areas (fuel tanks, control systems, cabin, pilot etc.) endangering the lives of the occupants, the survivability of the aircraft or the fulfilment of the mission.

To avoid or minimize these possible damages, it is necessary to develop ballistic protection systems. This process is not trivial, since increasing protection generally implies an increase in weight. That is why it is so interesting to study the behavior, from the ballistic point of view, of the different design parameters such as materials, geometry, location of the elements, internal protections and, in the case of composite materials, orientation of the constitutive layers or manufacturing methods..

To verify the properties of these designs, destructive tests are usually performed, however, these tests have a high cost and if the test fails, the complete cycle should be repeated. The target of the numerical simulation, is, firstly, reduce as much as possible the number of cycles design-manufacturing-test and, secondly, in the near future, when the simulations become mature enough, substitute the destructive test within the certification/qualification process.

1.1. Summary of content

This section provides a brief summary of the content of each of the chapters that make up this study.

1.1.1. Introduction

The first chapter contains a brief introduction to the work and an index that includes a summary of the work done in the different chapters of the project.

1.1.2. High Speed Impacts

In this chapter, the case studied is theoretically presented. First, the leading edge model used as the impact surface is defined, then, a brief description of the material used to model the leading edge has been made. The concept of ballistic limit is also defined as the minimum initial velocity at which the projectile begins to penetrate the leading edge. Finally, Thor's experimental equations are exposed and the specific case of this study is explained.

1.1.3. Introduction to Finite Element Model Methods

The third chapter focuses on finite element models, starting with a brief explanation and differentiating the two main types, implicit and explicit, as well as the Lagrangian and Eulerian approaches. The constitutive and the fracture models of the material are also explained within this chapter.

1.1.4. Development of numerical models

This chapter explains the process followed to make the simulation model. This process commences with the design of the leading edge and the different projectiles used, followed by the implementation of the materials properties and finalising with the boundary conditions.

After this, the process followed to perform the meshing of the model is exposed, starting with a simple initial meshing, followed by an iterative process to reach the convergence of the configuration, obtaining the final meshing that will be used in the simulations.

Once the final mesh of the model has been defined, the iterative process followed to obtain the ballistic velocity is exposed.

Finally, an analysis has been carried out on the influence of the contact of the elements of the leading edge with others of the same surface, to decide about the implementation or not of this parameter.

1.1.5. Outcomes

This chapter presents the results obtained from the simulations. Once decided which one will be used as a reference, different simulations modifying some of the parameters involved in the impact are performed. These simulations show how the ballistic velocity and leading edge breaking behavior changes with these modifications.

1.1.6. Conclussions and Future

In this chapter the conclusions obtained after analyzing the results of the previous chapter are shown and a brief description of the future steps to be followed to get deeper in this study is also made.

1.1.7. Appendix1: Model Creation

Finally, the appendix shows the step by step process followed in the program to make the model.

2

High Speed Impacts

This study will focus on the analysis by finite element simulation of an impact of a projectile on the leading edge of an aircraft wing using Simulia Abaqus Explicit Solver. The model will be composed by a leading edge made of 2024 T3/T351 aluminum and various impactors with different features.

As previously stated, increasing impact protection usually entails an increase in armor thickness, i.e., an increase in weight. This work will analyse the variation of the ballistic velocity considering the influence of different parameters such as the mass, speed and geometry of the projectile and the thickness of the profile.. For this, an initial simulation will be carried out that will be used as the reference and will be compared against other simulations performed varying some of the parameters previously exposed.

2.1. Impact Geometry

The airfoil chosen to carry out this study is a NACA standardized one, specifically NACA 2410. As it is a standardized profile, the 4 digits that name it correspond to different attributes of its geometry.

- The first digit (M) corresponds to the maximum camber divided by the chord and multiplied by 100. In the airfoil used in this study, M= 2 so the camber is 0.02 or 2% of the chord.
- The second digit (P) marks the position of the maximum camber in chord percentage divided by 10, in the case of the NACA 2410 the maximum camber is located at 40%.
- The last two digits correspond to the relative thickness divided by 100, in this case the thickness is 10% of the chord.

The Naca airfoil is created from a camber line and a thickness distribution plotted perpendicular to horizontal axis from both sides of the camber line. The camber line follows the next equations:

$$\begin{aligned} &Front(0 \leq x \leq P) \quad y_c = \frac{M}{P^2}\left(2Px - x^2\right) \\ &Back(P \leq x \leq 1) \quad y_c = \frac{M}{(1-P^2)}\left(1 - 2P + 2Px - x^2\right) \end{aligned} \tag{2.1}$$

For the airfoil Naca 2410 where M=0.02 and P=0.4, the equations are as follows:

$$\begin{aligned} &Front(0 \leq x \leq 0.4) \quad y_c = \frac{0.02}{0.4^2}\left(0.8x - x^2\right) \\ &Back(0.4 \leq x \leq 1) \quad y_c = \frac{0.02}{(1-0.4^2)}\left(1 - 0.8 + 0.8x - x^2\right) \end{aligned} \tag{2.2}$$

The thickness distribution is given by the equation:

$$y_t = \frac{T}{0.2}\left(a_0 x^{0.5} + a_1 x + a_2 x^2 + a_3 x^3 + a_4 x^4\right) \tag{2.3}$$

Where:

- y_t is half the thickness and is applied to both sides of the camber line.
- The constants values are a_0=0.2969, a_1=-0.126, a_2=-0.3516, a_3=-0.3516 and a_4=-0.1015.

Using the equations (2.2) and (2.3), for a given value of x it is possible to calculate the camber line position, the gradient of the camber line and the thickness. The position of the upper and lower surface can be calculated perpendicular to horizontal axis to each side of the camber line:

Calling

$$\theta = \arctan\left(\frac{dy_c}{dx}\right)$$

$$\begin{aligned} Upper\ Surface: &\quad x_u = x_c - y_t \sin\theta; \quad y_u = y_c + y_t \cos\theta \\ Lower\ Surface: &\quad x_l = x_c + y_t \sin\theta; \quad y_l = y_c - y_t \cos\theta \end{aligned} \tag{2.4}$$

The profile chosen for this study has the following geometry:

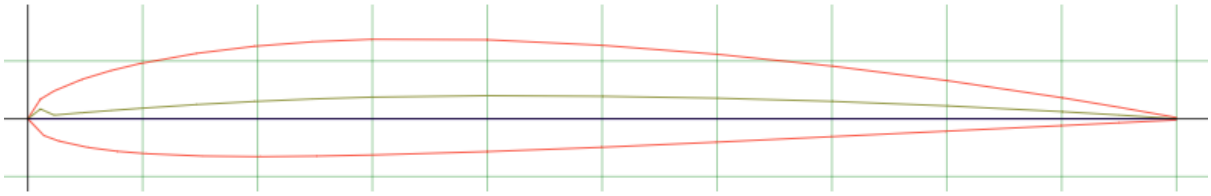

Figure 2.1: Naca 2410 Airfoil[15].

2.2. Material Chosen

The airfoil to be studied is made of 2024 T3/T351 material, an aluminum alloy subjected to certain heat treatments widely used in the aerospace industry due to its high stiffness and resistance to fatigue. Aluminum 2024 is an alloy made up of copper (4.3-4.5%), magnesium (1.3-1.5%), manganese (0.5% approx) and less than 0.5 % silicon, chrome, nickel, lead and zinc.

Aluminum 2024 has a low density of 2.77 g/cm3 and a Young's Modulus of 73 Gpa. The other mechanical properties will vary according to the heat treatment to which it has been subjected.

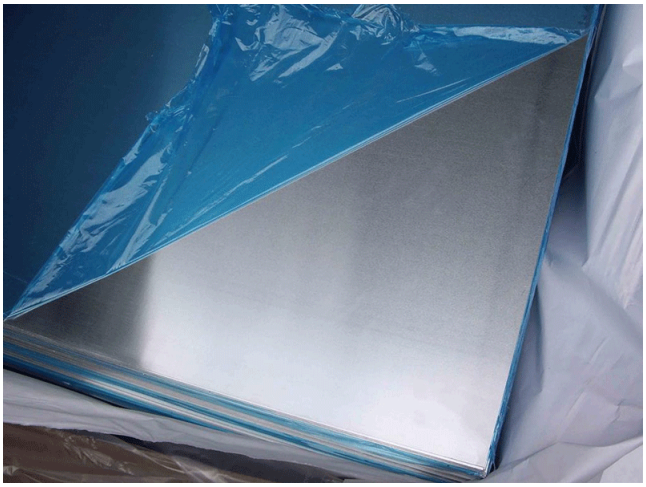

Figure 2.2: Aluminum 2024 T351 Sheets

Aluminum 2024 is treated with precipitation hardening to increase yield strength. Precipitation hardening relies on changes in solid solubility with temperature to produce fine particles of an impurity phase, which impede the movement of dislocations, or defects in a crystal's lattice. Since dislocations are often the dominant carriers of plasticity, this serves to harden the material. These impurities affect the aluminum alloy in a similar manner as particles in particle-reinforced composite material.

Unlike ordinary tempering, these alloys must be kept at elevated temperatures for hours to allow precipitation to take place, this time delay is called aging.

In the particular case of the aluminum 2024 T351, to achieve this temper, the metal is solution heat-treated, stress relieved (accomplished by stretching the metal) and finally naturally aged.

The mechanical properties of the aluminum alloy relevant to this study are presented in the table 2.1:

Density [kg/m$\hat{3}$]	Young's Modulus [MPa]	Poisson's Ratio	Yield Limit [MPa]
2770	73084	0.33	684

Table 2.1: Aluminum 2024 mechanical properties.

2.3. Ballistic Limit

When talking about the ballistic limit, it is important to look at the relationship between the probability to penetrate the impacted material and the impact velocity of the projectile. For low speeds, the probability that the projectile will be able to go through the material is nil, and it increases as the impact speed increases. When the speed is very high, the probability of the impactor to go through the material is close to 100%.

Between these two values, the point known as the ballistic limit is found, when for a certain velocity the projectile is capable of crossing 50% of the times.

The ballistic limit or limit velocity is defined as the speed required for a particular projectile to penetrate a particular piece of material 50% of the times. In other words, a given projectile will generally not pierce a given target when the projectile velocity is lower than the ballistic limit.

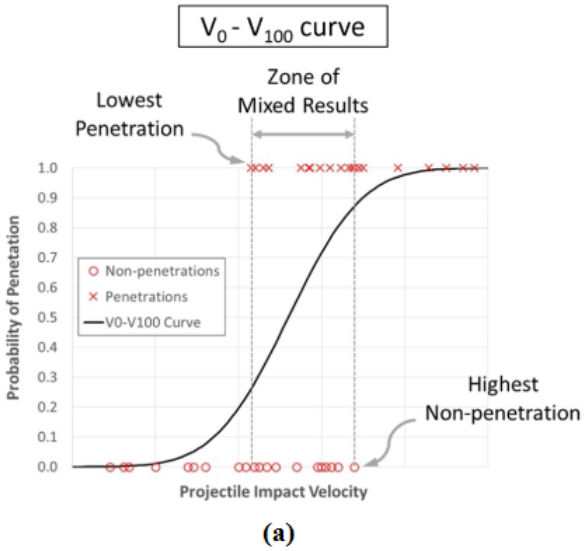

Figure 2.3: V0-V100 Probability distribution[12]

As can be seen in the experimental graph above, the distribution of the probability that the projectile will pass through the impacted material versus the velocity of the projectile corresponds to a Gaussian probability distribution. In this case, the expected value corresponds to the ballistic limit (or the V50 velocity) while the variance will depend on various factors such as the impacted material or the shape of the projectile.

The ballistic limit equation for laminates, as derived by Reid and Wen [17] is as follows:

$$V_b = \frac{\pi\Gamma\sqrt{\rho_t\sigma_e}D^2T}{4m}\left[1+\sqrt{1+\frac{8m}{\pi\Gamma^2\rho_t D^2T}}\right] \tag{2.5}$$

Where:

- V_b, is the ballistic limit.
- Γ is a projectile constant determined experimentally.
- ρ_t, is the density of the laminate.
- σ_e, is the static linear elastic compression limit.
- D, is the diameter of the projectile
- T, is the thickness of the laminate
- m, is the mass of the projectile

In the case of this study, since it is not an experimental work but a simulation using finite elements model, it has been decided to establish as a ballistic limit a velocity value with which the projectile is capable of crossing the leading edge and, after crossing its velocity residual is as close as possible to 0. In this way, the ballistic limit is defined as the minimum velocity at which a specific projectile is capable of traversing the material, guaranteeing that any higher velocity will traverse the leading edge.

2.4. Thor Equations

Thor's equations are two empirically derived equations that relate the initial velocity and initial mass of a projectile to the residual velocity and mass after impacting a material. These equations were developed from the experiments carried out in the Thor project, which consisted of studying the behavior of cylindrical and cubic projectiles after passing through a plate of metallic or non-metallic material. The impacts were analyzed using a logarithmic distribution that relates the aforementioned variables with material parameters using a series of constants.

Thor's equations are as follows:

- The residual mass of the fragment that remains after the impacted material has been penetrated.

$$m_i - m_r = 10^c\,(tA)^\alpha\,(m_s)^\beta\,(sec\theta)^\gamma\,V_i^\lambda \tag{2.6}$$

- The residual velocity of the ejected fragment after penetrating the impacted material.

$$V_r = V_i - 10^c\,(tA)^\alpha\,(m_s)^\beta\,(sec\theta)^\gamma\,V_i^\lambda \tag{2.7}$$

Where:

- m_i is the initial mass of the projectile
- m_r is the residual mass of the projectile after passing through the material
- t is the material thickness
- A is the impact area
- $\theta$is the angle between the trajectory of the projectile and the perpendicular to the impact material
- m_s is the initial mass of the projectile
- V_i is the initial velocity of the projectile
- V_r is the residual velocity of the projectile after passing through the material
- c, α, β, γ, $\lambda$are experimental coefficients

For the specific case of this project, both equations can be simplified.

First of all, the possible wear of the impactor has not been considered, it has been modeled as a rigid solid, therefore the equation 2.6 will not be relevant in this project.

Regarding the equation 2.7 and taking into account the definition that has been made in chapter2.3, the equation can be developed assuming a zero residual velocity (V_r = 0), the formula can be developed as follows:

$$0 = V_i - 10^c \, (tA)^\alpha \, (m_s)^\beta \, (sec\theta)^\gamma \, V_i^\lambda \rightarrow V_i = 10^c \, (tA)^\alpha \, (m_s)^\beta \, (sec\theta)^\gamma \, V_i^\lambda \tag{2.8}$$

$$V_0 = 10^{c1} \, (tA)^{\alpha 1} \, (m_s)^{\beta 1} \, (sec\theta)^{\gamma 1} \tag{2.9}$$

Where:

- V_0 is the balistic limit
- c1, α1, β1, γ1, λ1 are adjusted coefficients

These equations are particularized for certain types of impacts and show certain limitations. On the one hand, these equations hold for projectiles with a ratio between diameter and length of approximately 1 and do not correctly predict the impact behavior of projectiles with ratios between length and diameter are significantly bigger than one.

On the other hand, these equations have been developed to calculate the effect of impacting a flat plate [4]. In the case of this project, as the target is a curved leading edge, the equations will not be exactly fulfilled, but they will allow us to estimate the behavior that will be expected during the impact.

3

Introduction to Finite Element Model Methods

This section exposes the usefulness of the finite elements methods, shows the reasons for the choice of the explicit model to carry out the simulations and the different computational methods, as well as the theoretical characteristics of the materials that will be used in it.

3.1. FEM Solver

The finite element model method is a numerical problem solving methodology which subdivides the overall problem into simpler sub-issues (called finite elements) that are easier to solve. This is obtained performing a space discretization using what is called a mesh (the numerical domain for the solution, which has a finite number of points).

The typical work out of the method involves dividing the domain of the problem into different sub-parts, each represented by a set of element equations (often partial differential equations) to the original problem, and then, recombining them into a global system of equations for the final calculation.

The practical application of FEM, known as finite element analysis is used for analysing problems over complicated domains, when the domain changes or when the desired precision varies over the entire domain. FEM simulations provide a valuable resource as they remove multiple instances of creation and testing of hard prototypes for various high fidelity situations.

3.2. Differences between Explicit and Implicit models

Both explicit and implicit methods are numerical analysis methods used to solve a time dependant differential equation [14]. The main difference between them is that the explicit method calculates the future system state (y_{n+1}) using only the current system state (y_n) while the implicit method calculates the future system state using both the present and the future state.

The implicit method solves the position of the nodes through the inversion of the stiffness matrix. These solution is obtained using a series of linear approximations and several iterations might be needed to achieve convergence. Solutions are always stable and facilitate large time steps but can be extremely time consuming when solving dynamic and nonlinear problems.

The explicit method aims to solve the acceleration of the model using an inversion of the mass matrix. The equations become uncoupled and can be solved directly, no convergence checks are needed. Once the accelerations of one step are calculated, it is possible to obtain the velocity of the next half step and the displacement of the next step. The stability of this method is not guaranteed and thus, small time steps are required. In fact, the time step must be smaller than the Courant time step.

The Courant number is a dimensionless quantity which relates the timestep and the length between mesh elements with the speed of sound through that material.

$$C = \frac{\bar{v}\Delta t}{\Delta l} \tag{3.1}$$

In explicit analyses the Courant time step is the time taken by a sound wave to travel through an element [6]:

$$\Delta t \leq f * \left[\frac{h}{c}\right]_{min} \tag{3.2}$$

Where h is the characteristic length, c is the material sound speed and f is a safety factor. In case of a Quad Shell geometry, used in the airfoil mesh, the characteristic length would be the square root of the shell area [2].

It is clear that explicit integration is especially attractive for short, fast-dynamic problems such as impacts, crashes, and explosions. It is also advisable for some strongly non-linear problems, such as those in which frequent contacts between structures or parts of the same structure are developed; implicit methods do not find it easy to achieve convergence in such problems.

Even in some quasi-static problems where convergence is difficult for implicit methods, it may be more practical to opt for an explicit solution and, if the number of integration steps becomes excessive, artificially increase the density to reduce the wave speed, lengthen the integration interval and reduce the solution time. For this strategy to be valid, the problem must remain quasi-static and appropriate corrections must be introduced if changing time scales affects constitutive behavior [10].

As stated before, the case of study is a highly dynamic phenomenon where the model do not only need to account for the variation of stress with strain but also the strain rate [6] as well as the possible fracture of the elements. For this reason, the model will use an Explicit Finite Element Method simulation.

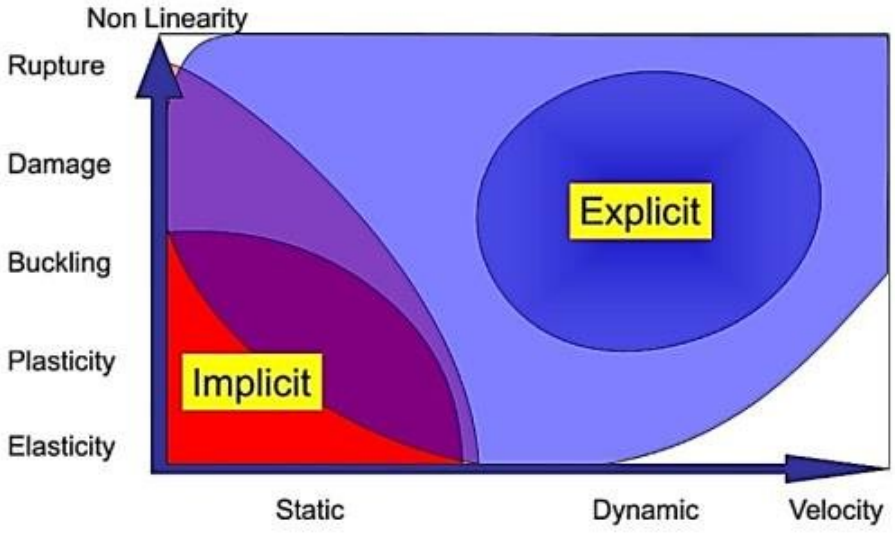

Figure 3.1: Implicit vs Explicit methods Application Zone [3].

3.3. Eulerian vs Lagrangian Approach

Within explicit finite element models, the majority of CFD models can be classified as: Eulerian approaches, where the unknown state variables are attached to stationary observers or Lagrangian approaches, in which the unknown state variables are attached to moving observers. The two approaches are vastly different.

Eulerian methods have been successfully applied and are very popular in CFD. The Lagrangian methods are used when seeking to analyze the deformation of a solid, and for this, meshing is performed on it.

In the case of this study, by focusing on studying the interaction between two solids, a Lagrangian mesh is used.

3.4. Constitutive models of materials

As stated before, the material used to model the airfoil is Aluminum 2024 T351. This material is defined by its physical and mechanical properties.

All materials must have a valid density defined for Explicit Dynamics simulations, the density property defines the initial mass/volume of a material at the start of the simulation.

In order to define the mechanical properties of the aluminum, the model will include the elastic and the plastic behaviour of the material.

The elastic behaviour is defined as the capacity of a material to recover their original shape after the external force that caused a deformation is removed. The material resists the changes up to the elastic limit. If the deformation continues beyond this point, this deformation would not be reversible.

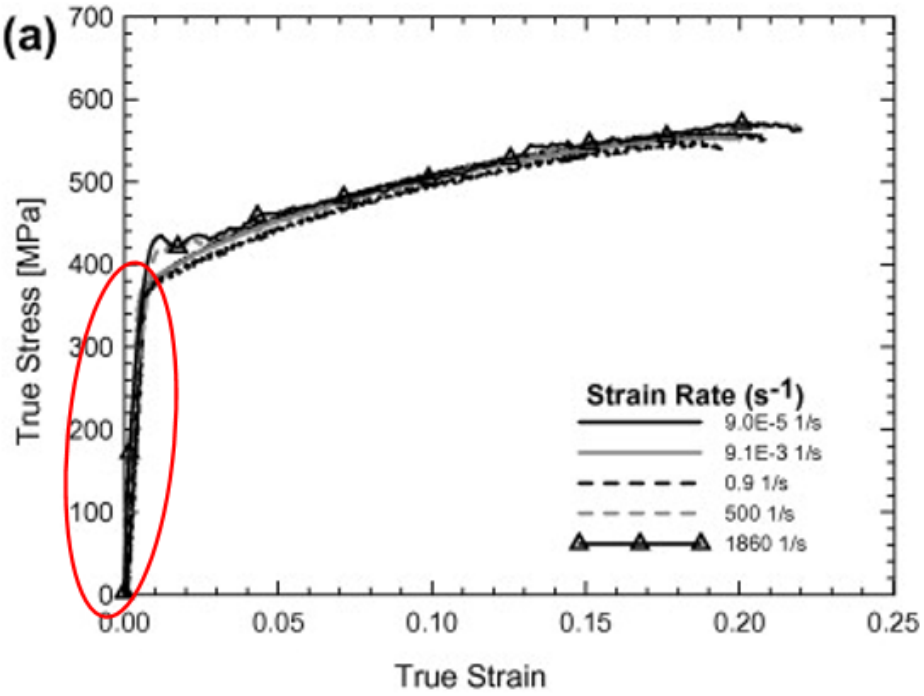

Figure 3.2: Elastic zone of the stress-strain graph of Aluminum 2024[13].

In the graph above, it can be observed that elastic behaviour is linear and, for a uni-dimensional material, corresponds to the Hooke Law that states that within the elastic limit, stress developed is directly proportional to the strain produced in a body:

$$\sigma_e = E * \varepsilon \tag{3.3}$$

For a tridimensional object subjected to loads in the different axes, the equations that express the elastic behaviour are the following[1]:

$$\begin{aligned} \varepsilon_x &= \frac{1}{E}\left(\sigma_x - \nu\left(\sigma_y + \sigma_z\right)\right) \\ \varepsilon_y &= \frac{1}{E}\left(\sigma_y - \nu\left(\sigma_x + \sigma_z\right)\right) \\ \varepsilon_z &= \frac{1}{E}\left(\sigma_z - \nu\left(\sigma_x + \sigma_y\right)\right) \end{aligned} \tag{3.4}$$

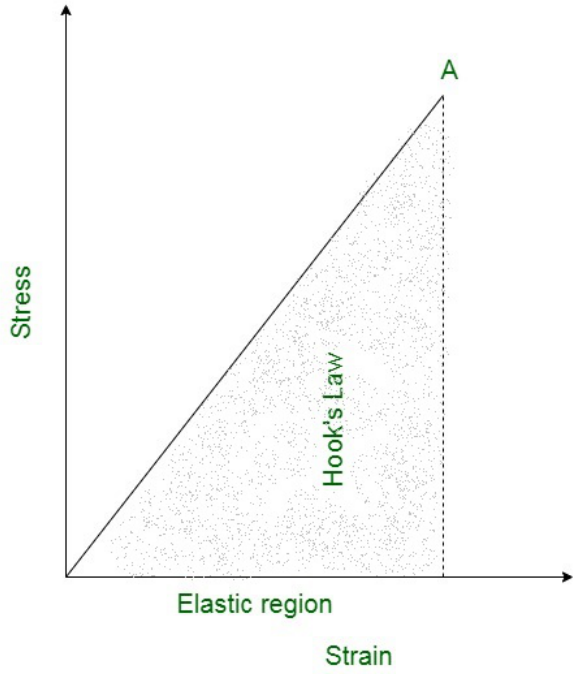

Figure 3.3: Hooke's Law Representation[18].

The properties defined for the elastic behaviour are the Young's Modulus (E) and the Poisson's Ratio (ν). From the defined properties, Shear modulus (G) and Bulk modulus (K) are derived using the following equations:

$$G = \frac{E}{2(1+\nu)} \tag{3.5}$$

$$K = \frac{E}{3(1-2\nu)} \tag{3.6}$$

As stated before, if a material is loaded elastically and subsequently unloaded, all the distortion energy is recovered and the material reverts to its initial configuration. If the distortion is too great, the material will reach its elastic limit and begin to distort plastically.

The model used to simulate the plastic deformation of the material will be the Johnson-Cook [7], it reproduces the behaviour of a material that is subjected to large strains, with high strain rates, at high temperatures, or a combination of all three.

The equation that shows the behaviour of the yield stress is as follows:

$$\sigma(\varepsilon, \dot{\varepsilon}, T) = (A + B^n)\left(1 + C\ln\frac{\dot{\varepsilon}}{\dot{\varepsilon_0}}\right)\left(1 - \left(\frac{T - T_0}{T_M - T_0}\right)^m\right) \tag{3.7}$$

Where:

- A is the yield limit at room temperature under conditions of low strain speed.
- B represents the strain hardening modulus of the material
- n is an exponent related to the strain hardening
- C represents the strain rate coefficient
- m is the thermal softening exponent
- ε is the effective plastic strain

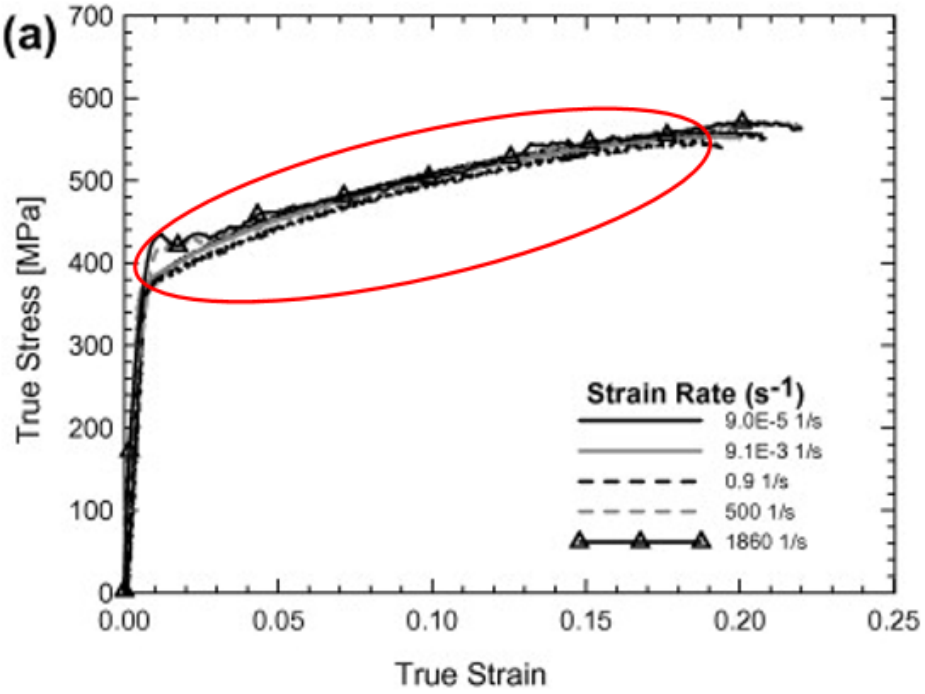

Figure 3.4: Plastic zone of the stress-strain graph of Aluminum 2024[13].

- $\dot{\varepsilon}$ is the rate of the effective plastic strain
- ε_0 is the reference strain rate
- T_M is the melting temperature of the material
- T_0 is the ambient temperature

Adiabatic conditions are assumed such that all internal plastic work is converted into temperature change [8]:

$$\Delta T = \frac{\overline{\sigma \varepsilon^P}}{\rho C_v} \tag{3.8}$$

Where σ is the effective stress, ε^P is the effective plastic strain, ρ is the mass density, and C_v is the constant volume specific heat.

The values of the parameters Johnson-Cook model for the Aluminum 2024-T3/T351 are presented in the following table:

A [MPa]	B [MPa]	n	C	m	T_M [K]	T_0 [K]
684	369	0.73	0.0083	1.7	775	294

Table 3.1: Aluminum 2024 J-C model parameters.

3.5. Fracture Models

To introduce the possible failure occurred by the impact in the model, Johnson-Cook failure model is used. The model, fully described in [7], defines the strain fracture as:

$$\varepsilon_{failure} = [D_1 + D_2 \exp(D_3 \sigma^*)] [1 + D_4 \ln(\dot{\varepsilon}^*)] [1 + D_5 T^*] \tag{3.9}$$

The first set of brackets correspond to the observation that strain to fracture decreases as the hydrostatic tension increases. The second set of brackets represent the effect of an increased strain rate on the material ductility. The last set of brackets represent the effect of thermal softening on the material ductility.

Where:

- D_1, D_2, D_3, D_4, D_5 are constants which value depends on the material studied
- σ^* is the ratio of the pressure to the effective stress:

$$\sigma^* = \frac{pressure}{\overline{\sigma}} \tag{3.10}$$

- $\dot{\varepsilon}^*$ is the non-dimensional plastic strain rate:

$$\dot{\varepsilon}^* = \frac{\dot{\varepsilon}^P}{\dot{\varepsilon}_0} \tag{3.11}$$

  Where:

  - $\dot{\varepsilon}^P$ is the equivalent plastic strain rate

- T^* is the non-dimensional temperature:

$$T^* = \frac{(T - T_R)}{(T_M - T_R)} \tag{3.12}$$

  Where:

  - T_M is the melt temperature of the material
  - T^R is the reference temperature at which the constants are determined.

With the Johnson-Cook model, facture occurs when the damage parameter (D) exceed 1.0. The value of D is given by the accumulated incremental effective plastic strains divided by the current strain at fracture:

$$D = \sum \frac{\Delta \bar{\varepsilon}^P}{\varepsilon_{failure}} \tag{3.13}$$

The values of the parameters Johnson-Cook failure model for the Aluminum 2024-T3/T351 are presented in the following table:

D_1	D_2	D_3	D_4	D_5	Melting Temperature [K]	Reference Temperature [K]
0.31	0.045	-1.7	0.005	0	775	294

Table 3.2: Aluminum 2024 J-C failure model parameters.

4

Development of numerical models

In this chapter, the different models that have been made to study the calculation of ballistic velocity will be presented, detailing the variations between them. It will be explained in a more detailed and focused way on the use of the simulation software in appendix 1 of this work.

The model will consist of a leading edge of a profile that is struck by an impactor whose geometry and speed will vary in the different simulations.

4.1. Impact Geometry

In this section, it will be briefly explained how the airfoil has been introduced in the simulation and how the final geometry has been reached.

As stated before, the airfoil chosen for this study is a normalized NACA 4 digit airfoil, NACA 2410. Using the equations (2.4) and selecting an array of points along the x axis between 0 and 1 meter, the values for the upper and lower surface points are obtained (See annex 1 for the complete array of points) and using the *Create Spline: Thru Points* function the airfoil section is modelled. Then, using the extrude function the airfoil is created:

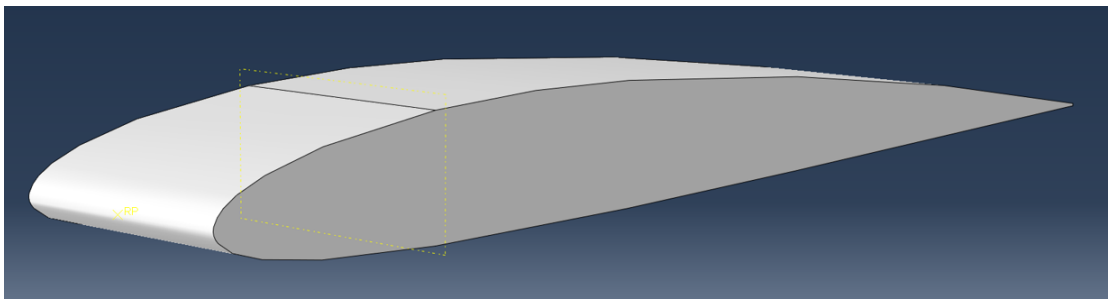

Figure 4.1: Initial Airfoil Model

The airfoil created in the previous steps is a solid object which does not correspond to the reality: the airfoils used in aviation are hollow, not solid. In order to solve this, the function *Create Shell: From Solid*, which transforms a solid into a shell-type object, is used in the whole airfoil.

Due to the fact that the area of interest during the impact is located on the leading edge of the airfoil and to reduce the simulation load, it has been decided to eliminate the area of the trailing edge of the airfoil so that the final geometry to be studied is the one shown in the following figure:

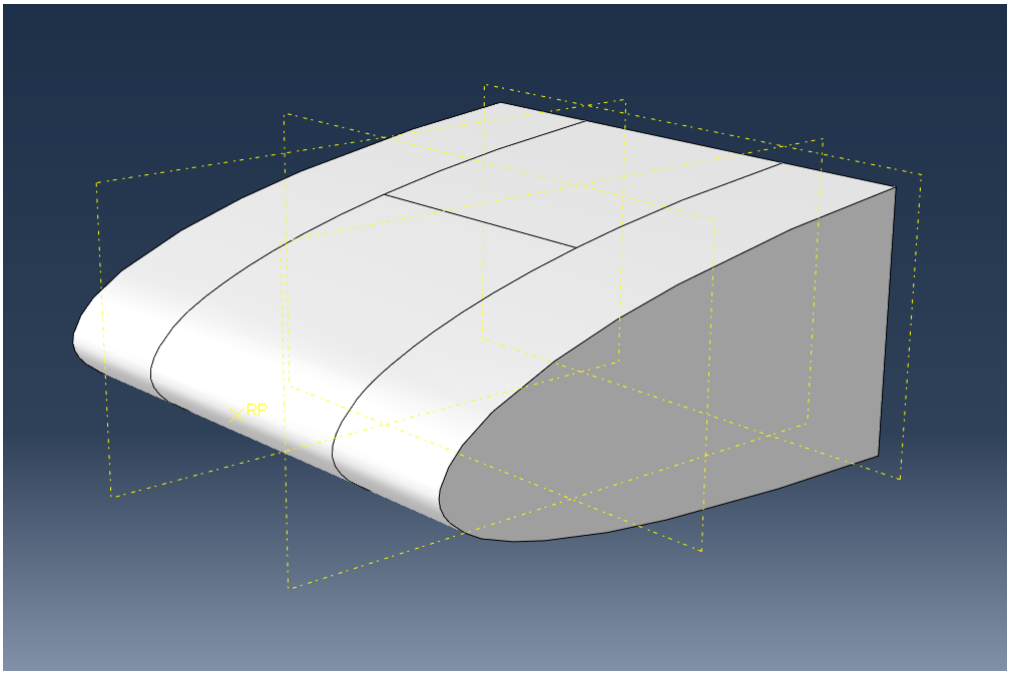

Figure 4.2: Leading Edge Model Used in the Simulation

4.2. Modeling of the impactor

This section shows the models of the impactors used in the different simulations in order to study how the ballistic velocity varies depending on their geometry.

The first impactor's geometry will be a 51 mm diameter sphere which will be considered the reference one for the simulations. The sphere has a weight of 0.54 kg introduced in the model as an inertia on the reference point. The mass of the spherical impactor is equivalent to what it would be if it was a solid sphere made of steel with density equal to 7.8 g/cm^3.

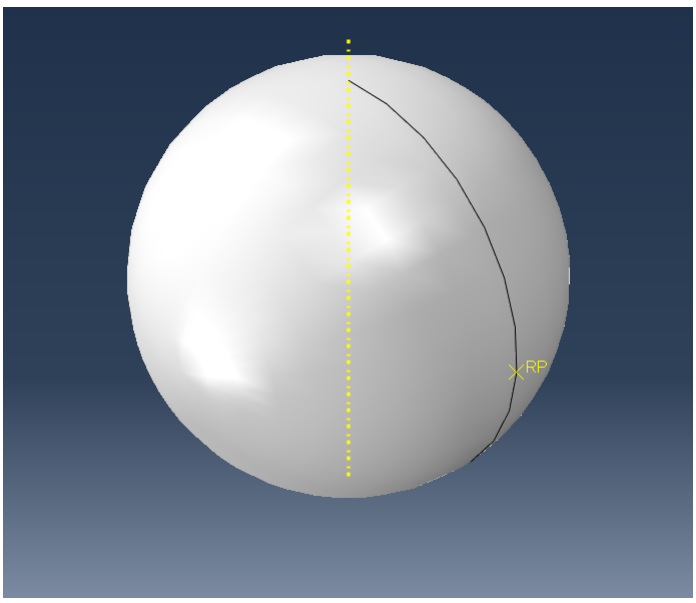

Figure 4.3: Spherical Impactor

The second geometry is a cylinder with the same diameter as the sphere mentioned above and such height that allows it to have the same volume as the sphere. Assuming that the material used for the impactor is identical to the one used in the spherical impactor, the weight (0.54 kg) is the same as the

reference geometry. The cylindrical projectile is oriented in such a way that the impact occurs at one of the bases.

The model used for the cylindrical impactor can be seen in the following illustration:

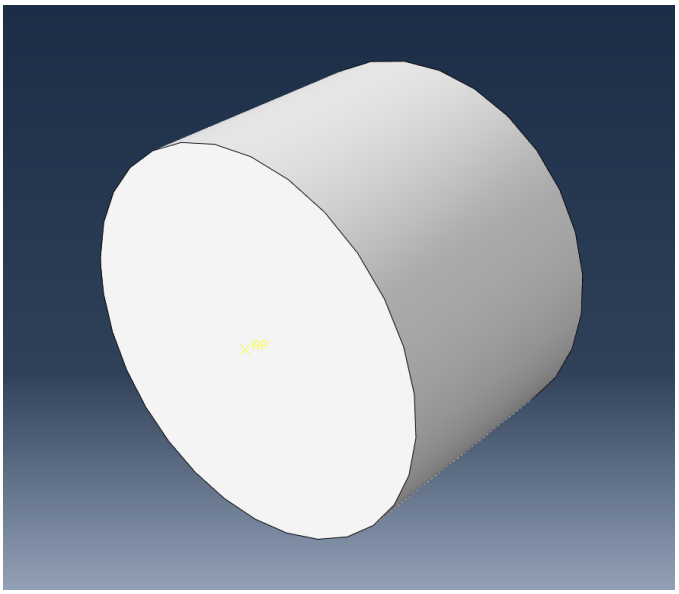

Figure 4.4: Cilindrical Impactor

The third geometry to study is a conical impactor, which generating triangle has a base of the same dimension as the radius of the sphere used as reference projectile. The height has been established so that the angle of the generating triangle opposite to the base is 30º. Since the interest of using these models with different geometry is to analyze its influence on the impact, the mass of the projectile remains constant with respect to the previous sections. Due to errors during meshing caused by the high skewness of the elements at the tip of the conical projectile, it has been decided to truncate the tip 1 mm from the vertex. This process is further detailed in Appendix 1.

Since the interesting aspect of making these models with different geometries is to study how the contact surface affects the ballistic limit and the residual velocity, as said before, the mass of the conical impactor remains constant with respect to previous projectiles.

The model used for the conical impactor can be seen in the following image:

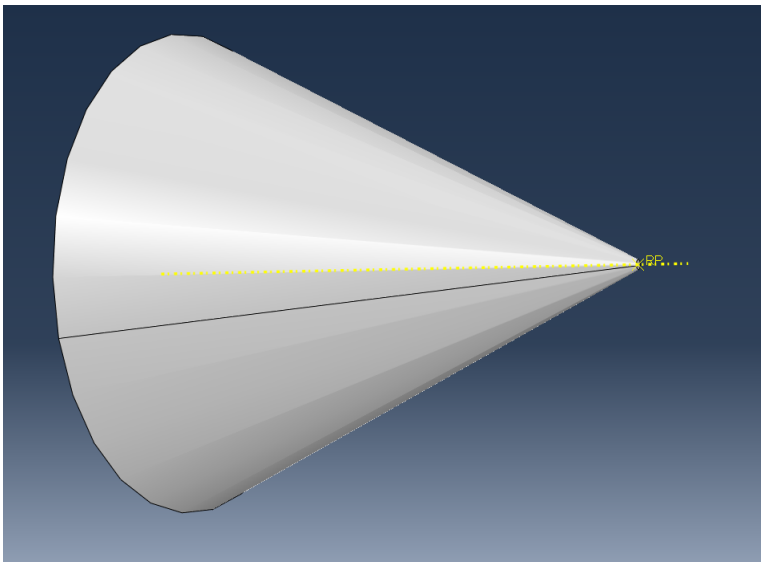

Figure 4.5: Conical Impactor

In order to study the effects of the contact surface between the impactor and the leading edge on the ballistic speed, another model has been generated using the same geometry as the sphere of the reference geometry but the diameter has been 20% reduced.

4.3. Materials

This section presents the numerical values used in the airfoil model material. The values are introduced in the property section of Abaqus and are distinguished between elastic, plastic and rupture properties.

The airfoil's leading edge is modelled using Aluminum 2024-T3/T351 Shell type elements which mechanical properties are shown within the following table:

Density [kg/m^3]	Young's Modulus [MPa]	Poisson's Ratio	Yield Limit [MPa]
2770	73084	0.33	684

Table 4.1: Aluminum 2024 mechanical properties introduced in Abaqus.

To simulate the plastic behaviour of aluminum, as previously stated, the Johnson-Cook model is used, which will be introduced in the simulation by means of a series of data collected within the following table:

Yield Limit [MPa]	Strain Hardening Modulus [MPa]	Strain Hardening Exponent	Thermal Softening Exponent
684	369	0.73	1.7

Table 4.2: Aluminum 2024 J-C model parameters introduced in Abaqus.

To analyse the potential failure produce by the impact in the model, Johnson-Cook failure model is used. In order to model this behaviour in Abaqus, the following values will be entered in the simulation properties section:

D_1	D_2	D_3	D_4	D_5	Melting Temperature [K]	Ref. Strain Rate [s^{-1}]
0.31	0.045	-1.7	0.005	0	775	0.0091

Table 4.3: Aluminum 2024 J-C failure model parameters introduced in Abaqus.

The impactor is modelled as a rigid solid with an inertia value equal to its desired mass. No material is created for the impactor.

4.4. Boundary Conditions

In order to correctly simulate the impact, it is required to define some boundary conditions that are applied to the profile. An encastre type boundary condition (restricted displacements and turns) is established on the edges of the airfoil as can be seen in the following image:

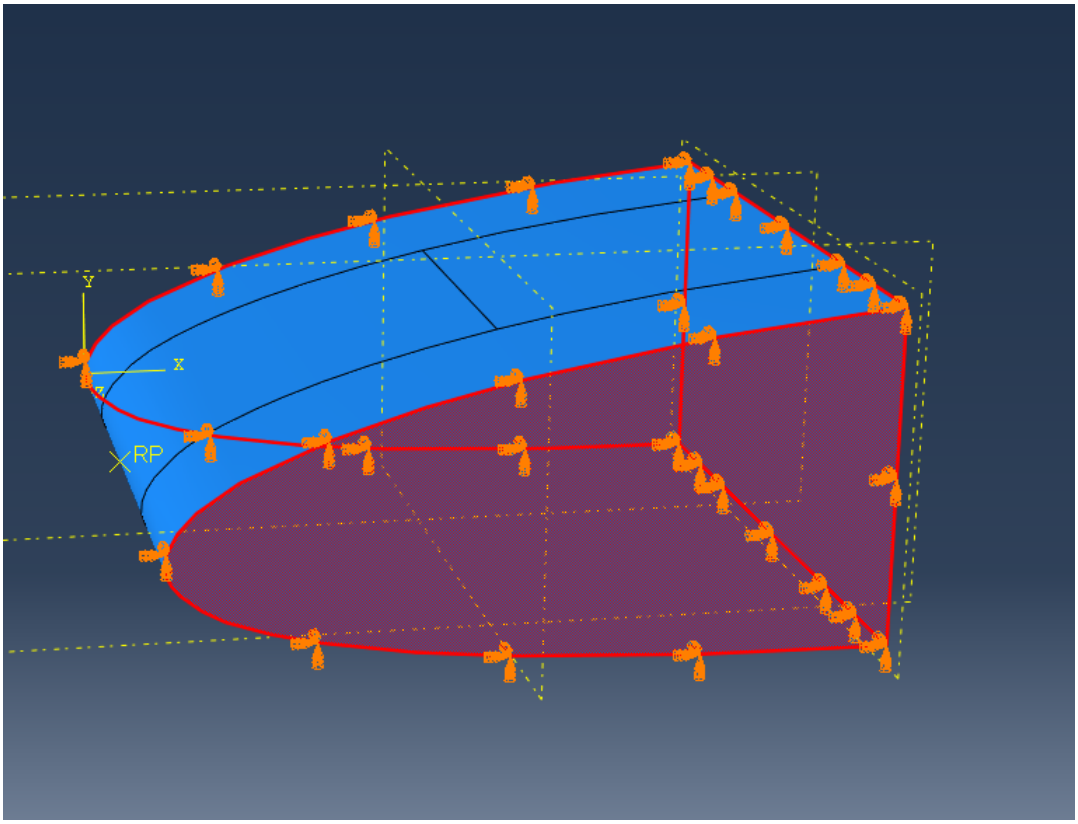

Figure 4.6: Boundary Conditions Applied to the Airfoil

Using the encastre boundary conditions, it is possible to model how an airfoil attached to a rig would be placed when performing impact tests.

Regarding the impactor, a boundary condition of the Displacement/Rotation type will be established in which the linear velocities that are not in the axis of the movement and all three rotations are restricted (U_2=U_3=UR_1=UR_2=UR_3=0).

4.5. Mesh Creation and Convergence

This section shows the meshing performed and the process followed to achieve mesh convergence.

When talking about the mesh, the two elements that make up the model are differentiated, the impactor on one hand and the airfoil on the other.

The impactor meshing has been carried out with Quad-dominated elements, assigning an approximate global size of 3 mm in the first simulation. The size of the elements will be reduced during the process of mesh convergence explained as below.

The airfoil mesh, described in more detail in Appendix 1, has been divided into two different zones: first, the zone close to the impact site, which has a finer mesh than the second zone, which includes the rest of the upper and lower surfaces of the airfoil leading edge. The meshing of the sides of the airfoil will not be relevant for the correct functioning of the model, since when the embedding conditions are applied, there will be no displacements or deformations in those areas.

To obtain the different mesh sizes for each of the zones, the divisions made in the profile (see Appendix 1) are used on which the *Seed Edge* function is applied, assigning different sizes depending on the zone.

The mesh used in the first simulation is shown in the following figure.

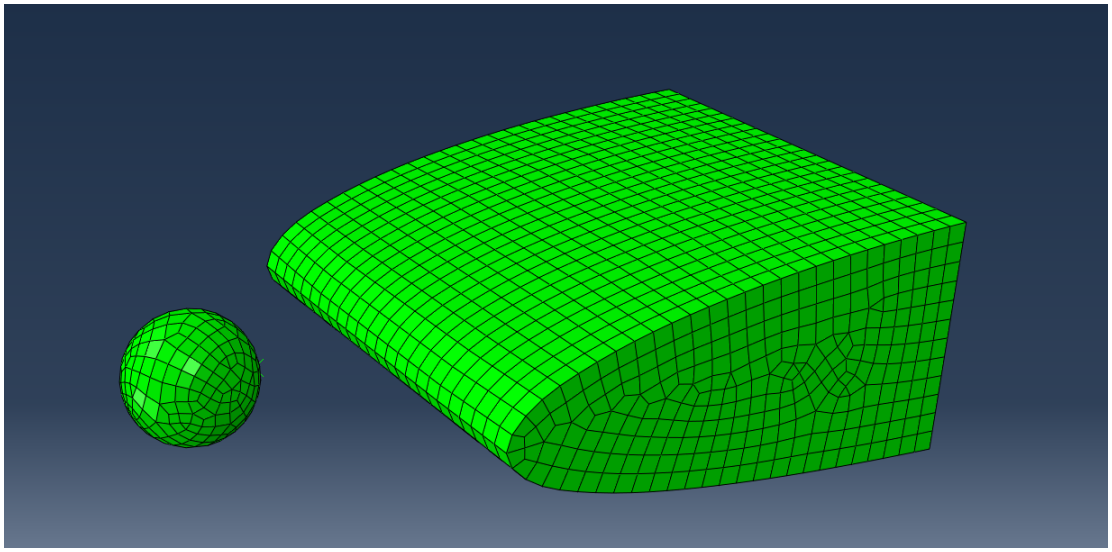

Figure 4.7: Initial Mesh

Once a simulation has been carried out with the previously defined mesh, and it has been verified that the simulation correctly reproduces the expected behavior, the process to obtain the mesh convergence is carried out.

When meshing a model for simulation, two initial considerations must be taken into account:

- A coarse mesh (with few elements) will be less precise than a finer mesh (one with more elements).
- A finer mesh will lead to an increase in simulation time, and it may even happen that the computer will not be capable of performing the simulation.

The process to achieve mesh convergence consists of reaching a compromise solution between the quality of this solution and the time required to get it.

To obtain mesh convergence, start with a coarser mesh (such as the one from the initial simulation), run the simulation, record its time, and observe the results obtained. Subsequently, we proceed to refine the meshing and repeat the previous process until reaching a point where the variations of the solution are small or the simulation times are too long.

In the case of this project, the mesh convergence has started with the mesh shown in the previous image and then, the mesh of the impactor and later, the leading edge one have been refined. To count the simulation time, both the time used to perform the iterations and the time consumed to initialise the model are taken into account. To observe the variation of the solution, the speed of the impactor is considered once it has crossed the profile.

Since the impactor is a rigid body, the influence of its mesh on the model solution will be relatively small. For this reason, to carry out mesh convergence, the number of elements on the leading edge is first left fixed and only the impactor element size is modified until an adequate number is obtained.

The results are collected within the following table:

Sim Name	Element Size	No Elements	Run Time [s]	Impactor Speed [m/s]
Conv1	0.003	1053	32	98.023
Conv2	0.002	2328	35	97.623
Conv3	0.001	9434	30	97.317
Conv4	0.0005	38952	46	97.561

Table 4.4: Mesh Convergence Process, Impactor.

As can be seen, the speed in the solution obtained for the different meshes does not significantly differ from each other.

The *Conv3* model is taken as the reference one to be used in the airfoils mesh convergence, which corresponds to an impactor mesh with 1 mm elements (9434 elements).

Once that model is selected, and therefore, the number of impactor elements is fixed, the size of the leading edge elements is modified, both in the central area and in the sides, and the influence that this has on the solution is analyzed.

The values obtained are collected within the following table:

Sim Name	Center Element Size	Side Element Size	No. Elements	Run Time [s]	Speed [m/s]
Conv3	0.006	0.01	2111	30	97.317
Conv5	0.003	0.01	5495	58	93.893
Conv6	0.003	0.005	8136	98	89.080
Conv7	0.002	0.005	14081	241	84.665
Conv8	0.002	0.003	19701	344	83.569
Conv9	0.001	0.003	50393	Err	Err
Conv10	0.0015	0.003	28601	>3600	Err
Conv11	0.002	0.002	27668	695	83.127

Table 4.5: Mesh Convergence Process, Leading Edge

As can be seen in the previous illustrations, reducing the size of the elements increases the number of elements and the simulation time, even leading to not being able to run the complete simulation (as is the case with the *Conv9* and *Conv10* simulations).

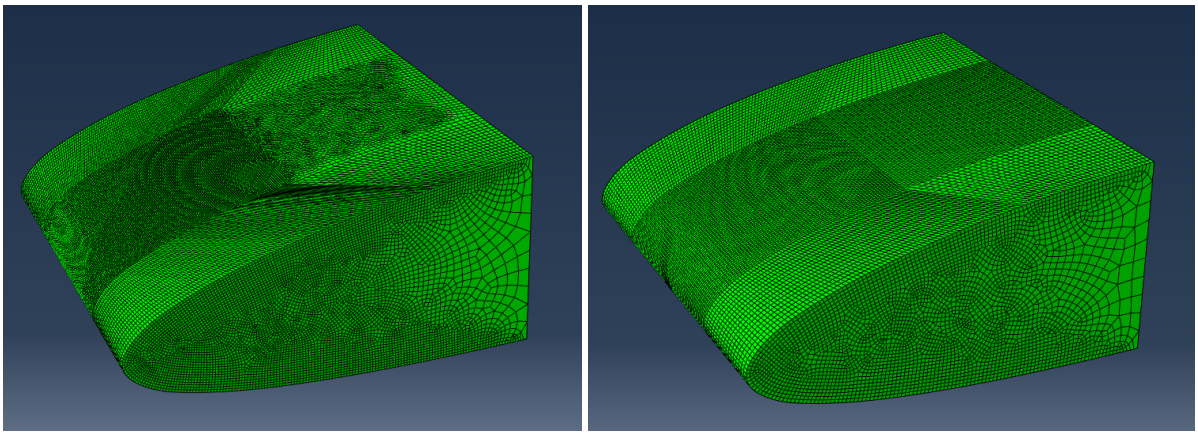

(a) Conv9 (b) Conv10

Figure 4.8: Convergence Process 1

On the other hand, it is observed that the velocity of the projectile after passing through the airfoil decreases as the mesh is refined. Experience using finite elements tells us that by refining the mesh of a structure, it becomes more flexible, that is, less impact energy would be required to cross the leading edge. In the specific case that is being studied, given that the initial velocity of the projectile remains constant, as the rigidity of the structure decreases, it is able to slow down the projectile less, so the velocity after crossing the profile should increase. .

As can be seen, this does not occur in the simulations being carried out and this is due to the fact that as the mesh size is reduced, the damage criterion should be adjusted by modifying the constitutive model of the material. This adjustment is outside the scope of this project since to do it correctly, different simpler models should be correlated with tested specimens.

Taking into account what has been described above, the most important criterion when choosing the mesh of the model that will be used in the study will be the simulation time, although the speed variation will be used as support. The first three simulations (*Conv3*, *Conv5* and *Conv6*), despite having a very short simulation time, present a greater difference in speed compared to the others, which is why they are discarded.

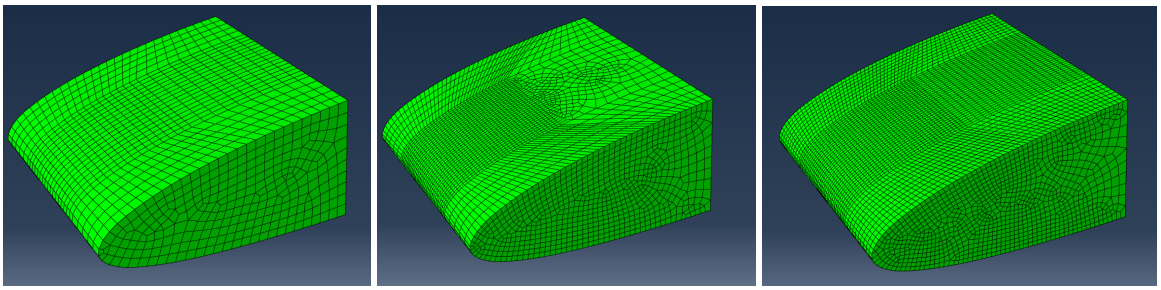

(a) Conv3 (b) Conv5 (c) Conv6

Figure 4.9: Convergence Process 2

The time increase in the *Conv11* simulation is not worth the small speed difference. Between the *Conv7* and *Conv8* simulation, both with similar simulation times (approx. 5 minutes), the mesh of the *Conv8* simulation has been chosen as the one to be used in the final model due to its greater regularity.

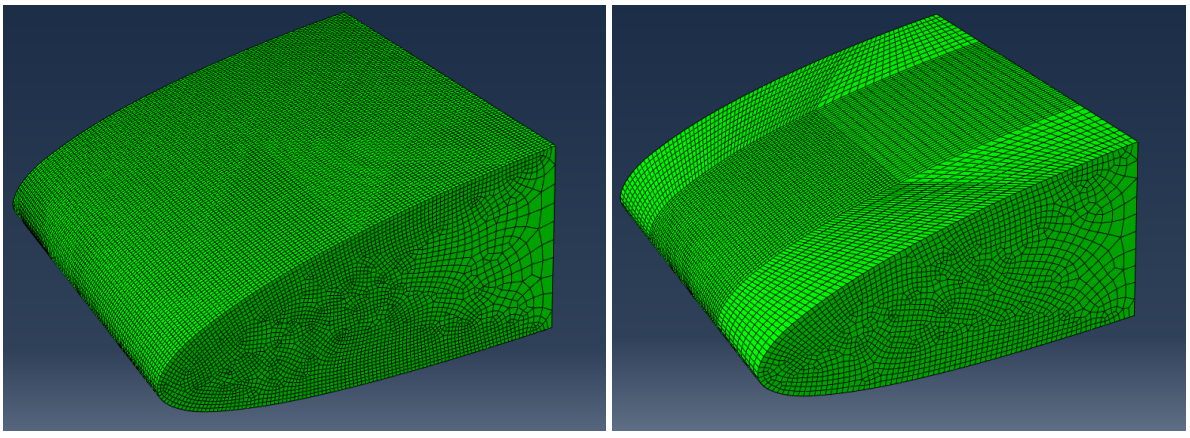

(a) Conv11 (b) Conv7

Figure 4.10: Convergence Process 3

The mesh used in the final model can be seen in the following illustration:

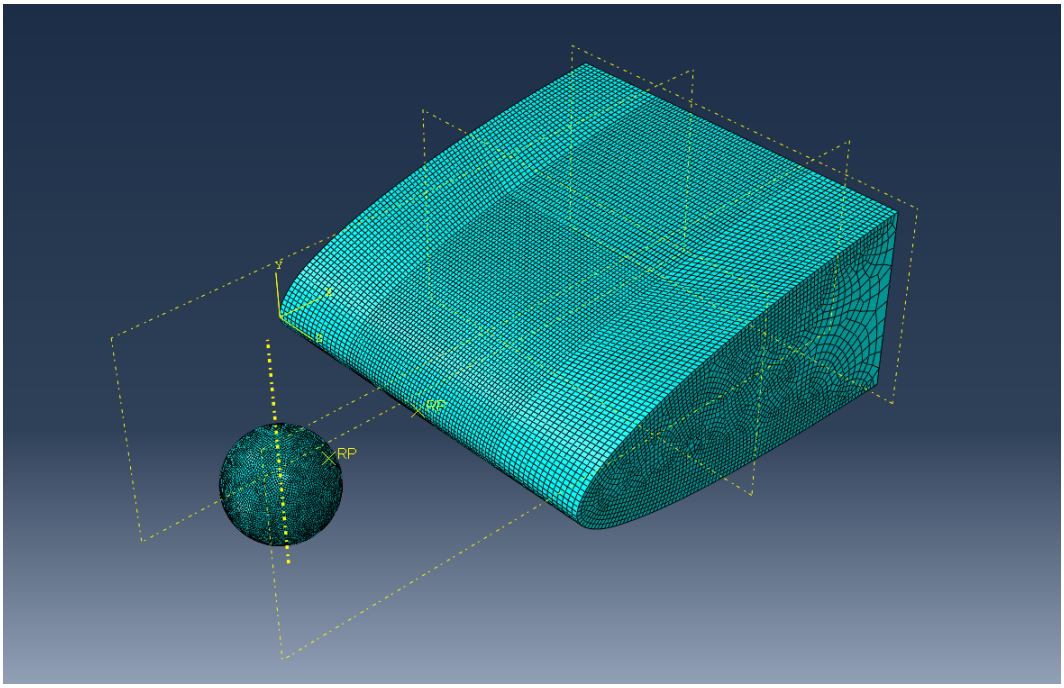

Figure 4.11: Model Mesh after Convergence

4.6. Impact Velocity

In this section is shown the process followed to obtain the speed of the projectile that will correspond to the ballistic limit.

As previously expressed, the ballistic limit concept corresponds to the speed at which a projectile has a 50% probability of passing through a structure. In the case of this work, the speed that is considered to be the ballistic limit is that at which the projectile crosses the leading edge. This assumption guarantees that any speed less than this does not cause breakage in it.

To calculate the speed of the projectile that corresponds to the ballistic limit, the mesh selected in the previous section is used and an iterative process will be followed, modifying the initial speed of the impactor.

The different iterations carried out are collected within the following table, where the initial velocity is shown, whether the projectile crossed the leading edge or not, and, if so, its residual velocity:

Sim Name	Initial Speed [m/s]	Break Through	Residual Speed [m/s]
BL1	200	Yes	83.569
BL2	160	No	-
BL3	180	Yes	51.217
BL4	170	Yes	29.508
BL5	165	Yes	19.527
BL6	162.5	Yes	5.858
BL7	161.5	No	-
BL8	162	No	-

Table 4.6: Balistic Limit Iterations.

As can be seen, as the initial velocity of the projectile decreases, the residual velocity after passing the profile airfoil decreases too, even reaching the point of not being able to cross it.

After carrying out the iteration, it is observed that for velocities smaller than 162 m/s, the projectile fails crossing the leading edge. Increasing the velocity slightly, it can be seen that for 162.5 m/s the residual velocity is barely 5.9 m/s, and although it does not reach 0 m/s, it is considered a sufficiently low velocity to be defined as the ballistic limit.

The initial speed of 162.5 m/s will be established as the reference one when carrying out the simulations.

4.7. Discussion on non-implementation of self-contact

After carrying out the simulations to obtain the ballistic limit, a discontinuity in the graphs has been observed, such as that of plastic dissipation. This is because this model does not include the contact behaviour that occurs when the detached portion of the leading edge, after breaking, hits the inside part of the rest of it. This can be seen in the following images:

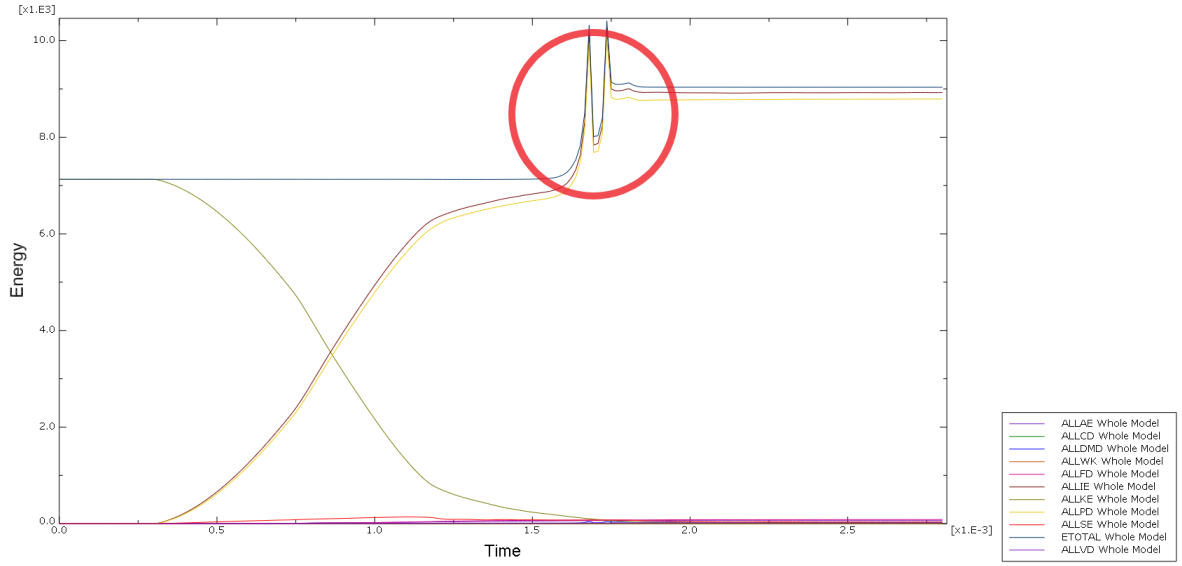

Figure 4.12: Discontinuity Detail

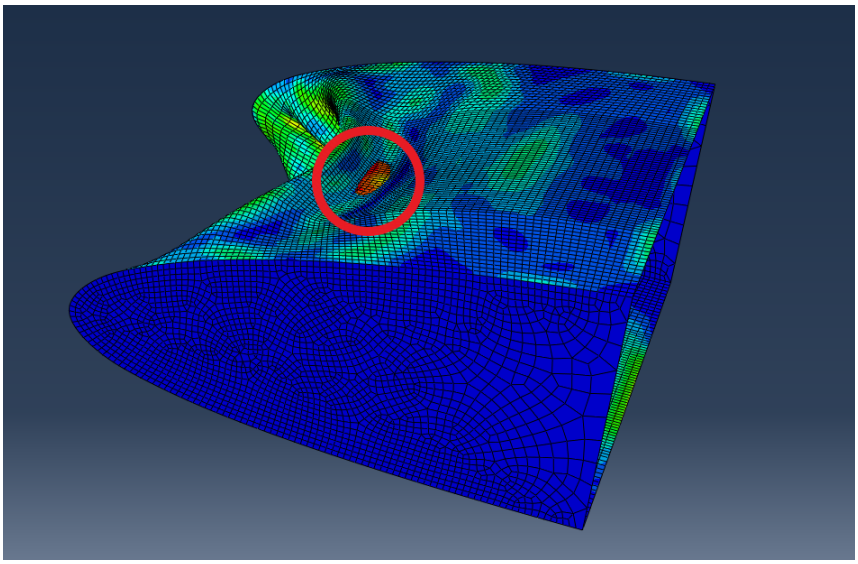

Figure 4.13: Detached area and upper surface contact

Taking the above into account, it has been decided to make an identical model but including the self-contact of the leading edge with itself.

When performing the simulation of these models, various errors occurred that prevented the simulation from being completed. To correct this issue, it was decided to reduce the timestep up to an order of magnitude and follow a process similar to the one carried out to obtain the ballistic limit. Despite this, depending on the velocity of the projectile, the model was not capable of converging without error, however, sufficient results have been obtained to justify the choice of not running the model with leading edge self-contact.

- Analyzing the initial and residual velocity results of the simulation carried out with self contact activated, it can be seen that for an initial velocity of 161.5 m/s the projectile is not able to cross the leading edge and ricochets. On the other hand, for an initial velocity of 162 m/s, despite the fact that the simulation is not capable of completing the whole time span, it can be seen that the projectile is capable of penetrating the leading edge.

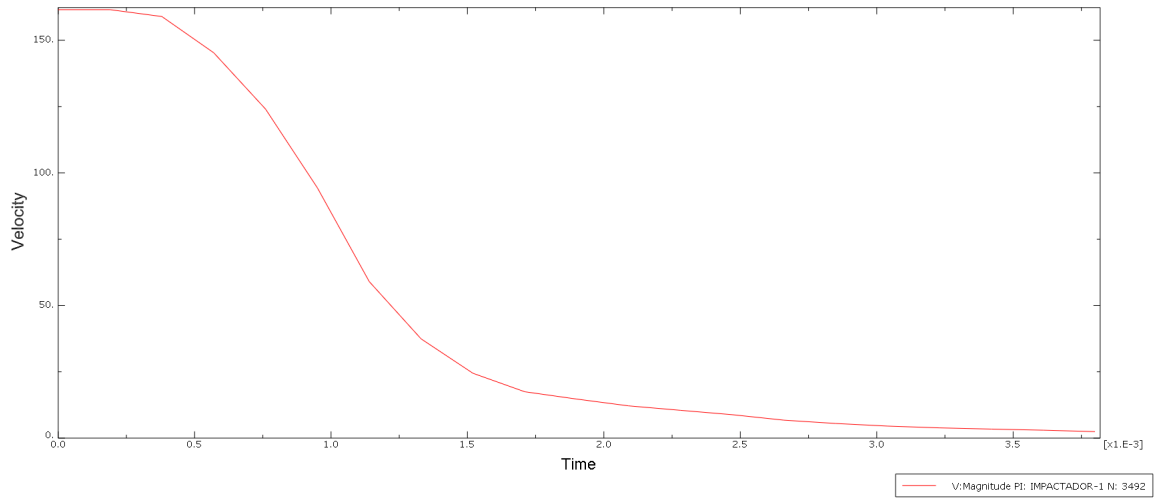

Figure 4.14: Speed Evolution 161,5 m/s

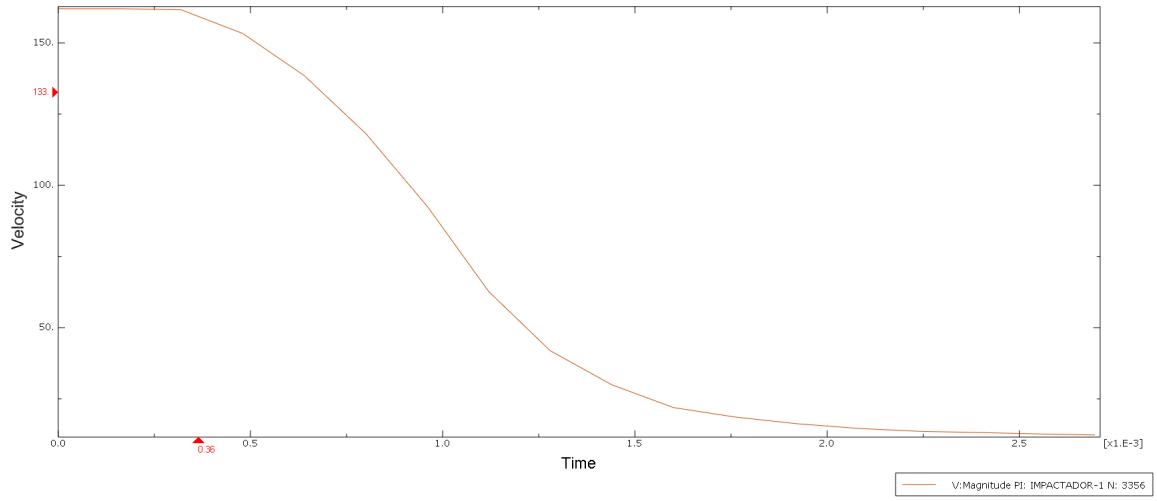

Figure 4.15: Speed Evolution 162 m/s

With these data we can assume that the initial velocity corresponding to the ballistic limit is between 161.5 and 162 m/s, that is, a difference of less than 1 m/s with respect to the simulation carried out without the self-contact activated. This difference in speed between one model and the other translates into a relative error of 0.6%, that is, a negligible error comparing the difference in simulation time.

- Analyzing the energies present in the model with the self contact deactivated (see graph 4.12) it is possible to clearly observe the discontinuity that occurs in the internal energy, the energy

dissipation caused by the plastic deformation and therefore the total energy, a once the projectile is no longer in contact with the leading edge.

Analyzing the behavior of the energies involved in the process in the model with self contact activated, it can be observed how, eliminating the part of the discontinuity in the simulation without contact, the variation of the two predominant energies during the impact occurs in a identical in both processes.

Although there are slight variations in some other energy involved, their influence is negligible on the whole process.

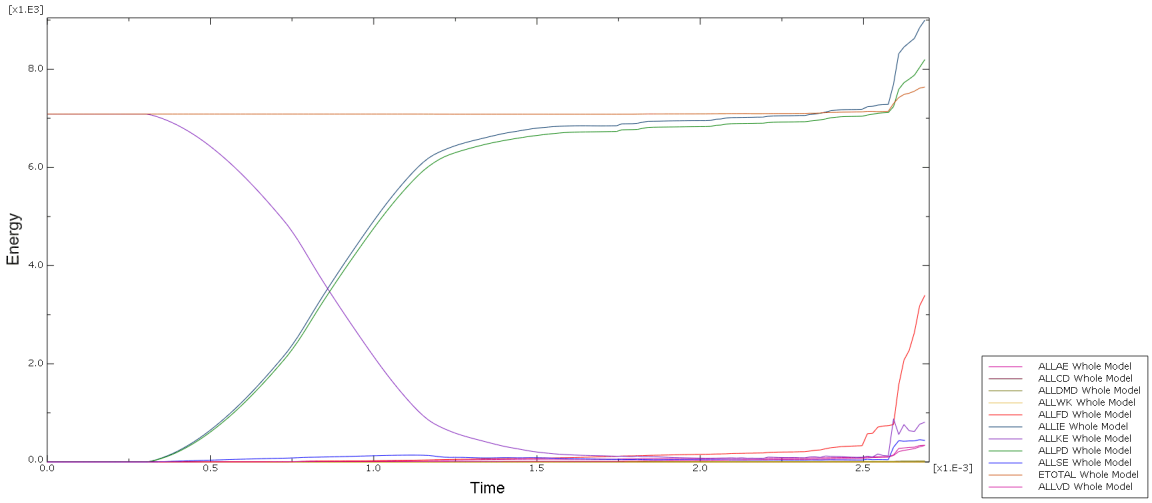

Figure 4.16: Energy Variation With Self-Contact Activated

For the reasons mentioned above, as well as the excessive increase in simulation times when the model is carried out with self-contact activated, it has been decided to carry out the model without considering the self-contact of the leading edge.

The results obtained with this model are shown in the next chapter.

5

Outcomes

The results obtained in the different simulations carried out after the choice of the model are shown in this chapter. These results will be analyzed and their variations will be emphasized according to the modifications made in each simulation compared to the reference model in order to appreciate the influence of the different parameters on the residual velocity and at the ballistic limit velocity.

5.1. Reference Model

The simulation considered as reference consists of the 1.5 mm thick leading edge model 2.1 and the spherical impactor 4.2 with an initial velocity (162.5 m/s) with which the ballistic limit has been obtained 4.6.

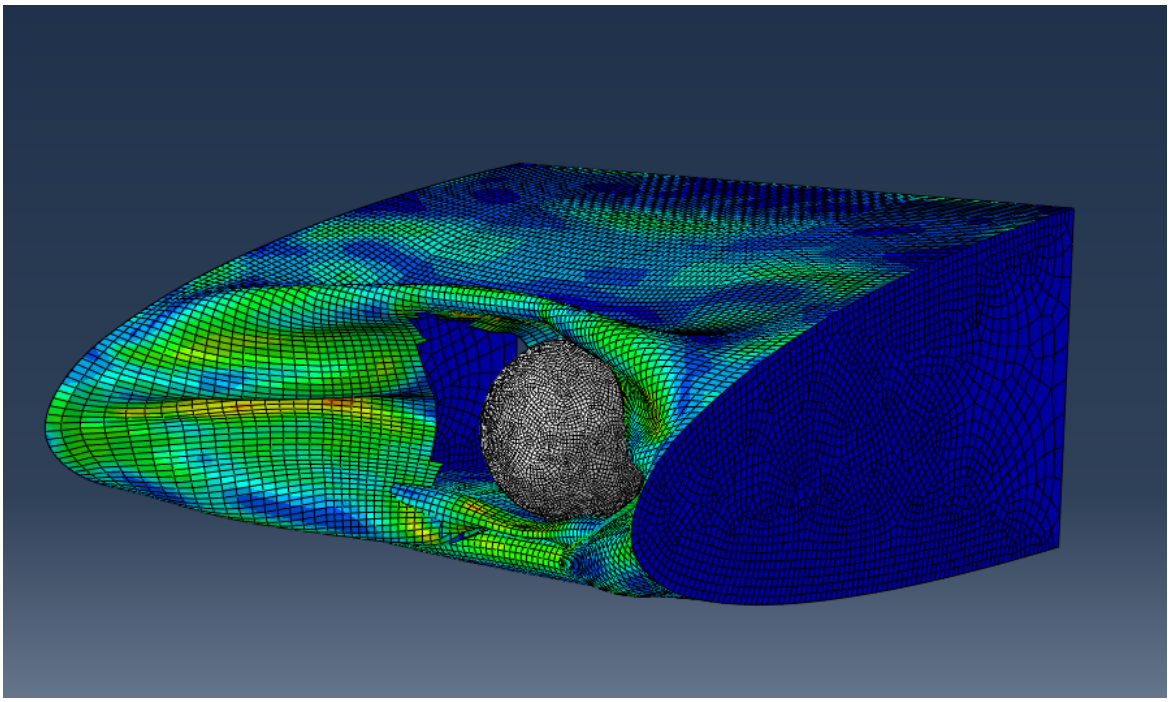

Figure 5.1: Reference Model Simulation

In the first place, the variation of the different magnitudes involved in the impact will be analyzed. It will begin by observing how the kinetic energy and the velocity of the projectile vary with time. Both magnitudes are related through the kinetic energy equation.

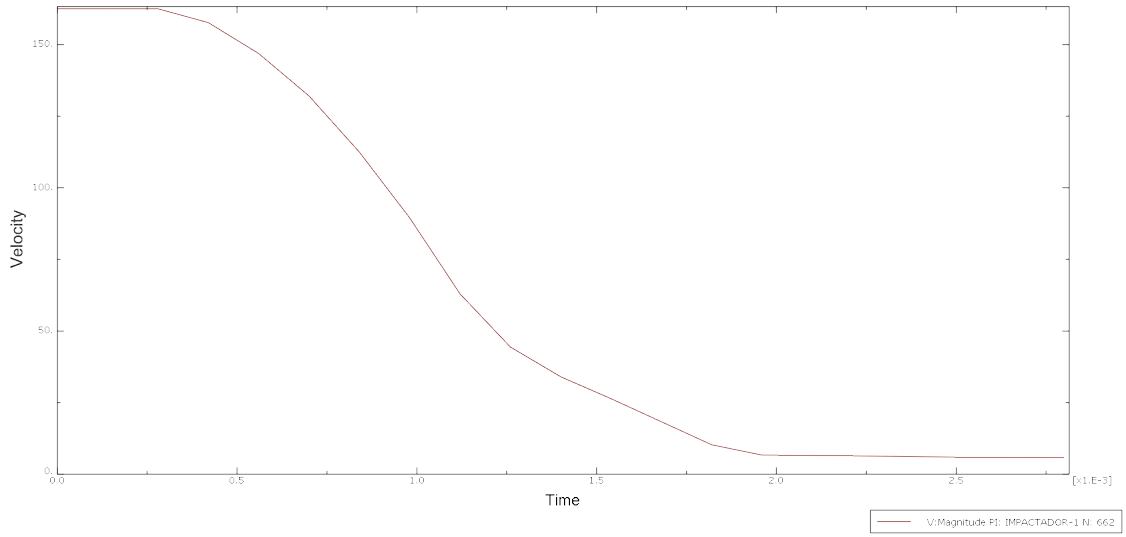

Figure 5.2: Reference Model Simulation Velocity Variation

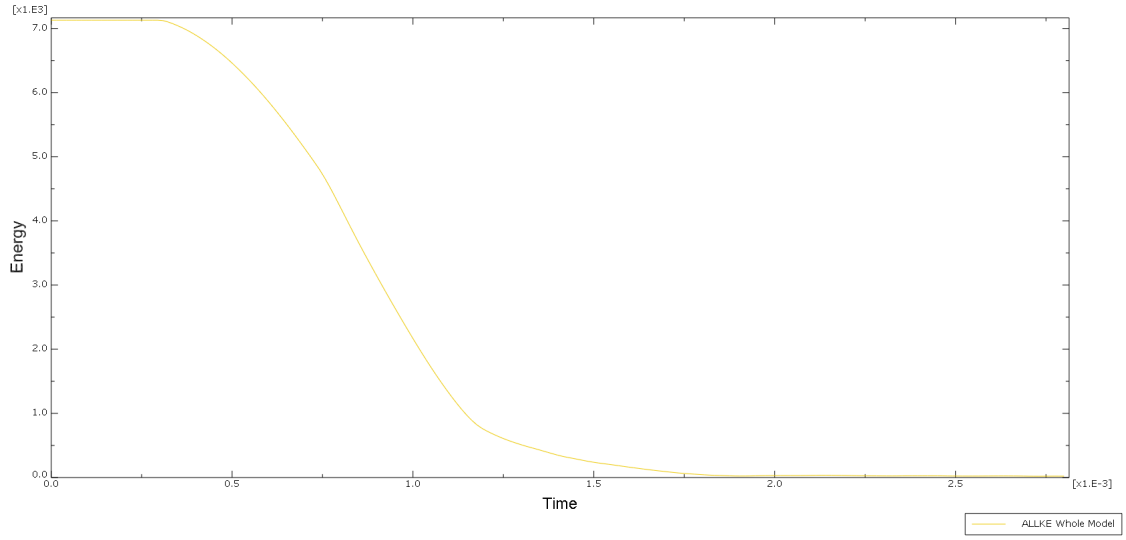

Figure 5.3: Reference Model Simulation Knetic Energy

As can be seen in the graphs 5.2 and 5.3, the velocity, and therefore, the kinetic energy remain constant until the moment when contact between the projectile and the leading edge occurs (around 2.5 e-4s). This is due to the fact that effects such as air resistance have not been considered in this model.

Once contact has been made, it can be observed that the velocity decreases, first more abruptly as the part of the projectile's surface increases and, after breaking the attack edge, more gently. Once it has completely crossed the leading edge, the speed remains constant at approximately 6 m/s.

Between the initial speed and the residual speed, a difference of 156.64 m/s can be observed.

Analyzing all the energies involved in the impact process, we can see that both the kinetic energy, already mentioned above, and the dissipation produced by the plastic deformation are the predominant energies.

In addition to these two main energies involved, the evolution of other energies can be observed, such as the energy dissipated by friction, the energy of deformation or the energy dissipated by damage. However, the influence of these energies is two orders of magnitude smaller than the prevailing ones.

As explained in the previous chapter, due to the not inclusion of the self-contact, the part detached from the leading edge of the airfoil crosses the upper surface, which is represented by a discontinuity

in the evolution of the different energies. This discontinuity occurs some time later than the projectile has passed through the leading edge. For this reason, when analyzing the behavior of the model, the discontinuity and the subsequent simulation time have not been taken into account.

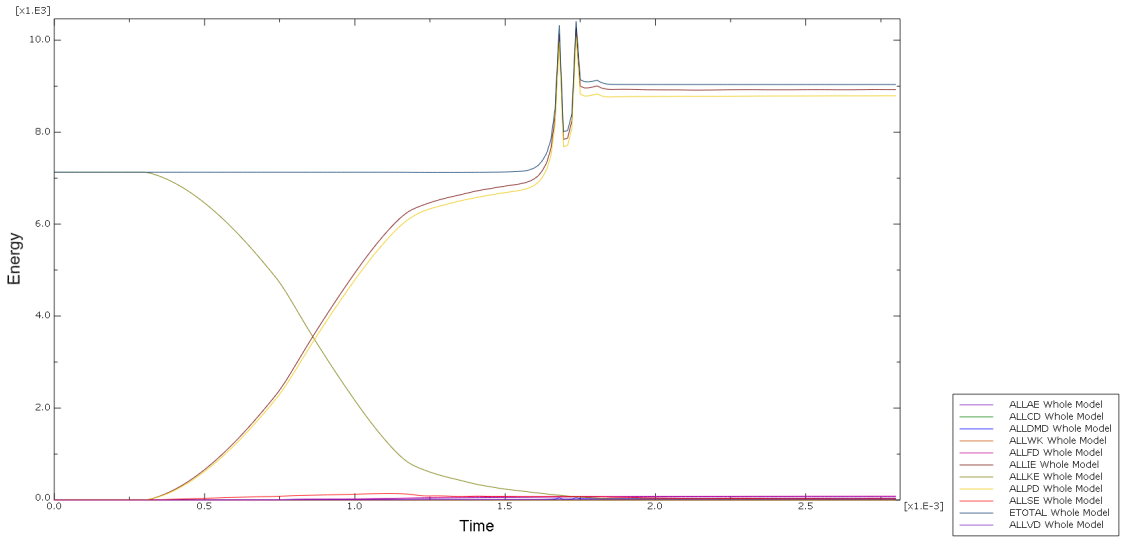

Figure 5.4: Reference Model Simulation Energies

Observing the variation of the kinetic energy against the plastic deformation dissipation one, the correlation between both energies can be highlighted, see 5.4.

On the one hand, the kinetic energy is conserved at its maximum value at the beginning of the simulation until the moment the projectile contacts the leading edge. At that moment, the velocity of the projectile begins to decrease, so does the kinetic energy. This progressive decrease is maintained until the projectile is no longer in contact with any surface and the velocity remains constant, in this case with the residual velocity.

On the other hand, it can be observed how the energy dissipation behaves opposite to the kinetic energy during the impact. As can be seen in the following graph 5.5, the dissipation is null until contact between the projectile and the leading edge occurs. Once this occurs, the dissipated energy increases until the projectile completely passes through the airfoil and then it remains constant when the projectile is no longer in contact with the airfoil.

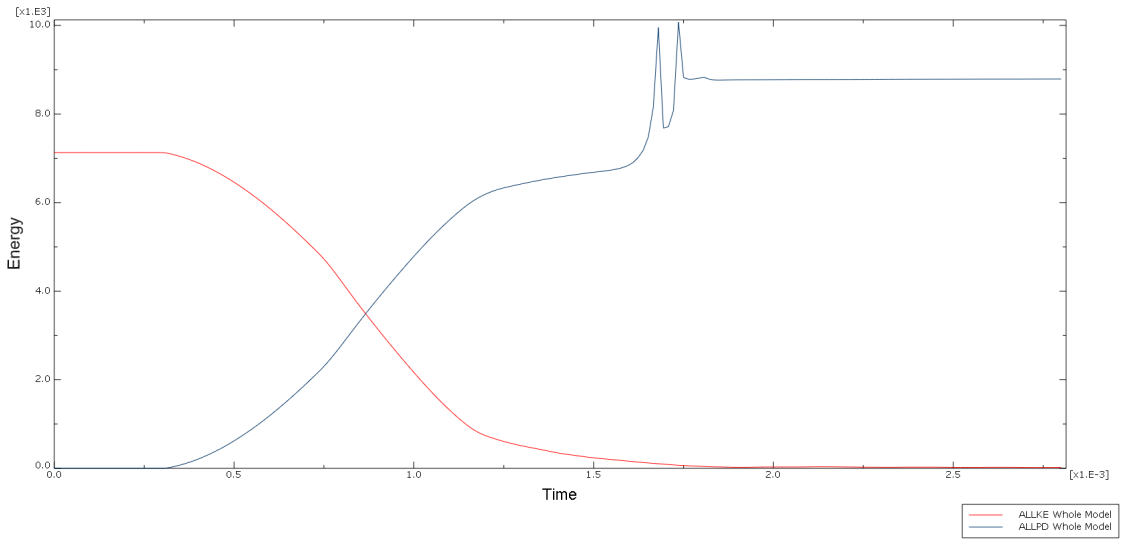

Figure 5.5: Reference Model Simulation Kinetic Energy vs Plastic Disipation

Analyzing the rest of the energies involved in the impact, it can be seen that their influence is less than the previously mentioned energies. Noteworthy is the strain energy, which is zero at the start of the simulation until contact between the projectile and the leading edge begins, reaching a maximum around 1.1 ms, at which point the damage dissipation energy begins to increase slightly. Once past the maximum, the strain energy decreases again.

On the other hand, two energies with a similar behavior can be observed, these are Artificial Strain Energy, which includes energy stored in hourglass resistances and transverse shear in shell and beam elements, and frictional dissipation. Both energies are zero until projectile-leading edge contact, at which point they increase slightly. As the projectile deforms and breaks the central zone of the leading edge, both energies increase until the projectile separates from the airfoil and these energies remain practically constant.

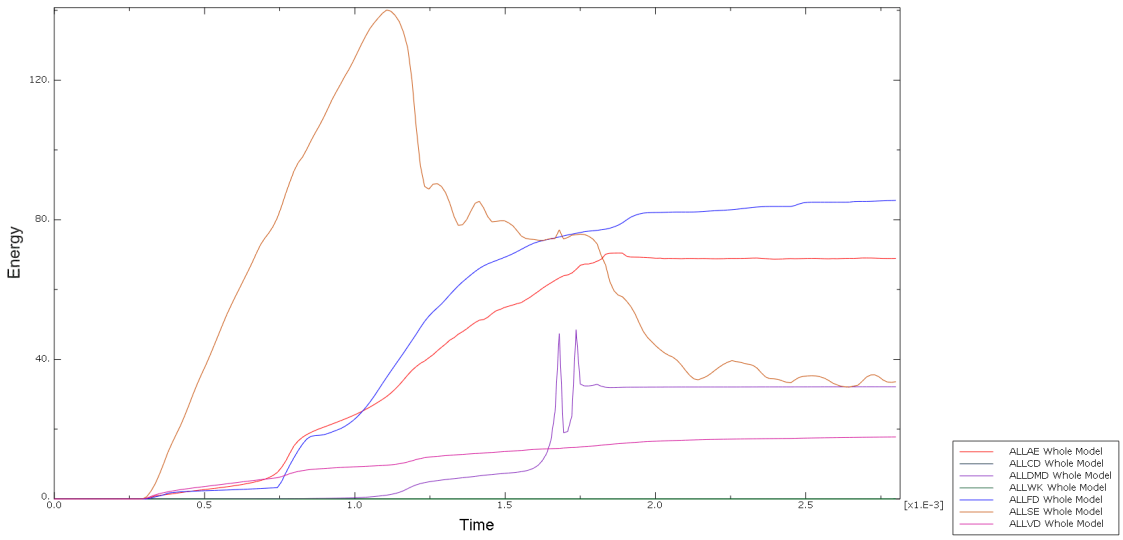

Figure 5.6: Reference Model Simulation Low Influence Energies

Finally, it is interesting to observe the behavior of the total energy. For this, the energy balance of the model is analyzed:

$$E_I + E_V + E_{FD} + E_{KE} - E_{IHE} - E_W - E_{PW} - E_{CW} - E_{MW} - E_{HF} = E_{total} = constant \tag{5.1}$$

Where

- E_I is the internal energy.
- E_V is the viscous energy dissipated.
- E_{FD} is the frictional energy dissipated.
- E_{KE} is the kinetic energy.
- E_{IHE} is the internal heat energy (not analysed in this model).
- E_W is the work done by the externally applied loads.
- E_{PW}, E_{CW} and E_{MW} are the work done by contact penalties, by constraint penalties, and by propelling added mass, respectively.
- E_{HF} is the external heat energy through external fluxes. (not present in this model)

The internal energy is composed in turn of the following energies:

$$E_I = E_E + E_P + E_{CD} + E_A + E_{DMD} + E_{DC} + E_{FC} \tag{5.2}$$

Where the internal energy is the sum of:

- E_E is the elastic strain energy.
- E_P is the energy dissipated through inelastic processes such as plasticity.
- E_{CD} is the energy dissipated through viscoelasticity or creep.
- E_A is the artificial strain energy.
- E_{DMD} is the energy dissipated through damage.
- E_{DC} is the energy dissipated through distortion control.
- E_{FC}, is the fluid cavity energy.

As can be seen in the graph 5.7, the total energy remains constant throughout the process until the discontinuity occurs. This corresponds to the aforementioned energy balance equation.

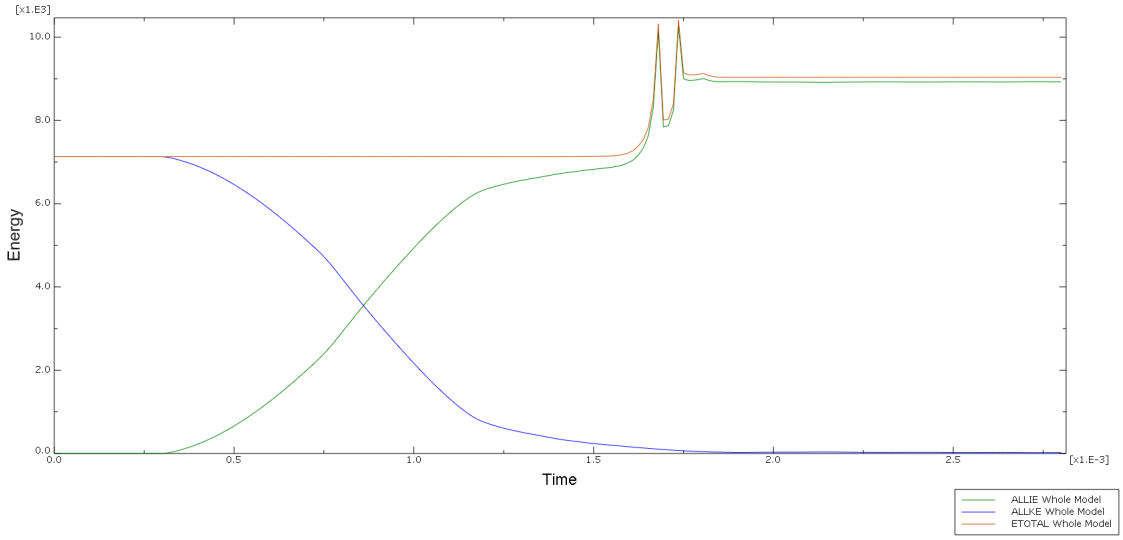

Figure 5.7: Reference Model Simulation Total Energy

The energies analyzed in this project with their respective acronyms are included within the following table:

Energy	Acronym
Artificial Strain Energy	ALLAE
Creep Dissipation Energy	ALLCD
Danage Dissipation Energy	ALLDMD
External Work	ALLWK
Frictional Dissipation	ALLFD
Internal Energy	ALLIE
Kinetic Energy	ALLKE
Plastic Dissipation	ALLPD
Strain Energy	ALLSE
Total Energy of the Output Set	ETOTAL
Viscous Dissipation	ALLVD

Table 5.1: Energy Acronyms

Finally, the behavior of the leading edge during the impact simulation will be analyzed. As can be seen in figure 5.8, after impacting the projectile, deformation occurs in the entire central zone followed by

the breaking of the leading edge in the lower and lateral of the impact zone. As the projectile continues to advance, the rupture zone grows until it is completely clear of the leading edge except for the top. After this the projectile continues advancing and displacing the piece detached from the leading edge towards the upper surface, until it completely passes through the airfoil.

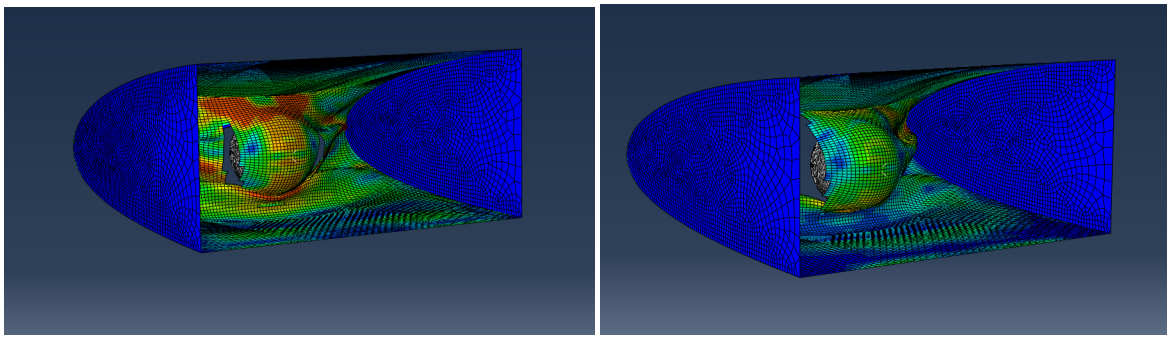

(a) t=1.26ms (b) t=1.68ms

Figure 5.8: Reference Simulation Impact Evolution 1

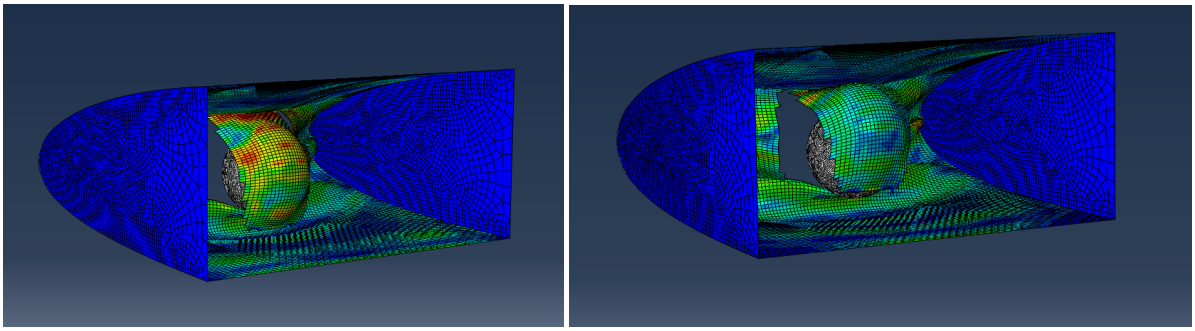

(a) t=2.24ms (b) t=2.8ms

Figure 5.9: Reference Simulation Impact Evolution 2

5.2. Projectile Velocity influence

In this section the behavior of the impact is analyzed modifying only the initial velocity of the projectile. In the first place, observing the behavior when the speed is lower than the ballistic limit and later analyzing the impact for a speed higher than the ballistic limit and checking the relationship between the initial and the residual speed.

5.2.1. Velocity below the ballistic limit

To analyze the behavior of an impact at a lower initial velocity than that corresponding to the ballistic limit, a model identical to the reference simulation has been made, considering the leading edge thickness of 1.5 mm and the spherical projectile. However, the initial speed has been slightly reduced from 162.5 m/s to 160 m/s.

As can be deduced from the very definition of the ballistic limit that has been presented in this work and by looking at the images below, it can be seen how the projectile is not able to completely cross the leading edge but rather bounces and changes direction.

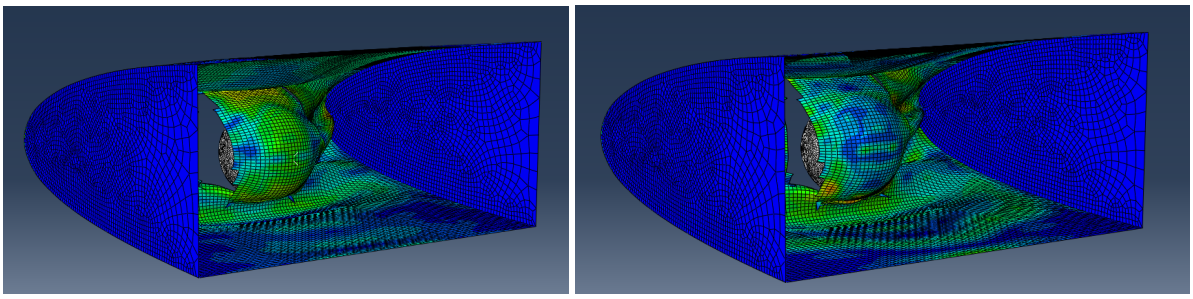

(a) t=1.9 ms (b) t=2.8 ms

Figure 5.10: Velocity Lower than Ballistic Limit Simulation

The effect of the ricochet can be observed more clearly if we analyze the behavior of the velocity of the projectile:

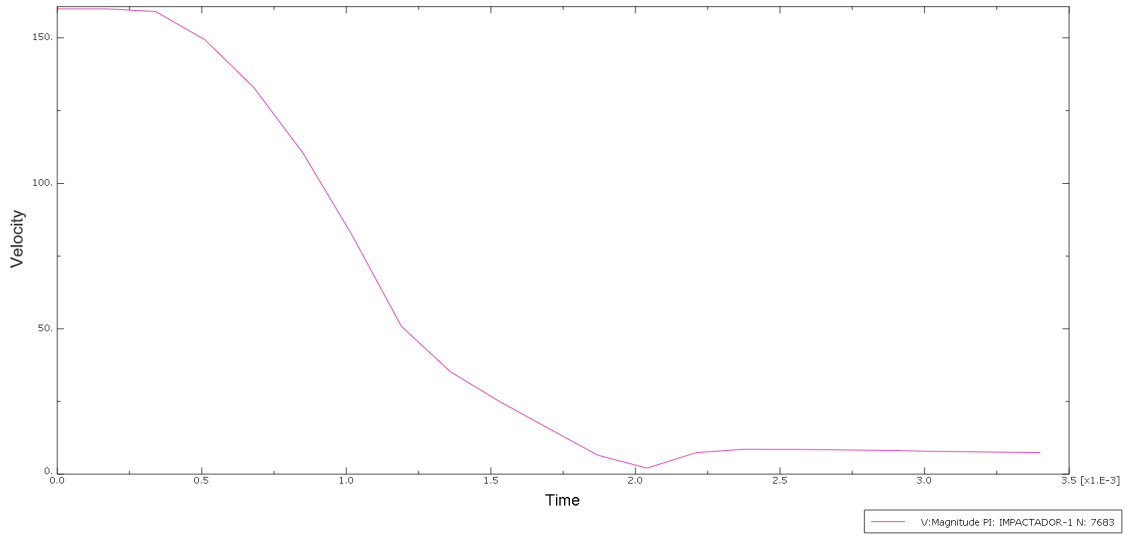

Figure 5.11: Velocity Lower than Ballistic Limit Simulation: Speed Evolution

If the graph of the velocity of the projectile is analyzed, a shape practically identical to the one in the reference simulation is observed. Firstly, the speed remains constant until impact and then, the speed decreases while the contact between the projectile and the leading edge is maintained. However, since the speed is below the ballistic limit, the impact energy of the projectile is not enough to cross the leading edge, but rather it is capable of completely absorbing the kinetic energy of the projectile. This is observed in the velocity graph itself where, in time 2ms, the velocity of the projectile is zero. Once this point is reached, due to the elastic behavior of the material, the projectile rebounds, that is, the magnitude of the velocity increases although the direction changes. Finally, the speed increases until it reaches 7.4 m/s and since there is no contact or influence from external effects such as gravity or friction with the air, this speed remains constant.

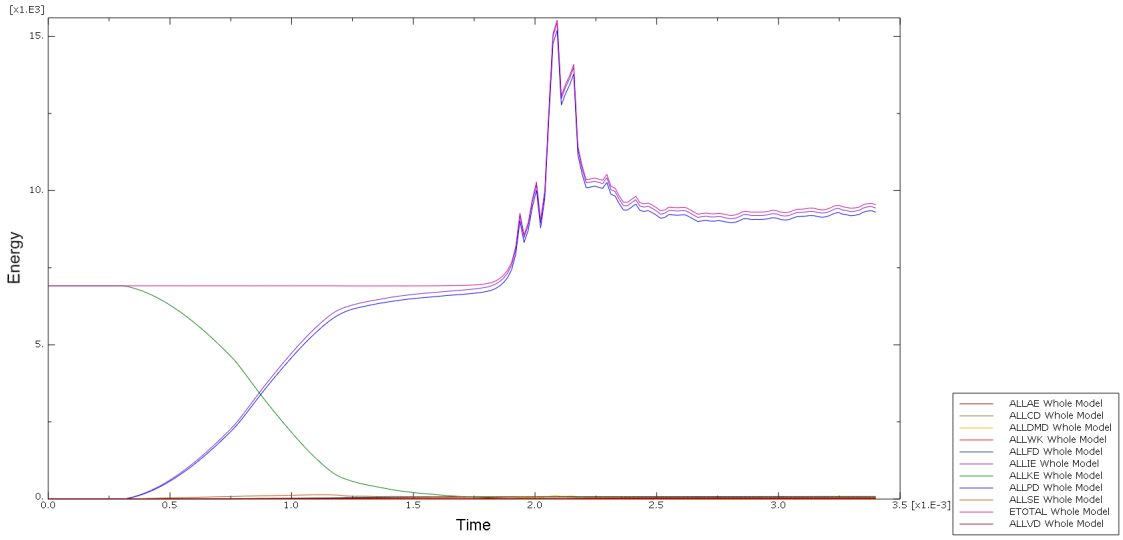

Figure 5.12: Velocity Lower than Ballistic Limit Simulation: Energies Involved

Analyzing the behavior of the energies involved and comparing them with those obtained in the reference simulation (5.4), ignoring the part after the discontinuity, a very similar behavior can be observed. As is logical, the initial kinetic energy is lower than in the reference model since the initial velocity is lower in this simulation. It can be concluded that because the kinetic energy of the projectile is less than the energy that is capable of dissipating the leading edge, the projectile is not able to pass through it.

In this case, the behavior of the leading edge against impact is very similar to what occurs in the reference simulation. The rupture zone begins in the lateral area of the point of impact and as the projectile advances, this rupture grows. However, in this case, the material does not break in the lower area of the impact zone, which prevents the projectile from continuing through, and causes it to loose speed until it stops and bounces in the opposite direction of the movement.

5.2.2. Velocity above the ballistic limit

In this section we analyze the behavior of the impact when the velocity of the projectile is higher than the ballistic limit. It is obvious to assume, and this can be observed in the simulations, that by having greater speed, and therefore greater kinetic energy, the projectile will always cross the leading edge. The interesting objective of this section is to carry out a series of simulations with different velocities above the ballistic limit and to analyze how the residual velocity varies accordingly.

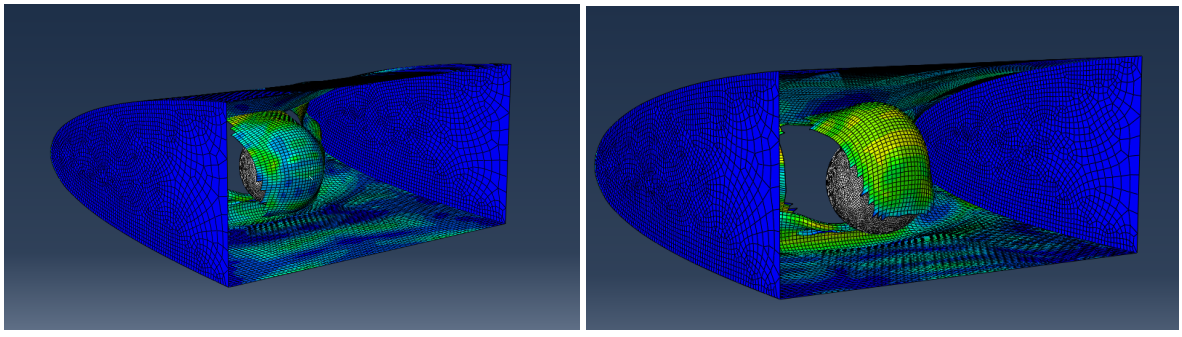

(a) t=1.68 ms (b) t=1.9 ms

Figure 5.13: Velocity Higher than Ballistic Limit Simulation 1

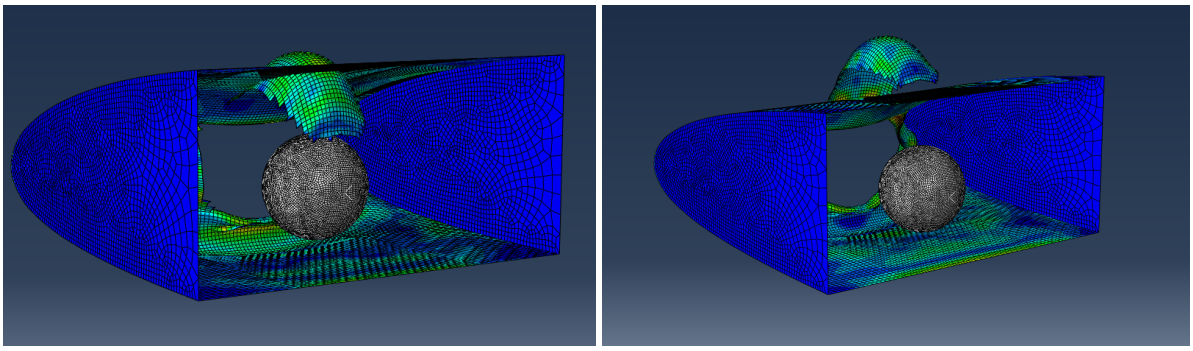

(a) t=2.38 ms (b) t=2.8 ms

Figure 5.14: Velocity Higher than Ballistic Limit Simulation 2

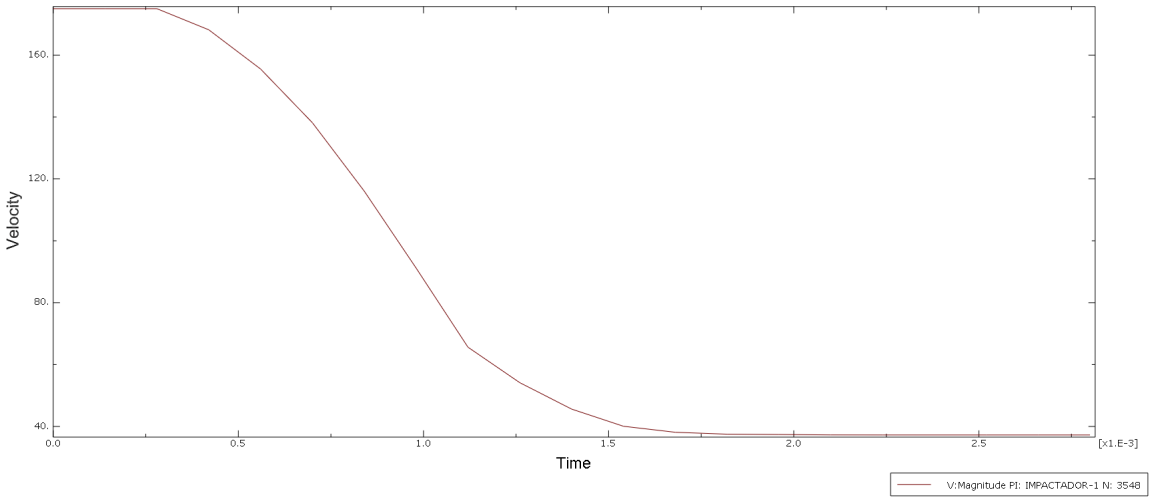

Figure 5.15: Velocity Higher than Ballistic Limit Simulation: Velocity Evolution

If the previous graph (5.15) is compared with the one obtained for the velocity corresponding to the ballistic limit (5.2), it can be observed that the increase in initial velocity does not exactly correspond to that with the increase in the residual velocity of the projectile.

To study the relationship between both speeds, a series of simulations have been carried out for different initial speeds, and have been collected within the following table:

Sim Number	Initial Speed [m/s]	Residual Speed [m/s]
1	162.5	5.8
2	165	19.527
3	170	29.508
4	175	37.246
5	180	51.217
6	185	60.296
7	200	83.569
8	220	108.833
9	250	156.168

Table 5.2: Initial vs Residual Speed.

Analyzing the values obtained, a graph (5.16) is obtained where the variation of residual speed can be observed against the variation of the initial one.

As can be seen in the graph, the residual velocity compared to the initial velocity does not vary linearly throughout the range of velocity, but this variation decreases as we move away from the ballistic velocity. That is, the slope of the curve decreases as the initial speed is increased and, the slope will become 1 for really high speeds.

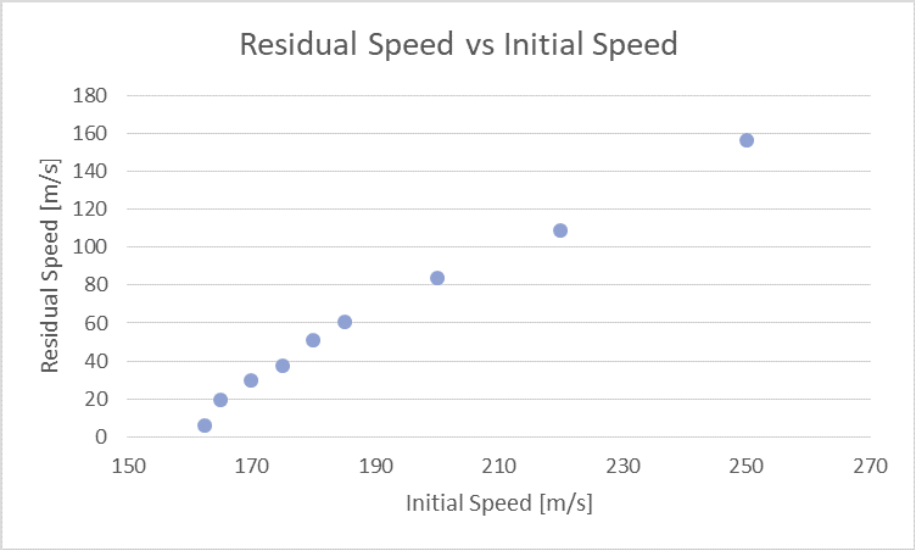

Figure 5.16: Residual vs Initial Speed

Analyzing Thor's equation for projectile speeds (5.3) and particularizing it for the current case, that is, in which the only impact parameter that is modified is the initial speed, the equation 5.4 is obtained.

$$V_r = V_i - 10^c \, (tA)^\alpha \, (m_s)^\beta \, (sec\theta)^\gamma \, V_i^\lambda \tag{5.3}$$

$$V_r = V_i - CV_i^\lambda \tag{5.4}$$

As can be seen from the equation 5.4 and from the data analyzed in the graph, the residual velocity increases as the impact velocity increases if the other parameters are kept fixed. Comparing the equation with the results obtained, the constant C that encompasses the other parameters,such as the mass, the thickness of the leading edge and the contact area between the projectile and the airfoil, must be a positive number and therefore the parameter λmust be less than 1.

5.3. Influence of the contact surface

In this section we study the influence of geometry of the impactor on the velocity of the ballistic limit. In the first place, it is analyzed how this velocity varies by reducing the contact surface and then it will be observed how the ballistic velocity varies and how the different energies evolve when modifying the geometry of the projectile keeping the rest of the constant parameters.

5.3.1. Smaller Contact Surface

In this subsection the influence of the contact surface between the projectile and the profile will be analyzed, in this case reducing it. To carry out this analysis, a model identical to the one created for the reference simulation has been made, only modifying the size of the projectile used. A spherical projectile has been used with 20% smaller radius than that of the original model, in other words, the total area of the sphere has decreased by 36%, keeping the mass of the projectile constant.

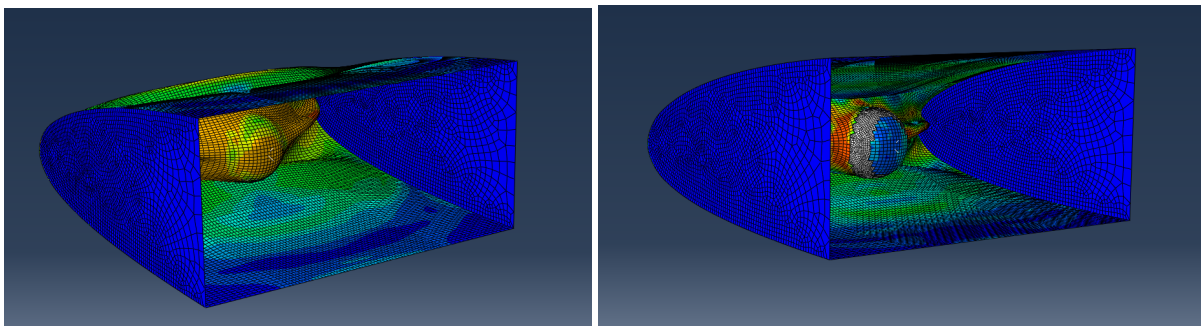

(a) t=1.12 ms (b) t=1.26 ms

Figure 5.17: Lower Surface Simulation 1

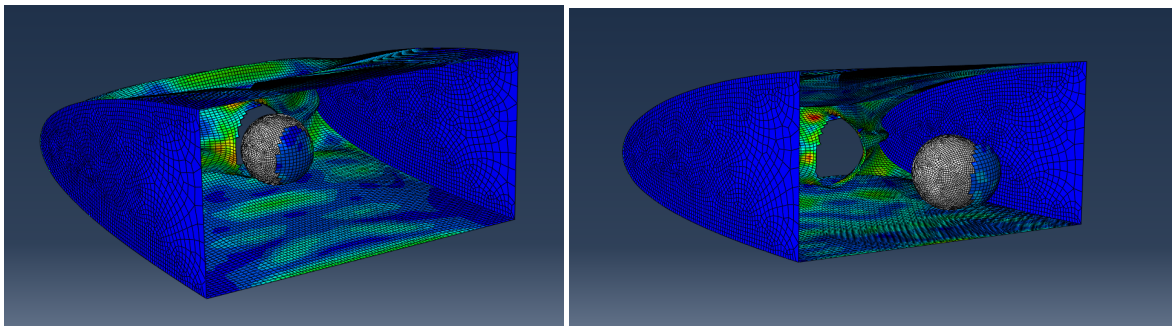

(a) t=1.54 ms (b) t=2.8 ms

Figure 5.18: Lower Surface Simulation 2

Firstly, a simulation has been carried out using the speed obtained as the ballistic limit for the reference simulation as the initial speed for this model. As can be seen in the images above, the breaking behavior of the leading edge is different from that observed in the reference simulation.

In this case, since the surface of the projectile is smaller, the deformation is concentrated in a smaller area of the leading edge. The airfoil rupture occurs around the impact zone, completely tearing off a section and traveling at the same time as the projectile, unlike in the reference simulation, with the projectile with the largest contact area, in which what happens is that the detached area of the leading edge is pushed up.

On the other hand, analyzing the behavior of the velocity of the projectile, it can be observed that the residual velocity (69 m/s) is substantially higher than that resulting from the reference simulation.

As will be seen when analyzing the energies involved, this is due to the reduced ability of the leading edge to dissipate energy through plastic deformation.

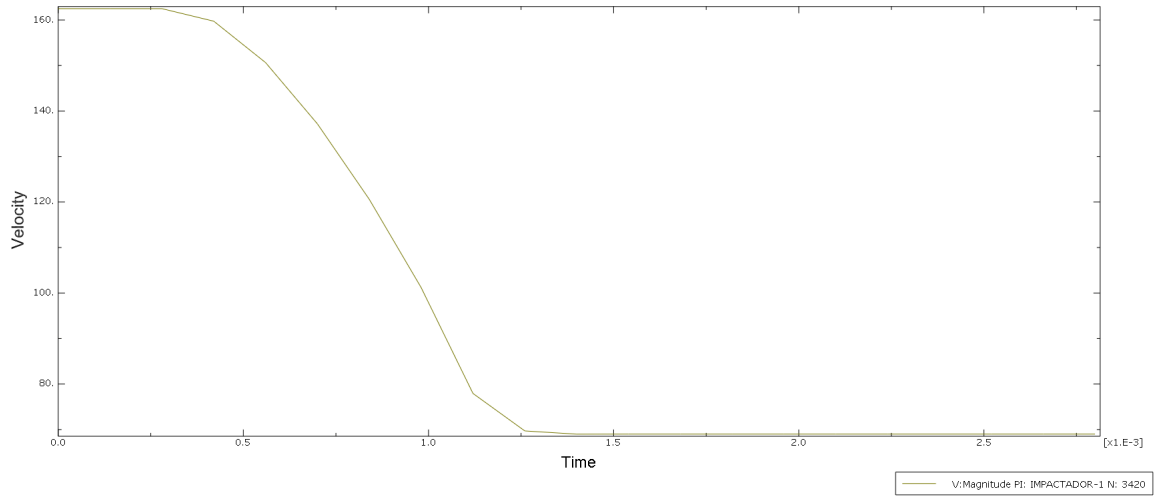

Figure 5.19: Less Surface Simulation: Velocity Evolution

If we analyze Thor's equation for the residual velocity and keep constant the parameters that have not changed between the simulations, the following equation is obtained:

$$V_r = V_i - C_1 (tA)^{\alpha} V_i^{\lambda} \tag{5.5}$$

Analyzing the equation, if the initial velocity remains constant but the contact area is decreased, the residual velocity should increase, which corresponds to the results obtained in the simulation.

On the other hand, by analyzing the energies involved in the process, certain variations can be highlighted compared to their behavior in the reference simulation.

As previously mentioned, the kinetic energy is not completely dissipated, but after impact, it gradually decreases until it completely passes through the leading edge and remains constant at a value of approximately 1300 Joules, which corresponds to a residual velocity of 69 m/s.

As can be seen, the predominant energy dissipation is produced by plastic deformation, although in this case, its influence is less than in the reference simulation.

Finally, note that because the leading edge breakage is produced in a different way, the discontinuity observed in the reference simulation does not occur when the contact area decreases.

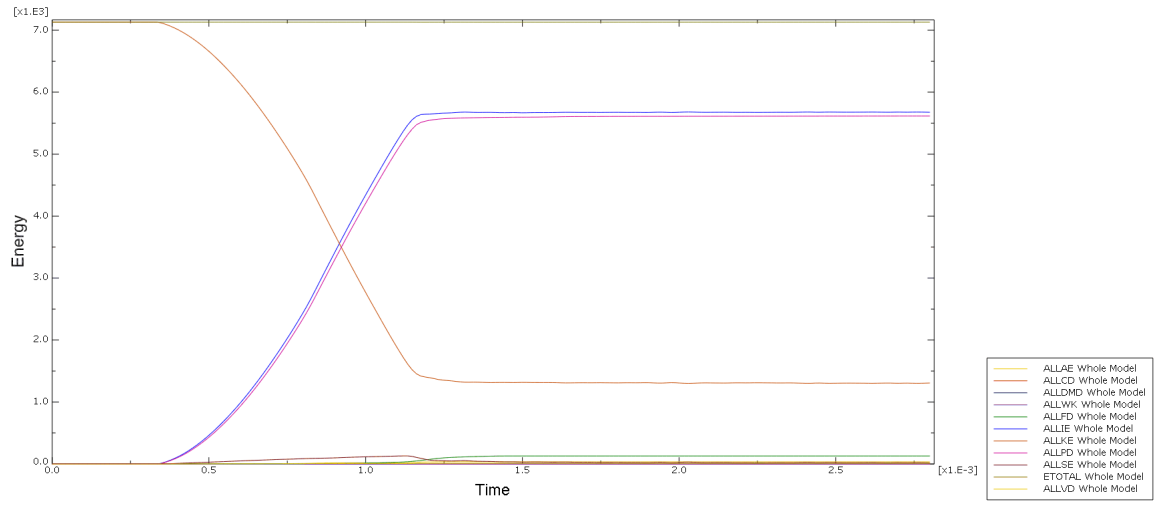

Figure 5.20: Less Surface Simulation: Energy Evolution

Once the behavior of the impact has been analyzed for a reduced surface of the projectile, an iterative process identical to the one done in section 4.6 is carried out to obtain the ballistic limit velocity with this projectile. The values obtained during the iteration are collected in the following table:

Sim Number	Initial Speed [m/s]	Break Through	Residual Speed [m/s]
1	162.5	Yes	68.999
2	120	No	-
3	130	No	-
4	140	No	-
5	150	Yes	43.469
6	145	No	-
7	147.5	No	-
8	148.5	No	-
9	149	No	-
10	149.5	Yes	41.763
11	149.2	Yes	40.288
11	149.1	No	-
12	149.12	Yes	37.886

Table 5.3: Lower Surface Balistic Limit Iterations.

As can be seen after analyzing the iterative process carried out, it can be concluded that the ballistic speed using the projectile with the reduced surface area is between 149.1 and 149.12 m/s. However, the resulting residual velocity after impact at 149.12 m/s is too high (37.9 m/s).

The specific value of the ballistic velocity is not so relevant, rather what is important is that it is verified through simulation that a reduction in the contact surface, keeping the other parameters fixed, implies a reduction in the ballistic velocity.

5.3.2. Changes in Geometry

In this subsection it is analyzed how the variation of the geometry affects the ballistic velocity. For this study, two geometries have been developed whose contact surface at the moment of impact differs greatly from the contact surface of the spherical projectile. In the first place, a cylindrical model has been made with the same diameter as that of the spherical projectile, despite having the same contact surface, in this case, since the surface of the cylinder is flat, the speed with which the contact surface increases is much greater than with the spherical projectile.

On the other hand, a conical projectile has been modeled that behaves in the opposite way to the cylinder, the impact surface is very small at the beginning and increases progressively but slower than the sphere.

Starting with the cylindrical projectile, it can be seen how, due to the increase in the initial contact surface, for the speed established as the ballistic limit of the spherical projectile, this one is not able to pass through the leading edge.

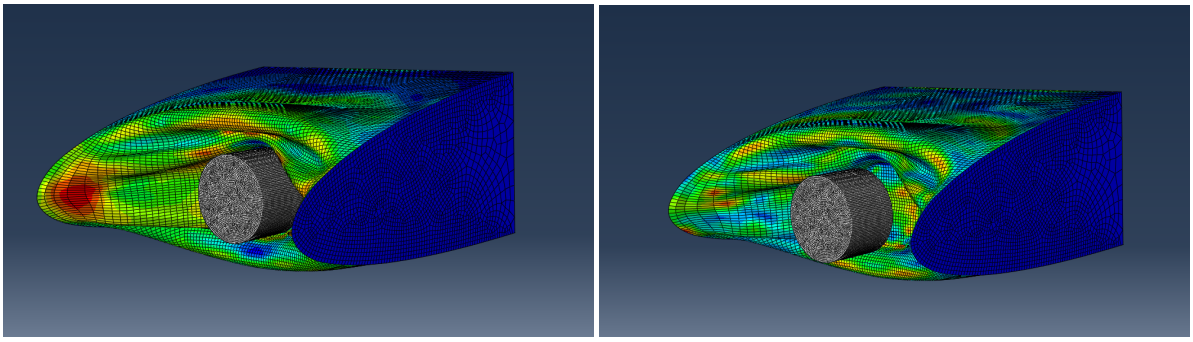

(a) t=1.4ms (b) t=2.8ms

Figure 5.21: Cylindrical Impactor Reference Simulation

Analyzing the graph of the velocity of the projectile (5.22), several differences can be observed compared to the reference simulation:

- First of all, as already mentioned above, it is appreciated that the projectile is not capable of trespassing the leading edge. The speed becomes zero (around 1.26 ms). At which point the projectile bounces, its speed increases again and remains constant at a value of 18.8 m/s, more or less double than in the sphere case. This means that the relation between elastic and plastic deformation is bigger in the case of the cylinder than in the sphere.
- On the other hand, a greater downward slope can be seen in the graph, that is, the projectile loses speed faster than the spherical projectile. This effect occurs due to the increase in contact surface from the instant of impact compared to the spherical projectile.

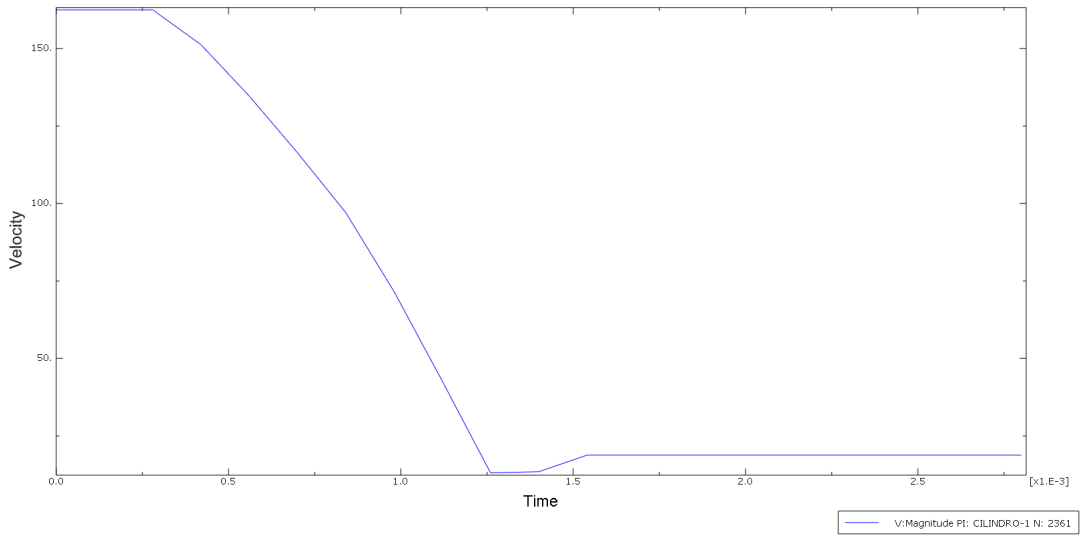

Figure 5.22: Cylindrical Impactor: Speed Evolution

Analyzing the energies involved in the process, a behavior very similar to the one in the reference simulation with the spherical projectile can be observed. As can be seen in the lower graph, the discontinuity that occurs with the spherical projectile does not occur. This is because in this simulation, the leading edge material does not break through itself.

As in the model with the spherical projectile, the predominant energies are the kinetic energy and the energy dissipated by plastic deformation and they behave practically identically except for the increase in slope.

It can also be seen that, as no discontinuity occurs, the total energy remains constant.

Analyzing the behavior of the leading edge against impact, it can be observed how the lower and upper

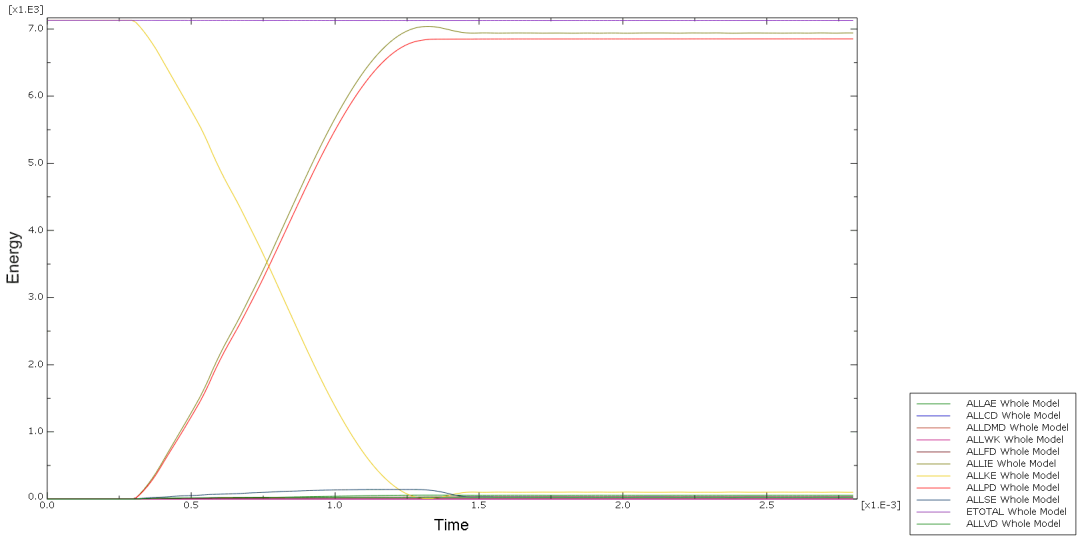

Figure 5.23: Cylindrical Impactor: Energy Evolution

surfaces deform more than in the spherical model and how the impact zone does not present any type of break.

Analyzing Thor's equation, it must be taken into account that the tests were carried out by impacting a flat face of a cylinder or cube against a flat plate, so the variation of the contact surface with time is not represented. Despite the fact that the spherical and cylindrical projectile have the same diameter, the contact surface in the sphere grows progressively while in the cylinder the speed with which the contact surface increases is much greater than with the spherical projectile. That is, guided by the Thor equations, the increase in the contact area translates into a reduction in the residual velocity after traversing, or in this case, even preventing the penetration of the material. That is, the ballistic limit velocity is higher.

To verify that the results agree with the above, following the same iteration process as in section **4.X**, the ballistic velocity can be obtained using the cylindrical projectile. As can be seen in the table that includes the different values, the ballistic limit is 174.5 m/s, that is, 12 m/s greater than in the reference simulation.

Sim Number	Initial Speed [m/s]	Break Through	Residual Speed [m/s]
1	162.5	No	-
2	170	No	-
3	180	Yes	40.564
4	175	Yes	18.839
5	172.5	No	-
6	173	No	-
7	174	No	-
8	174.5	Yes	9.601

Table 5.4: Cylindrical Projectile Balistic Limit Iterations.

Analyzing the behavior of the model for a velocity equal to its ballistic limit, it can be observed that, in this case, the leading edge rupture begins in the upper area of the impact, the fracture extends to the sides and finally the projectile passes through, pushing the lower edge towards the lower surface of the airfoil.

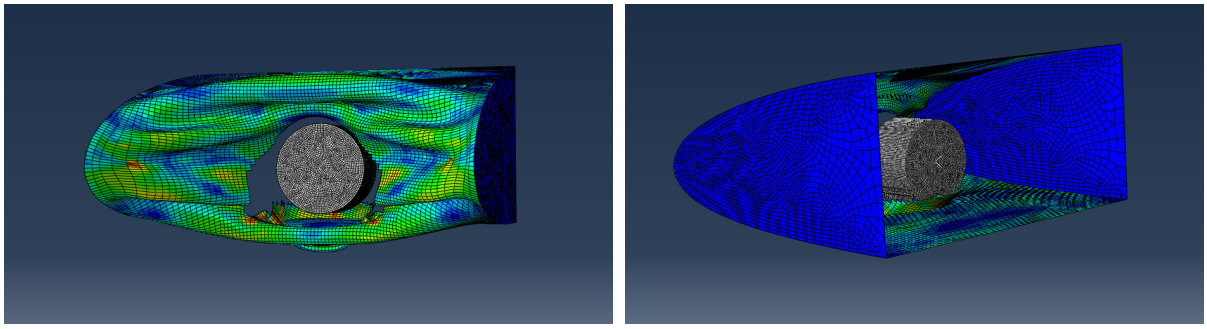

Figure 5.24: Cylindrical Impactor Balistic Limit Simulation

Observing the behavior of the velocity during the impact for a velocity close to the ballistic limit, a behavior similar to that observed in the reference simulation can be seen, differing in that the slope of the velocity curve is more pronounced from the beginning of the impact, mainly due to to increase the initial contact surface.

As can be seen, the resulting residual velocity is approximately 9 m/s, a much lower value than the initial 174.5 m/s, which is why 174.5 m/s has been considered an acceptable value to be considered as a ballistic limit velocity. If the iteration were continued, it would be obtained that the real ballistic velocity is between 174 and 174.5 m/s.

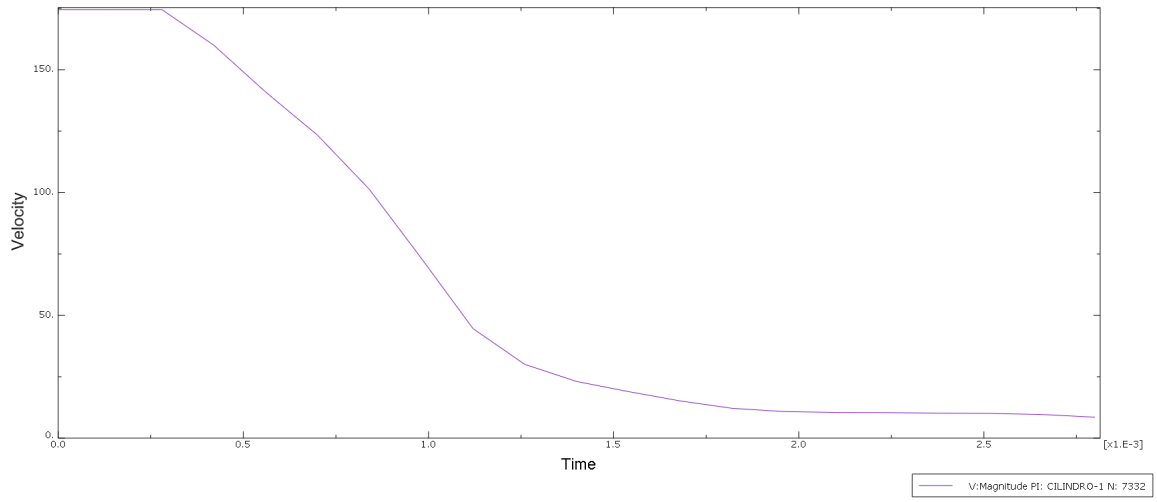

Figure 5.25: Cylindrical Impactor Ballistic Limit: Velocity Evolution

Lastly, looking at the evolution of the different energies involved in the impact, it can be observed that, as is logical, the increase in the initial speed leads to an increase in the kinetic energy before the impact. In the same way that occurs in the curve of speed versus time, in the kinetic energy and in the dissipation due to plastic deformation an increase in the absolute value of the slope is observed from the beginning of the impact compared to the reference simulation.

It can also be seen that due to the fact that the breaking mode of the leading edge is different than in the simulation with a spherical projectile, the discontinuity in the energies no longer occurs, but rather the total energy remains constant.

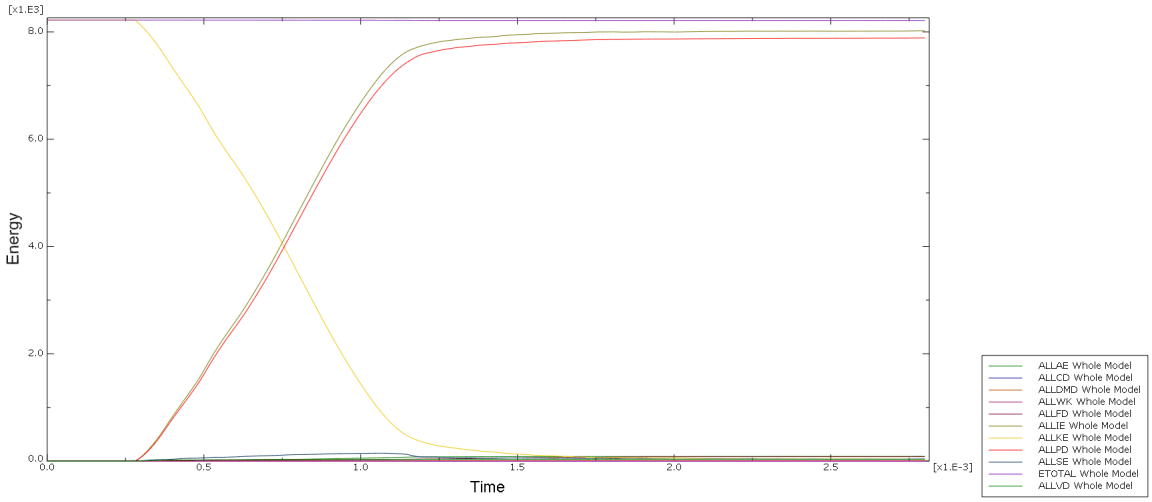

Figure 5.26: Cylindrical Impactor Ballistic Limit: Energy Evolution

Analyzing the behavior using a model identical to the one used in the reference simulation and only varying the geometry of the projectile, the following results are obtained:

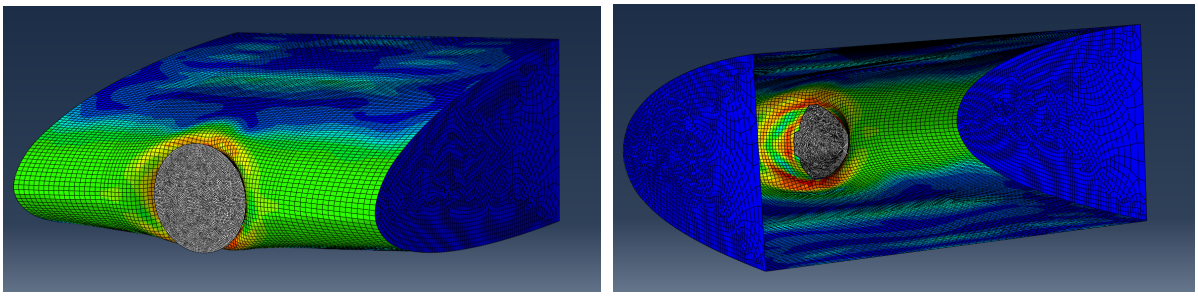

Figure 5.27: Conical Impactor Reference Simulation 0.7ms

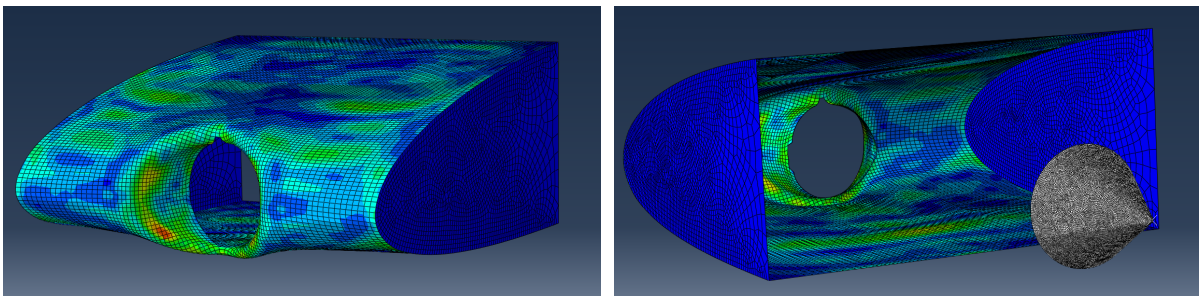

Figure 5.28: Conical Impactor Reference Simulation 2.66ms

First of all, as can be seen in the previous images (5.27 and 5.28), the way the projectile passes through the leading edge is completely different from what happens with both previous projectiles. The deformation that occurs is much smaller and is concentrated around the impact zone. On the other hand, since the cone initially hits a small surface, the break occurs at the point of contact and grows as the projectile passes through the break.

Analyzing the variation in velocity, using for the ballistic velocity of the spherical projectile, in this case, the velocity is barely reduced by 15 m/s (dropping from 162.5 m/s to 147.3 m/s 5.29). Analyzing these results and comparing them with Thor's equations, we can affirm that they are consistent and behave contrary to the case of the cylindrical projectile. In this case, the initial contact surface is very small and grows as the projectile passes through the material. By simplifying this behavior so that it is consistent

with Thor's equations, the contact surface between projectile and leading edge it decreases compared to the surface considered as reference (model with spherical impactor), that is, the residual velocity will be higher and with the definition of ballistic limit exposed in chapter 2, it will be lower.

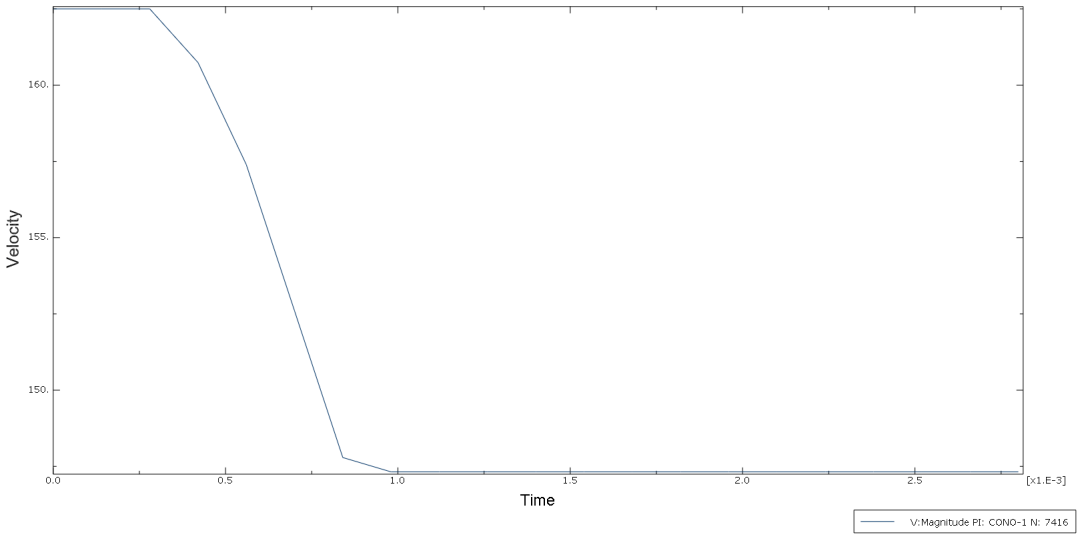

Figure 5.29: Conical Impactor: Velocity Evolution

Analyzing the behavior of the energies involved in the impact, notable differences can be observed when comparing them with the reference simulation with the spherical projectile. In this case, the kinetic energy and the dissipation due to plastic deformation continue to predominate, however, the dissipation that occurs is much smaller and is not capable of absorbing the majority of the kinetic energy of the projectile, which is why the projectile hardly lose speed.

Analyzing the influence of the other energies involved, although its effect is still one order of magnitude smaller than the two previously mentioned, a comparatively greater influence of energy dissipation due to friction can be seen. This is mainly due to the increase in the surface area of the projectile that is in tangential contact with the leading edge.

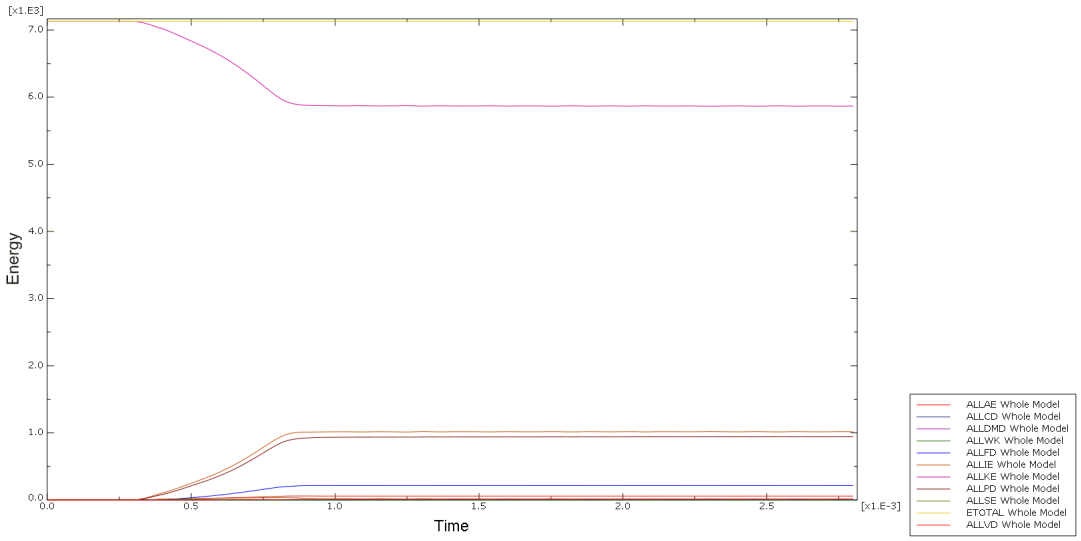

Figure 5.30: Conical Impactor: Energy Evolution

Once the behavior of the model for the reference velocity has been analyzed, the process to obtain the ballistic limit velocity for the case of the conical projectile has being carried out. As previously stated, the ballistic limit speed will be lower than in the reference simulation. The process followed and the ballistic limit velocity obtained are shown in the following table (5.5):

Sim Number	Initial Speed [m/s]	Break Through	Residual Speed [m/s]
1	162.5	Yes	133.781
2	120	Yes	99.545
3	100	Yes	74.828
4	70	Yes	25.386
5	40	No	-
6	50	No	-
7	55	No	-
8	60	No	-
9	65	No	-
10	67	Yes	15.408
11	66	Yes	11.561
12	65.5	Yes	6.463

Table 5.5: Conical Projectile Balistic Limit Iterations.

After carrying out the iterative process, it has been found that the ballistic velocity for the case of the conical projectile is approximately 65.5 m/s, that is, about 100 m/s smaller than that obtained in the reference simulation.

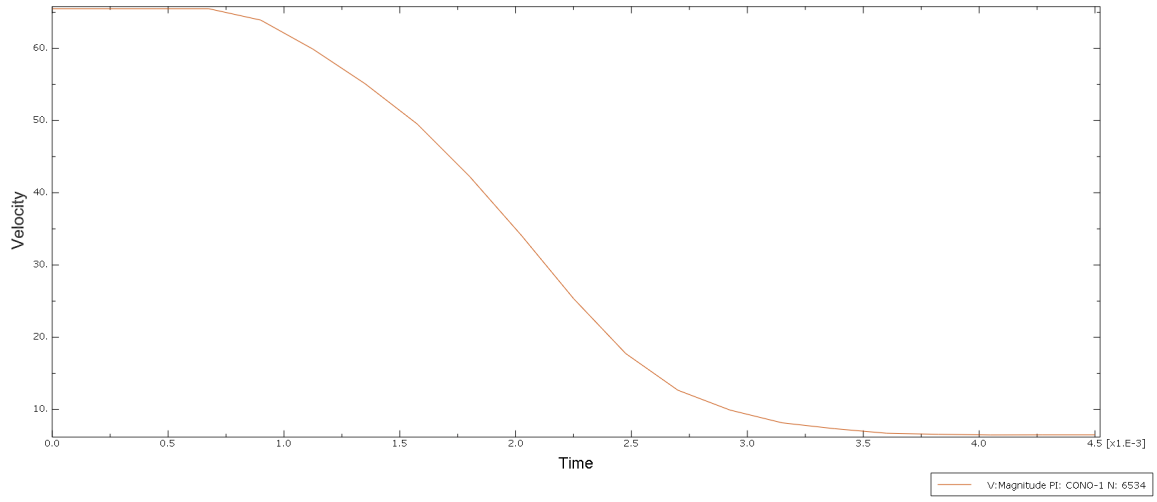

Figure 5.31: Conical Impactor Ballistic Limit: Velocity Evolution

As previously stated, the conical projectile has a smaller contact area, especially at the beginning of the impact, so that the leading edge material breaks more easily and can absorb less kinetic energy from the projectile.

Analyzing the behavior of the energies involved when the velocity is equal to the ballistic velocity, it can be observed that, due to the drop in ballistic velocity, the kinetic energy at the beginning of the simulation has decreased considerably.

In this case, contrary to other models, the internal energy of the complete model is not equal to the initial kinetic energy after impact, since the energy dissipated by friction greatly influences the energy dissipation of the projectile (200 J dissipated by friction against the 800 J approx dissipated by plastic deformation 5.32).

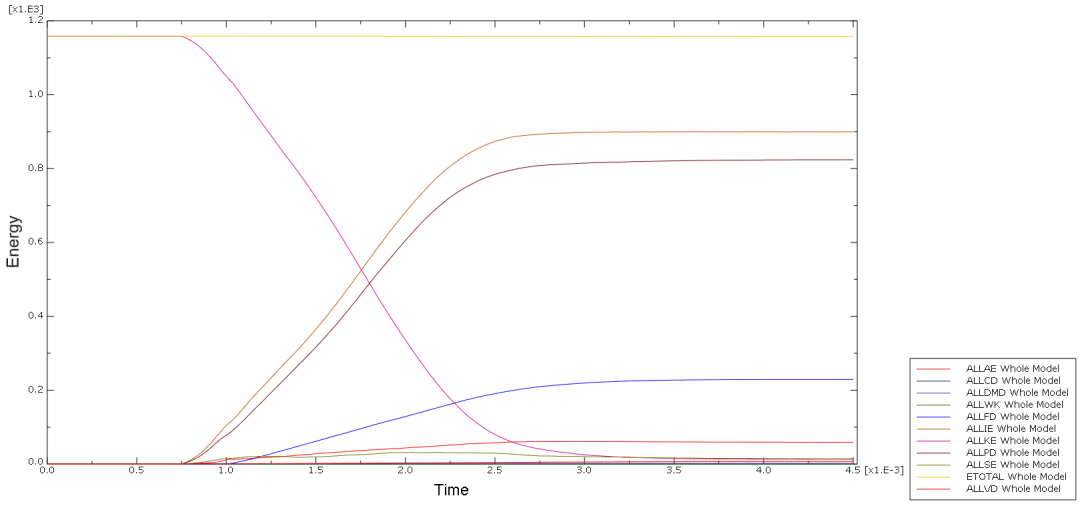

Figure 5.32: Conical Impactor: Balstic Limit Energy Evolution

5.4. Ballistic Protection Improvements

In this last section, the possibility of increasing the ballistic protection of the leading edge against a projectile is studied.

First of all, to improve ballistic protection it is necessary to reinforce the area of the leading edge where the impact occurs. To carry out this reinforcement, different actions can be done, such as changing the material of the leading edge to one with bigger yield strength, increasing the thickness of that area or placing a reinforcement such as a rib.

The influence of the thickness of the leading edge on the ballistic velocity is going to be studied. For this, a model identical to the reference simulation has been carried out, in which only the thickness of the leading edge has been varied, increasing it by 10%.

To analyze the variation of the ballistic velocity, the same iterative process performed in previous sections and shown in the following table (5.6 is carried out:

Sim Number	Initial Speed [m/s]	Break Through	Residual Speed [m/s]
1	162.5	No	-
2	165	No	-
3	170	No	-
4	175	No	-
5	180	Yes	11.827
6	178	No	-
7	179	Yes	2.213

Table 5.6: Increased Thickness Balistic Limit Iterations.

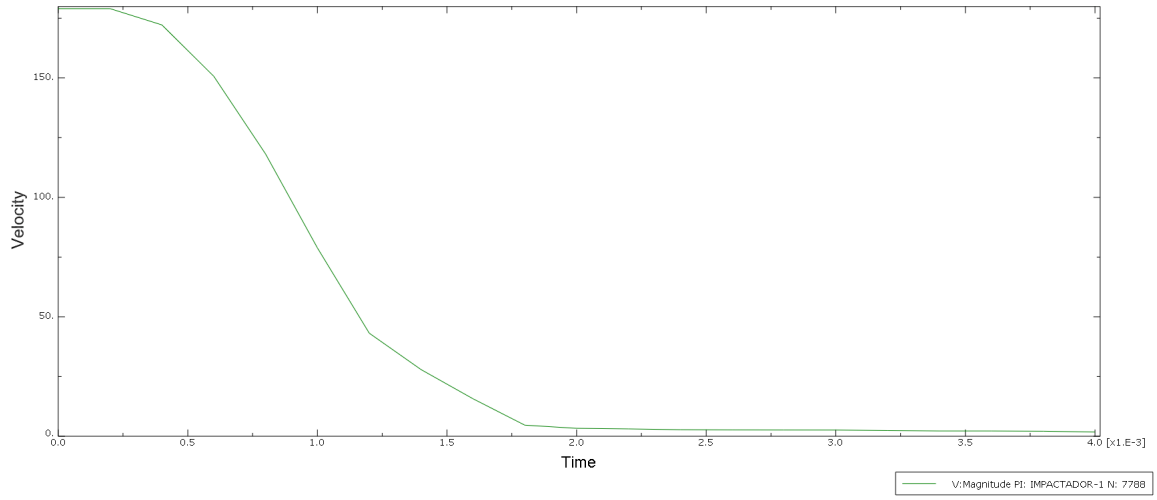

Figure 5.33: Increased Thickness: Velocity Evolution

As can be seen once the iterations carried out, the ballistic speed of the model when increasing the thickness by 10% increases up to 179 m/s. Analyzing the previously mentioned Thor equation 2.9 and assuming constant all the parameters except the thickness, we obtain the following equation:

$$V_0 = 10^{c1} (t)^{\alpha 1} C \tag{5.6}$$

From this equation it can be seen that as the thickness increases, the ballistic limit velocity also increases. In this specific case, the ballistic velocity has increased by 10.15% by increasing the thickness by 10%, so through the simulations we can obtain an approximation of the constant gamma1, which will have a value of 1.0146.

Finally, analyzing the energies involved, it can be seen that the discontinuity reappears again since the model is practically identical to the reference one (5.1).

Due to the increase in the flight speed of the projectile, there is an increase in the initial kinetic energy that gradually decreases until it is practically null after crossing the leading edge. This greater capacity to dissipate kinetic energy is mainly due to the increase in energy dissipated through plastic deformation due to the increase in thickness.

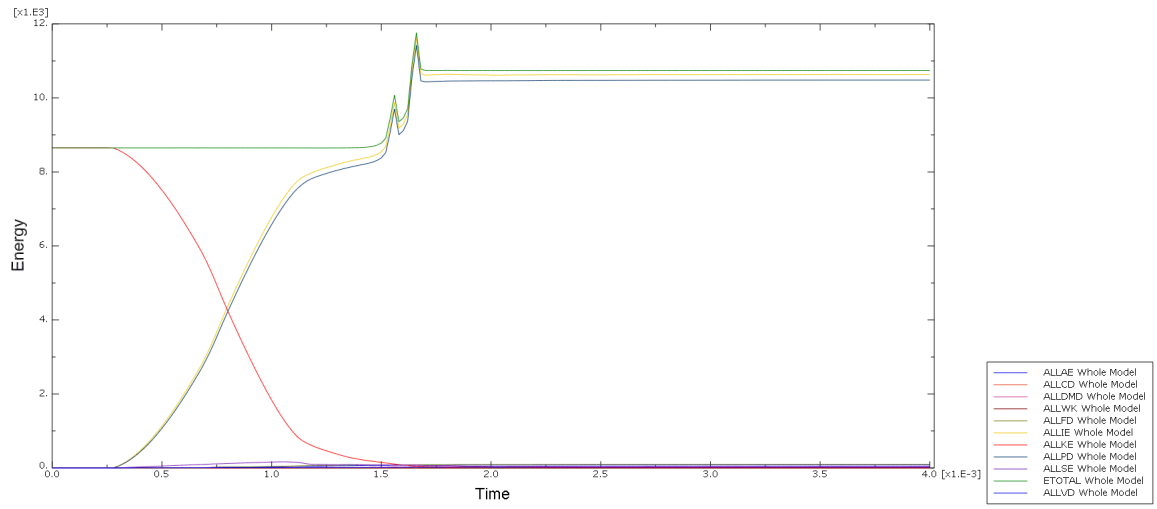

Figure 5.34: Increased Thickness: Energy Evolution

6

Conclussions and Future

The results obtained within the previous chapters are analysed and summarised in this one and a series of conclusions are shown, as well as a proposal for future steps that could be followed to advance and get deeper in this project.

First of all, it should be noted that when carrying out the mesh convergence process, an unexpected behavior has been observed in the results.

In general, experience with finite element models tells us that when refining the mesh of a structure, the stress peaks in the material tend to increase. In the specific case of a high velocity impact, this would result in an increase in the residual velocity of the projectile because the first material failure occurs before.

During the mesh convergence process performed, it was observed that the residual velocity of the projectile decreased as the mesh was refined, in the opposite way to the expected behaviour. This is because by reducing the size of the mesh, from certain size on, the criteria for damage and breakage of the material must also be adjusted. In order to carry out this process correctly, the results of a simpler simulation must be correlated with those obtained from tests with test samples, an aspect that is outside the scope of this project.

On the other hand, identical models have been made with the only difference that a self-contact parameter has been introduced in one of them. That is, a parameter that prevents the leading edge elements from interpenetrating with other elements of the same surface. Comparing the results obtained from both simulations, it has been observed that for a ballistic velocity difference of 162.5 to 161.5 m/s, that is, a variation of 0.6%, the simulation time has been multiplied by more than three.

Therefore, When studying the implementation of the self-contact parameter in the model, in view of the previous results, low influence and high computational cost, the decision taken was to proceed with the model without self-contact parameter.

Analyzing the results obtained, it can be seen that although Thor's equation does not accurately predict the numerical results of different type of projectiles on a surface that is not flat, it does reproduce the behavior in a similar way when initial parameters are modified.

As a summary we can observe that the ballistic limit velocity varies proportionally to the thickness and the speed of the contact area variation.

As mentioned in the previous paragraph, it is important to note that although Thor's equations did not take into account since the impact occurred between two flat surfaces, a very important parameter is the variation of the contact surface since a small initial contact surface generates a zone of concentrated efforts that favors the breakage of this zone beforehand. This is why a conical-shaped projectile has a much lower ballistic velocity than a projectile with a blunt impact face. In other words, if you want to stop a target use an as plain as possible bullet, but if you want to penetrate it, use a sharp one.

In the impact process, a series of energies are involved that have to be balanced. In the initial state, the energy is provided by the speed of the impacting projectile, that is, its kinetic energy. This kinetic

energy is transformed into others that are: the energy of deformation and breakage of the material, the residual kinetic energy of the projectile and the energy dissipated by friction and thermally.

Actually, in the case at hand, in which the residual kinetic energy of the projectile has to be minimized, the only two relevant energies are the initial kinetic energy of the projectile and the deformation and breakage of the material, the other ones are two or three orders of magnitude smaller (see Fig. 5.4). The only exception is the frictional energy during the impact of the conical projectile which is an order of magnitude higher than for the other projectiles, but in any case, much smaller than the principal energies (see Fig. 5.32).

6.1. Future Steps

The next steps to complete the full validation of the model will be the following:

First of all, a more powerful computer or a cluster should be used to be able to design more complex simulations that are more similar to real life situations.

In order to correctly model the behavior of the material used and the influence of the mesh, it will be necessary to carry out a series of tests with small specimens of that material.

Finally, after having carried out the previous steps and a satisfactory simulation, it will be necessary to perform a real impact test. For this, a leading edge of the selected material will be manufactured and placed on a rig. By means of a cannon, for example compressed air one, the projectile will be launched at ballistic speed and the behavior of the leading edge will be observed when impacted.

As previously mentioned, the ballistic velocity that has been defined for the simulation is not exactly the one that is defined in a real test. This is why a test must be carried out to obtain the V50 speed and it will be compared with that obtained in the simulation.

Appendix1: Model Creation

In this chapter it will be shown step by step how the simulation has been built, following the same order as the workflow in Abaqus.

6.2. Part

In this first section, the process followed for impactors and airfoil creation is shown:

Beginning with the airfoil, a 3D deformable solid is defined based on extrusion of the airfoil section. After defining the solid properties, using the equations (2.4) and selecting an array of points along the x axis between 0 and 1 meter, the values for the upper and lower surface points shown in the table below are obtained. This points, then, are introduced in the *Section Sketch* using the function *Create Isolated Point* and adding each point's x and y coordinates, being x the position in the x axis and y the height of the upper or lower surfaces.

Position in X axis [m]	Upper surface [m]	Lower Surface [m]
0.00000	0.00000	0.00000
0.01402	0.01694	-0.01448
0.02703	0.02411	-0.01927
0.05258	0.03420	-0.02482
0.07783	0.04169	-0.02809
0.10290	0.04766	-0.03016
0.15278	0.05665	-0.03227
0.20239	0.06276	-0.03276
0.25186	0.06668	-0.03230
0.30125	0.06875	-0.03125
0.40000	0.06837	-0.02837
0.49951	0.06356	-0.02468
0.59915	0.05580	-0.02024
0.69898	0.04551	-0.01551
0.79903	0.03296	-0.01074
0.89933	0.01816	-0.00594
0.94959	0.00990	-0.00352
1.00000	0.00105	-0.00105

Table 6.1: NACA 2410 point distribution

As it is shown in the table above, the upper and lower surfaces do not meet at the same point in the trailing edge of the airfoil. In order to create a solid body it is necessary that the section is not open. Knowing that the trailing edge of the airfoil is not really relevant for the study, it is closed with a vertical line that connects the lasts points of the upper and lower surfaces.

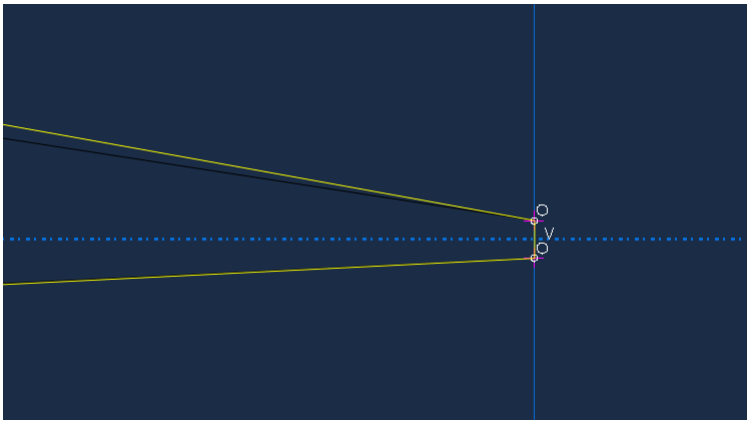

Figure 6.1: Closed Trailing Edge

The *Create Spline: Thru Points* function is used to connect the rest of the points in order to conform the airfoil section, as can be seen in the image below.

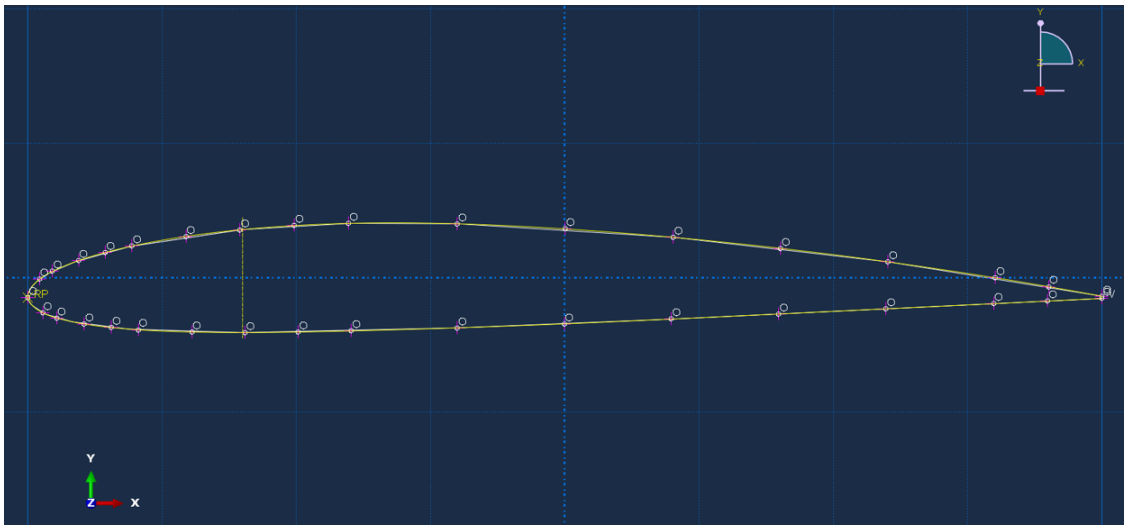

Figure 6.2: Airfoil Section in Design

Once the airfoil section is created in the sketch, it is time to create the extrude characteristics. In this case, the final geometry is a 20 cm blind extrude with no twist or draft angle in the z plane. The final geometry can be seen in the image below.

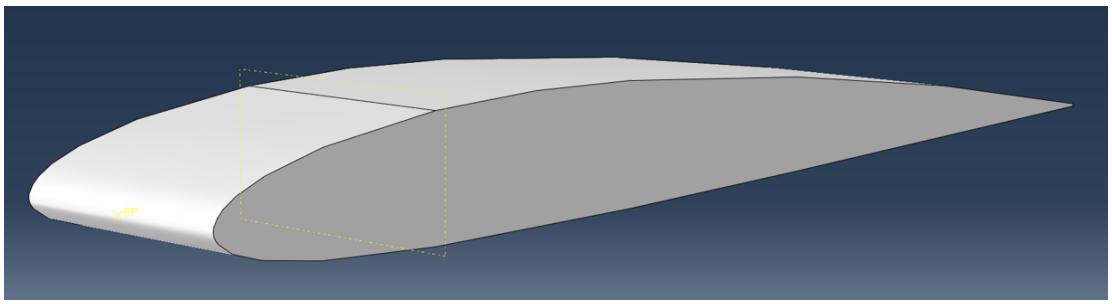

Figure 6.3: Airfoil Model

Looking at the airfoil created in the previous steps, it is obvious that the model does not correspond to the reality: the airfoils used in aviation are hollow, not solid. In order to solve this, the function *Create Shell: From Solid*, which transforms a solid into a shell-type object, is used in the whole airfoil.

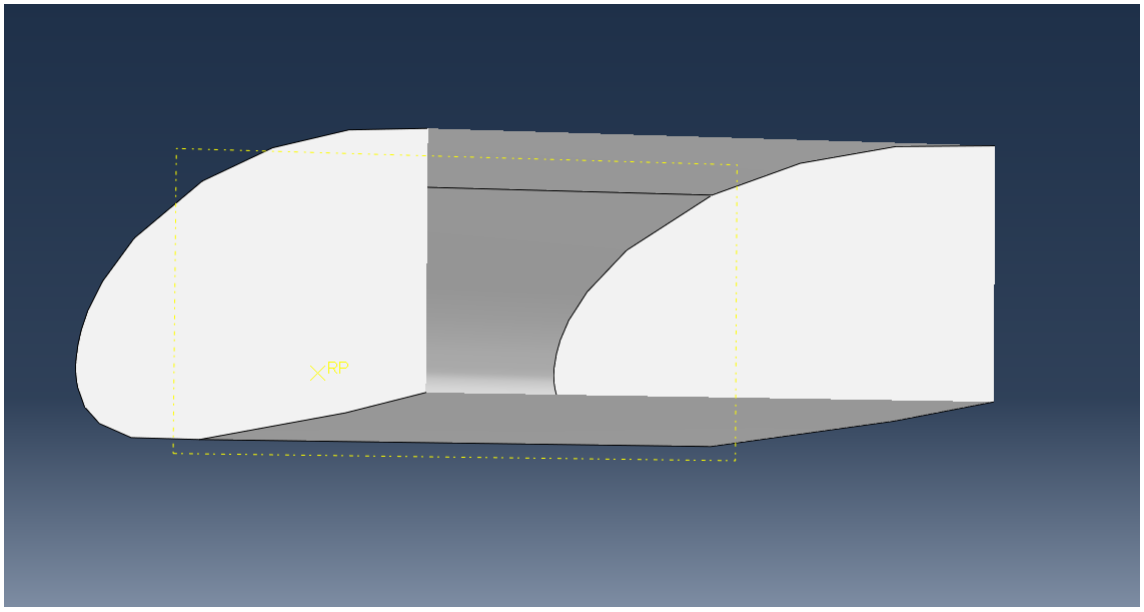

Figure 6.4: Airfoil Shell from Solid

The last two steps to create the airfoil are intended to facilitate the construction of the model and the mesh optimization.

In the first place, to facilitate the construction of the model, a Reference Point (shown as RP in the Abaqus CAE) is created, this point is used as a reference in the assembly of the whole model. In this case, the Reference Point is created in the middle of the airfoil frontal section located in global coordinates (0, 0, 0.1).

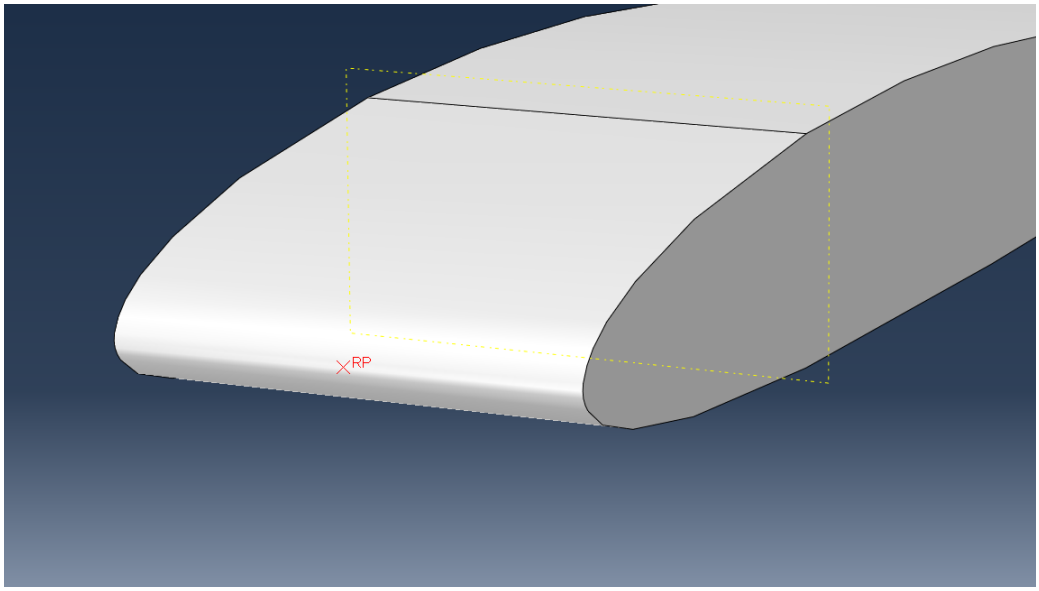

Figure 6.5: Airfoil Reference Point

Knowing that the impact will be happening in the leading edge of the airfoil, the mesh should be smaller in that section than in the rest of the airfoil. In order to be able to achieve this, the upper and lower surfaces of the airfoil are divided into two parts. To partition each of the faces, the function *Partition Face: Use Datum Plane* is used, so, a datum plane is needed. A datum plane is a geometrical tool with no mechanical functions used for references or section operations for example. The datum plane is created using the function *Create Datum Plane: Offset from Principal Plane* parallel to the YZ plane with an offset of 20 cm from the reference point. After the datum plane is created, the partitions in the upper and lower surfaces are created using the above mentioned datum plane.

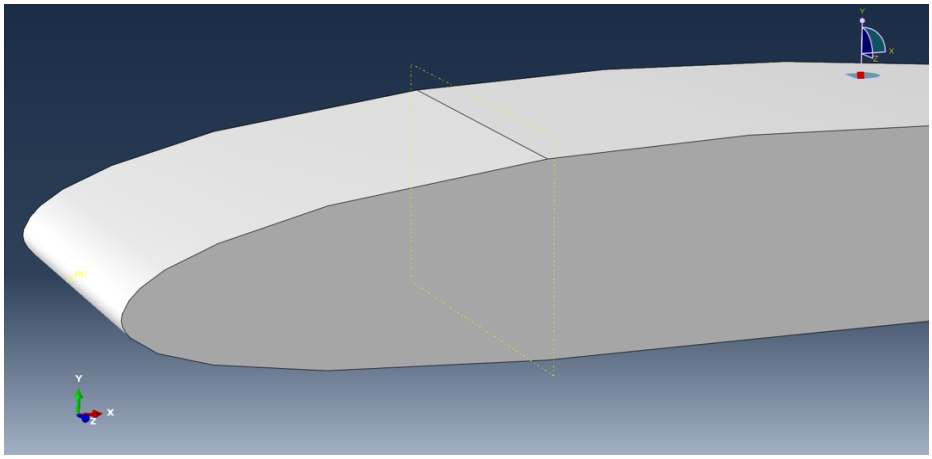

Figure 6.6: Datum Plane Division

After carrying out a series of initial simulations, it has been observed that the trailing edge of the airfoil has no influence on what is to be calculated. This is why it has been decided to cut the airfoil and use in the model only the part corresponding to the leading edge. For this, the *Datum Plane* created previously, has been used.

Identical to the process followed for partitioning the upper and lower faces, the partitioning of the lateral faces is carried out. Once done, using the *Remove Faces* option removes the rear partition of the top, bottom and side faces, as well as the vertical surface created to close the airfoil.

Once this process is done, the impact geometry consists only of the leading edge of the airfoil.

On the other hand, in order to make a more refined mesh in the area where the impact occurs, two *Datum Planes* perpendicular to the previous one have been created, located 5mm on the Z axis on both sides of the *Reference Point*.

The final geometry of the leading edge is shown in the following illustration:

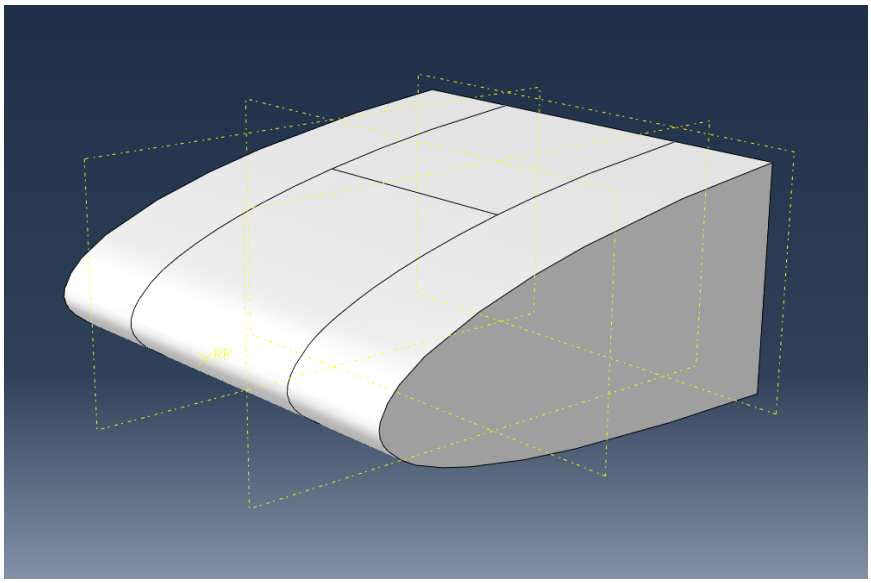

Figure 6.7: Leading Edge Final Geometry

The impactor is created as a discrete rigid solid based on revolution of different shapes. The first impactor tested is a 5.1 cm diameter sphere created using a circular section and applying a 180º revolution. In a similar way to the procedure followed to establish the reference point on the leading edge, one is placed on the outside of the sphere that marks the point of impact and that facilitates the placement of the model in the assembly.

The sketch and the geometry of revolution of the spherical projectile are shown in the following illustrations:

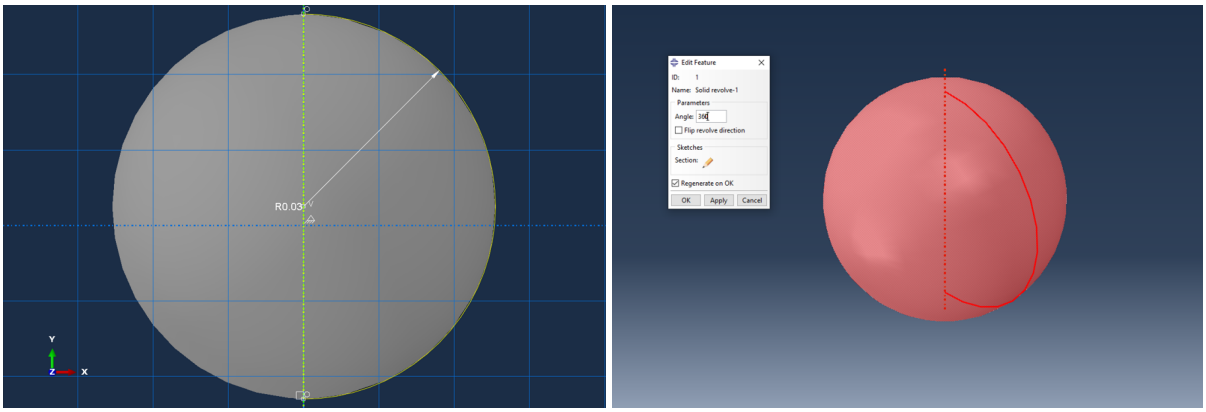

(a) Spherical Impactor Sketch (b) Spherical Impactor Revolve

Figure 6.8: Spherical Impactor Model

In order to analyze the influence that the variation of the contact surface has on the ballistic limit velocity and on the residual velocity, two more projectiles with different geometries have been modelled.

First, a cylindrical projectile has been designed, created by extruding a circle with an identical diameter to the sphere. The extrusion has been carried out with a depth of 3.4 cm so that the volume of the cylinder is the same as that of the sphere.

The reference point of the cylindrical projectile is located in the center of the base that comes into contact with the profile.

The model used for the cylindrical projectile is shown in the following illustration:

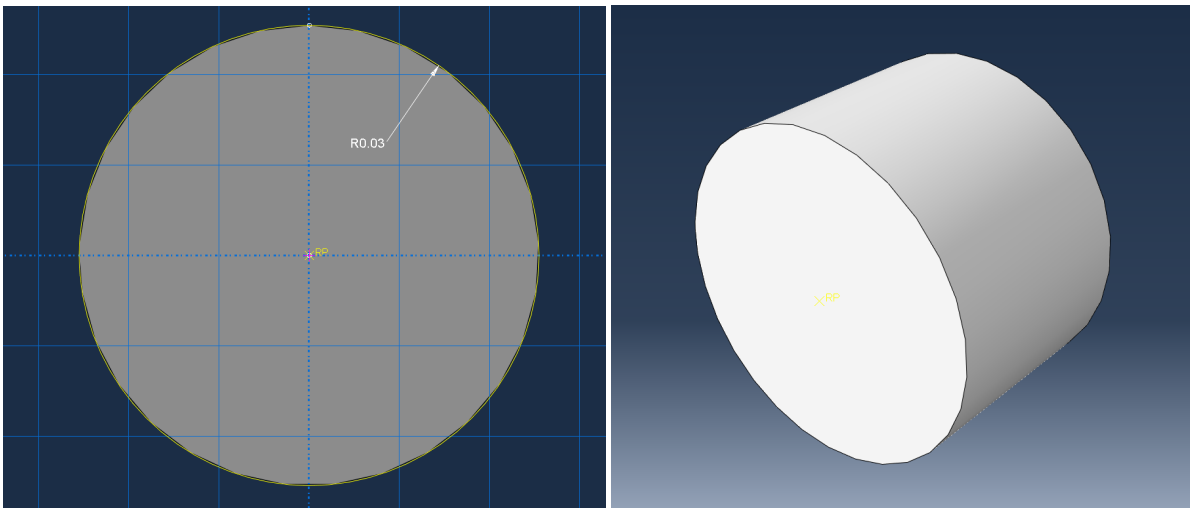

(a) Cylindrical Impactor Sketch (b) Cylindrical Impactor Extrude

Figure 6.9: Cylindrical Impactor Model

On the other hand, a conical projectile has been made, modeled as the revolution of a right angle triangle whose base measures 2.55 cm, that is, the same as the radius of the spherical projectile and its height is twice that of the base so that the angle formed at the vertex opposite the base is 30º. The generating triangle and the model of the cone are shown in the following illustrations:

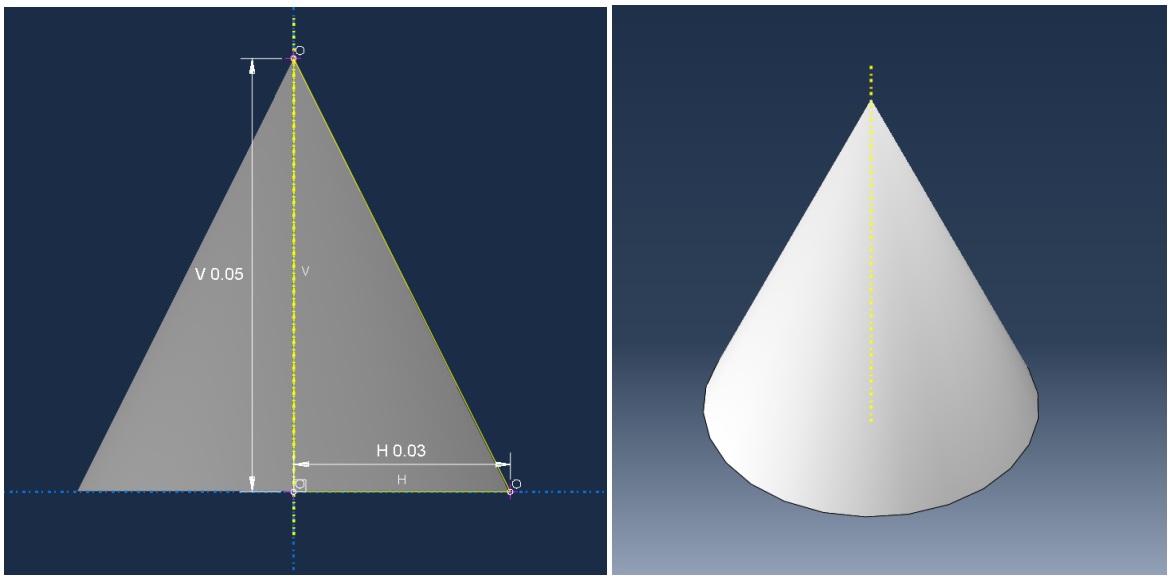

(a) Conical Impactor Sketch (b) Conical Impactor Revolve

Figure 6.10: Conical Impactor Model

As can be seen in the following illustration, when meshing the conical projectile, the elements of the tip exhibit excessive distortion. This is because the mesh elements are not able to adapt to the vertex of the cone.

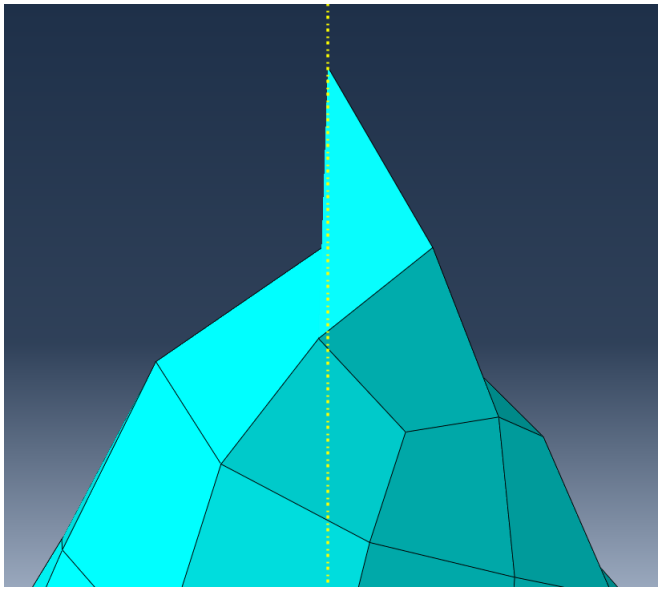

Figure 6.11: Element Excessive Distorsion

To solve this problem it has been decided to cut the tip of the projectile. In the sketch made previously, a line has been created parallel to the base 1 mm from the tip of the projectile and the area above it has been erased (see image 6.10a). With this sketch, the same procedure is carried out to generate the cone per revolution and once the projectile is obtained, the reference point is assigned in the center of the upper face of the projectile.

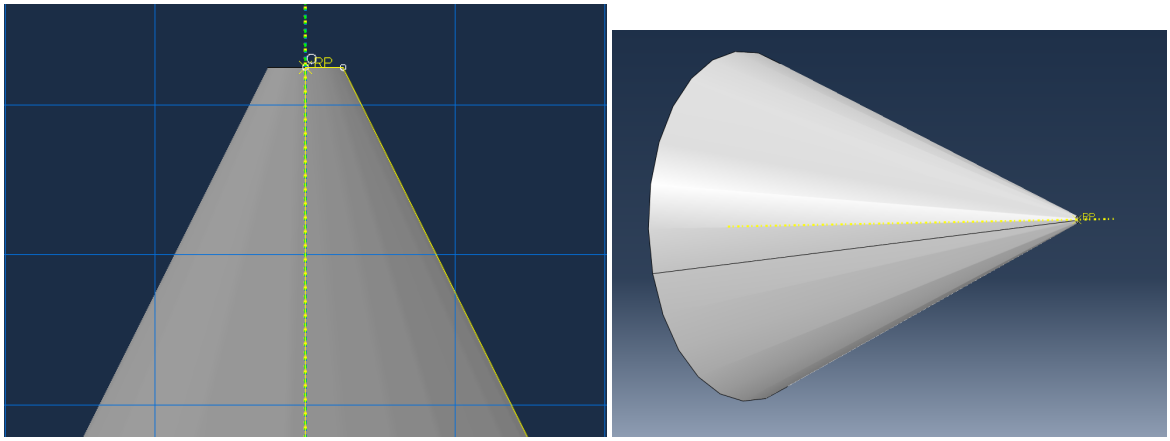

(a) Conical Impactor Sketch Detail (b) Conical Impactor

Figure 6.12: Conical Impactor Model

Although the impactor is created as a solid rigid body, when trying to include it in the assemble, Abaqus shows the following error. In order for the impactor to be included in the assembly, it must be converted to a shell body using the *Create Shell: from Solid* explained above.

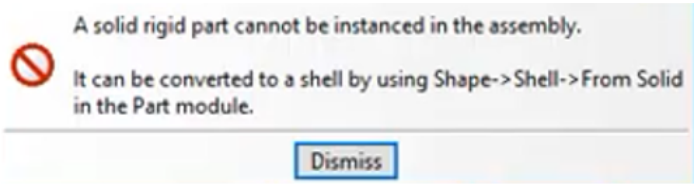

Figure 6.13: Solid in assembly error

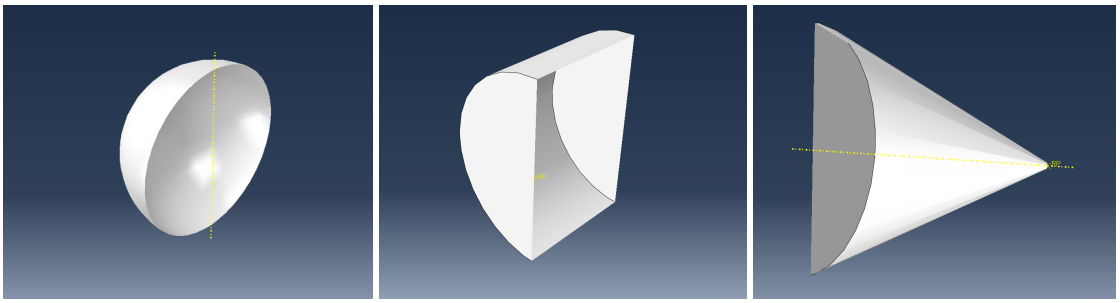

(a) Spherical Impactor in Shell type (b) Cylindrical Impactor in Shell type (c) Conical Impactor in Shell type

Figure 6.14: Shell Impactor Models

The last step in the impactor definition is the addition of the mass using inertia. Inertias can be added selecting *Engineering Features* in the display tree of each part located in the left hand side of the screen. The inertia is modelled as a Point mass/inertia assigned to the reference point created before. The mass of the spherical impactor is equivalent to what it would be if it were a solid sphere made of steel with density equal to 7.8 g/cm3. Calculating the volume of the sphere and the density of the steel it is valid to assume a weight of 0.54 kg.

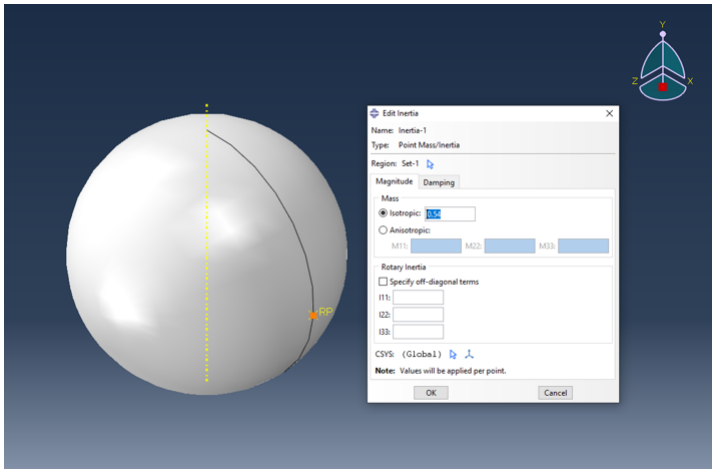

Figure 6.15: Reference point and Inertia Assignment

6.3. Property

This section will explain the process followed to model the material of the airfoil and how it is assigned to the part.

The first step in order to create the material is opening the Material Manager tab, then selecting the option create. After assigning the name, in this case *Aluminio2024T3*, a list of different material behaviours will appear divided into five different categories:

- **General**, which contains options like density, depvar (define the internal state variables for a user-defined material), regularization, etc. For this project, density is applied introducing the value in kg/m3 detailed in the fourth section of this project.

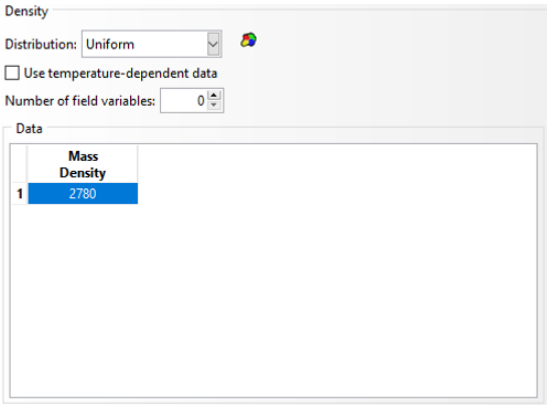

Figure 6.16: Property: Density

- **Mechanical**, which contains different options to model the behaviour of the material when subjected to external forces. Some of the options presented are elasticity, plasticity, damage for different materials, viscosity, etc. The Aluminum defined for this project is modelled using an elastic behaviour, plastic behaviour and Johnson-Cook damage model.

  – The elastic behaviour is defined as isotropic, without temperature dependent data, using the Young's Modulus and the Poisson's Ratio using the values defined in the Materials subsection of the fifth section of this report.

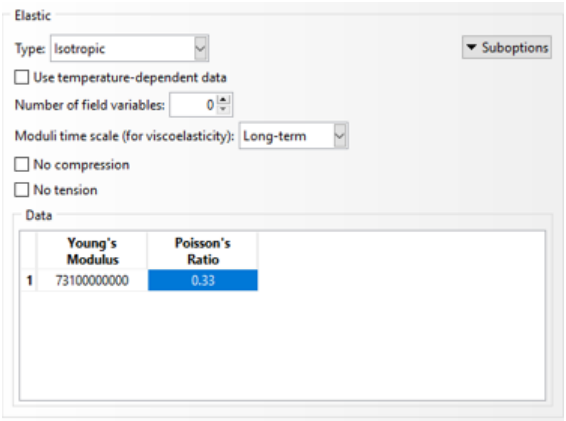

Figure 6.17: Property: Elastic Behaviour

– To simulate the plastic behaviour of aluminum, as previously stated, the Johnson-Cook model is used, which will be introduced in the simulation by means of a series of data collected in the table 4.2

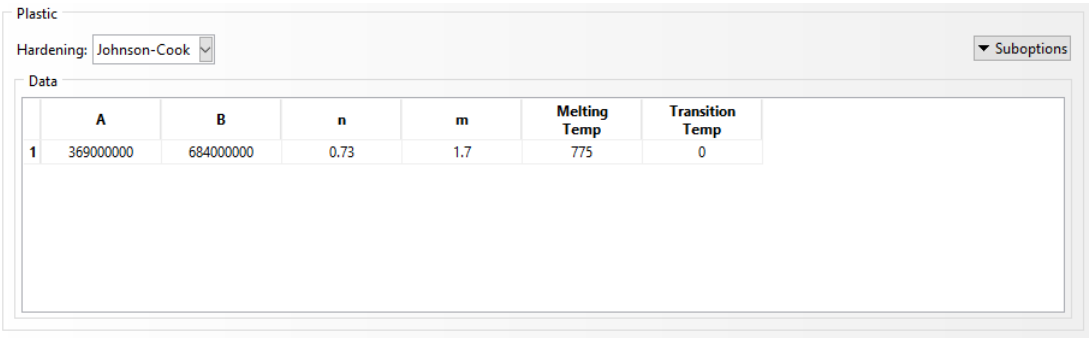

Figure 6.18: Property: Plastic Behaviour

– To simulate the fracture of a ductile metal, it is necessary to simulate the damage initiation and propagation. The Johnson-Cook damage model is incorporated to the model using the parameters shown in the table 4.3.

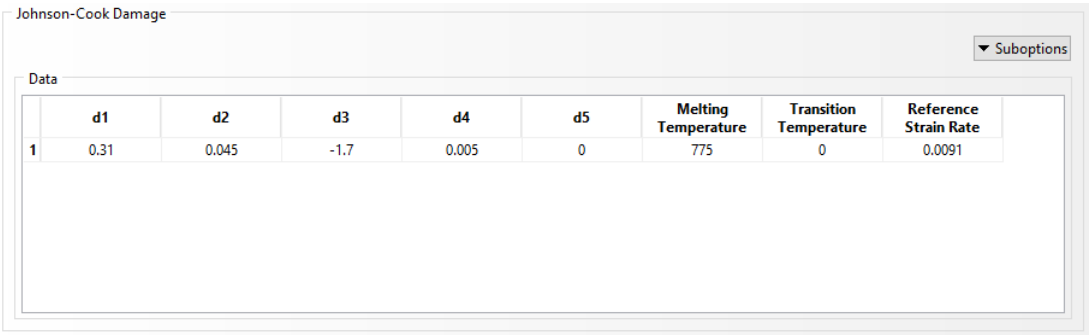

Figure 6.19: Property: Johnson-Cook Damage Model

To incorporate the propagation of the damage, inside the Johnson-Cook Damage window there is a display that shows Suboptions and inside it has Damage Evolution. After selecting damage evolution, a Suboption Editor window is opened where the Displacement at Failure or Energy at Failure can be introduced. In the case of this study, a displacement at failure value of 0.002 is introduced.

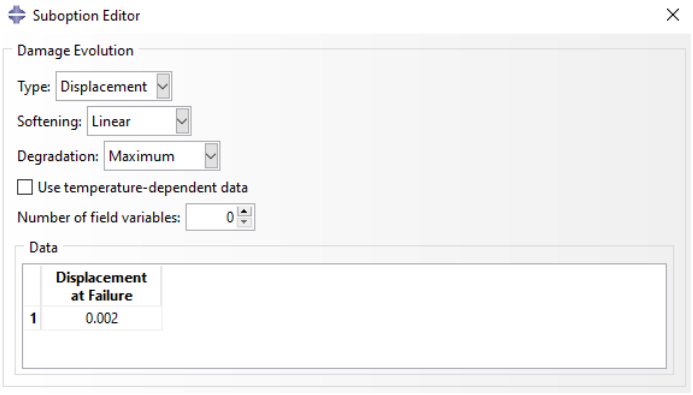

Figure 6.20: Property: Damage Propagation

- **Thermal**, where different thermal properties such as conductivity, heat generation, latent heat or specific heat can be implemented into the model. In the case of study, knowing that the temperature is not a relevant factor, none of this properties will be applied.
- **Electrical/Magnetic** properties like electrical conductivity, piezoelectric and electrical and magnetic permeability. Due to no electric/magnetic interaction, none of this properties will be applied.
- **Other**, which contains properties like acoustic medium, mass diffusion, pore fluid, etc. None of this properties are going to be applied to the model.

Once the material is created, the next step is creating the material section of the airfoil opening the section manager window and selecting the option create. In the *Create Section* window, after assigning the name, one can select the category and type of the section (in this case the section will be a shell with a homogeneous distribution of material).

After confirming the previous selection, an *Edit Section* window will appear. In this window, a list of basic and advanced options will appear. For this study, only some basic properties will be modified, the shell thickness is assigned an initial value of 1.5mm, the material is the previously described *Aluminio2024T3* and the Simpson's thickness integration rule will be chosen.

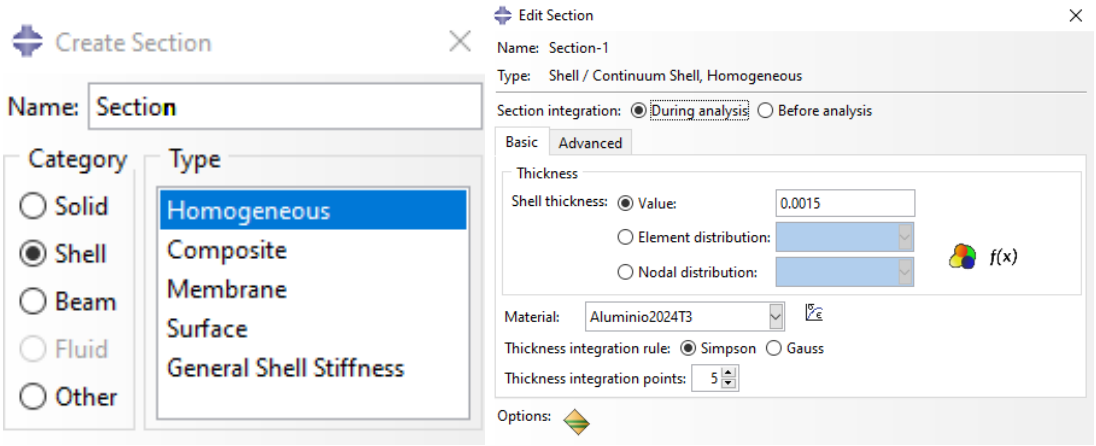

(a) Create Section (b) Edit Section

Figure 6.21: Property: Section Definition

Once the section is defined, it is applied to the airfoil using the *Assign Section* option and selecting the whole part. In the *Edit Section Assignment* window, the thickness should be from section and the shell offset is defined as middle surface.

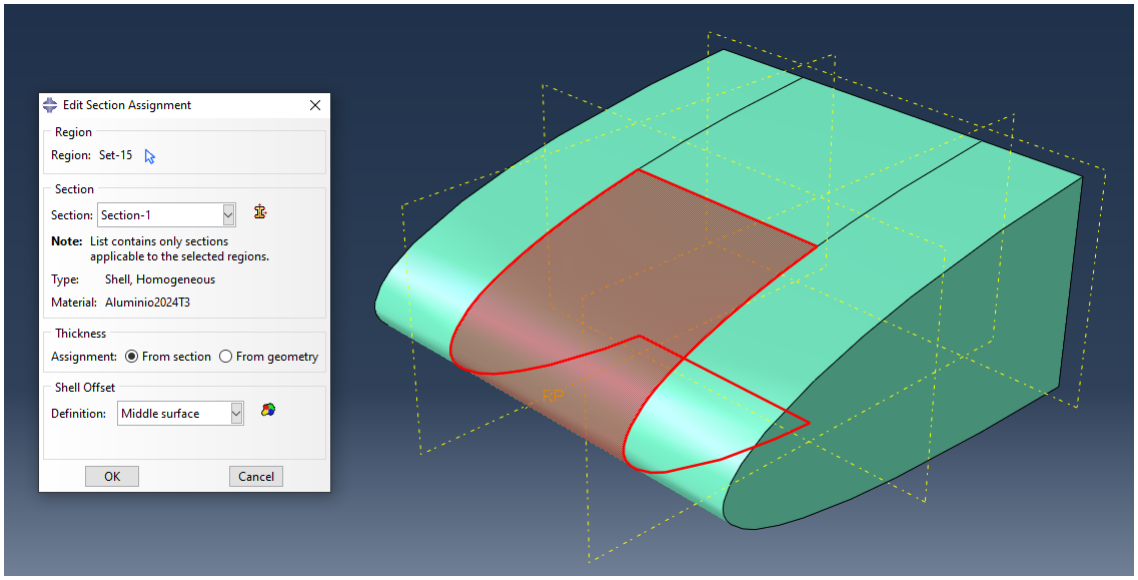

Figure 6.22: Property: Section Assignment

6.4. Assembly

This section will explain the process followed to combine the airfoil and the impactor in the same model.

The first step that must be followed in order to create the assembly is choosing the parts created in the previous steps with the function *Create Instance*. Inside the dialog window *Create Instance*, the option create instances from parts must be chosen and then, the impactor and the airfoil can be added to the assembly.

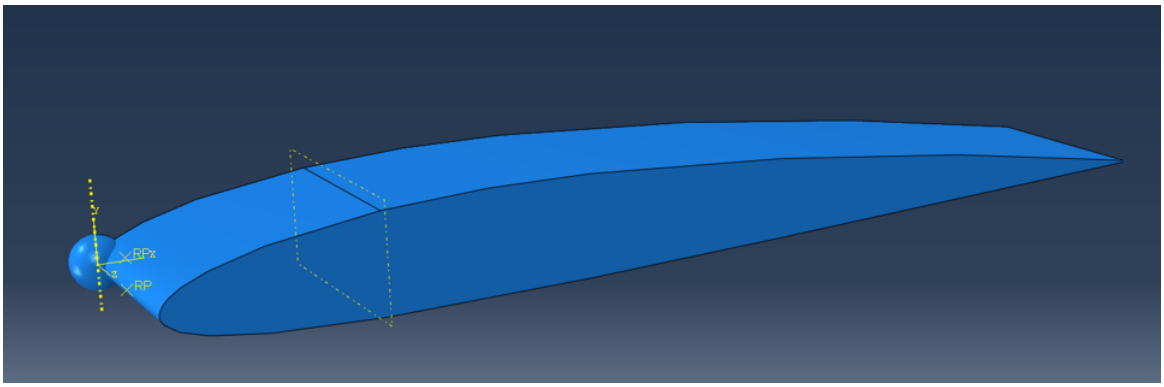

Figure 6.23: Assembly: Create Instance

As seen in the image above, both parts are added to the assembly but they are not in their correct positions. In order to create the correct assembly the impactor must be rotated and translated to its final location using the functions *Rotate Instance* and *Translate Instance*.

The impactor must be rotated in a way that the revolution axis that contains the reference point is parallel to the global x axis. Once the impactor is rotated correctly, it must be translated using the assistance of the reference points created for both, the airfoil and the impactor. With the *Translate Instance* function, selecting the impactor as the instance, it must be translated in a way that the reference points of each of the parts its located in the same place using the reference point of the impactor as the starting point of the translation and the reference point of the airfoil as the end point.

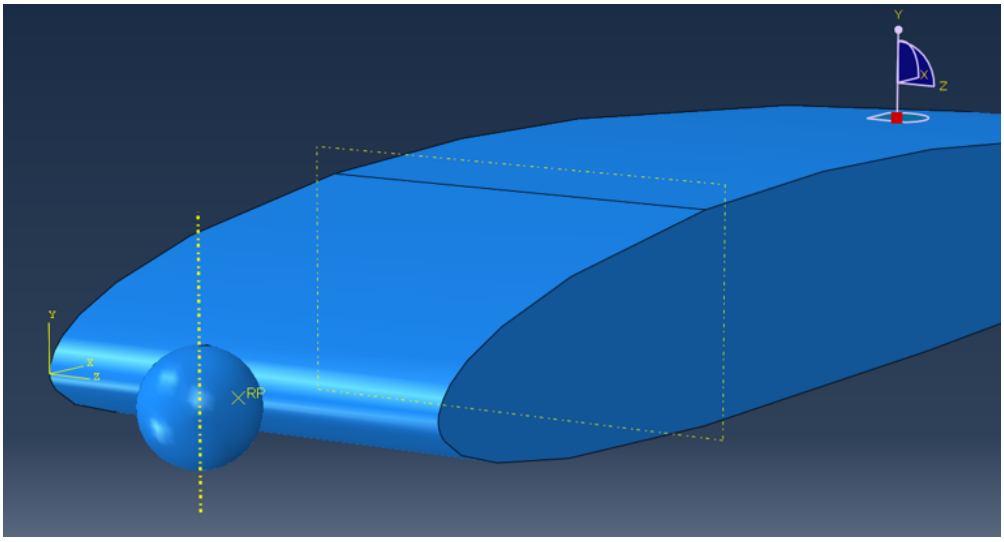

Figure 6.24: Assembly: Correct location

With the operations realised above, the impactor is located in its correct position in the YZ plane but is already making contact with the airfoil, to solve this, the impactor is translated 5 cm (0.05m) to the negative side of the X axis.

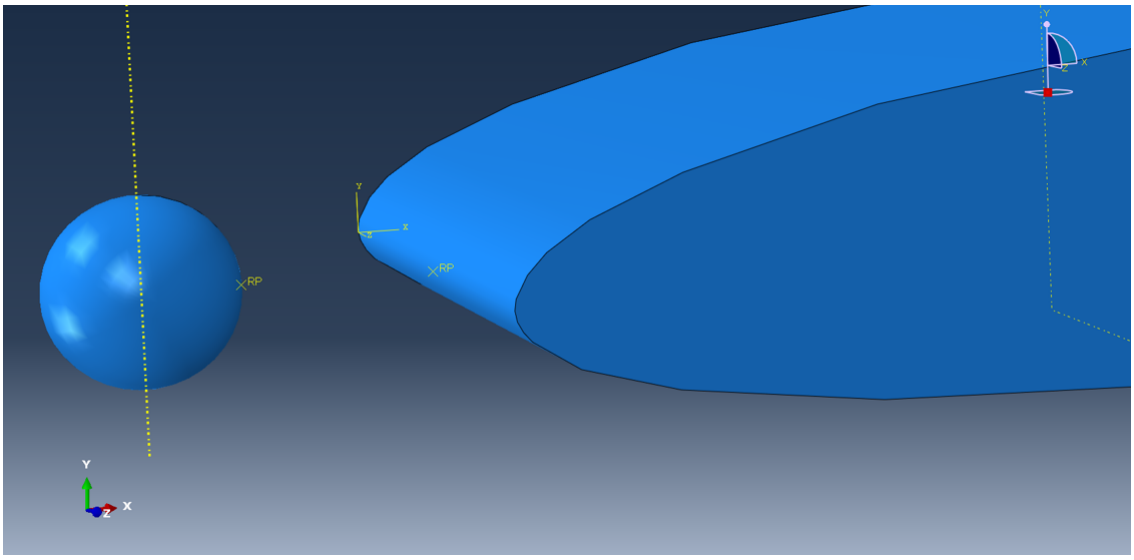

Figure 6.25: Assembly: X Axis Separation

6.5. Step

This section will explain the process followed to determine the duration of the phenomenon to be simulated and the variables of interest that will be analysed in the results.

To create the simulation event to be carried out, the Step Manager tab must be opened, where only one event called initial will appear. Opening the create option and after assigning the name, in this case Impact1, you must select the type of event to be studied. Abaqus presents various options for static, heat transfer, mass diffusion, etc. In this case, as explained above, the phenomenon to be studied is an explicit dynamic phenomenon.

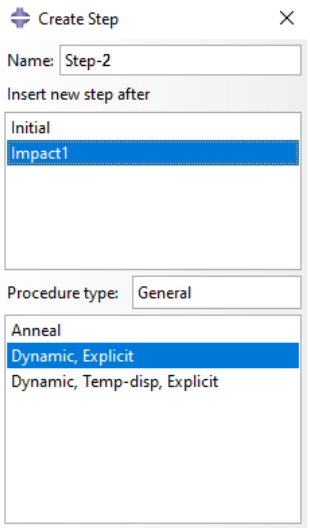

Figure 6.26: Step: Create

Once the type of phenomenon to be simulated has been created, it must be assigned a duration time. In this case, the interesting phenomenon occurs when the impactor comes into contact with the leading edge of the airfoil.

Bearing in mind that the impactor is separated 5cm from the leading edge and that the impact velocity to be studied will be about 160 m/s, the time it takes for the impact to occur is 3.125*10-4 seconds. To guarantee a small margin, and to be able to check the speed of the projectile after passing through the leading edge, it has been decided to establish a simulation time of 2*10-3 seconds. After the first simulations were analysed, it was observed that the time was not enough to fully study the effects of the impact, so it was decided to extend it to 4*10-3 seconds.

No incrementation or mass scaling will be defined for this simulation.

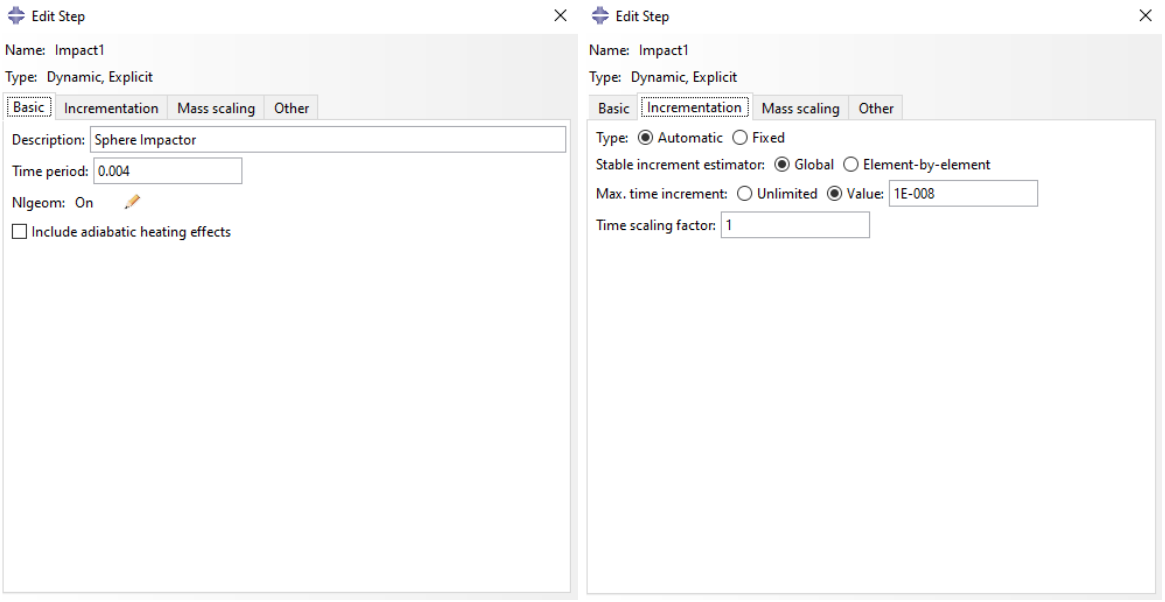

(a) Edit Step Basic

(b) Edit Step Incrementation

Figure 6.27: Step: Edit

Once the event to be simulated has been defined, it is necessary to define the variables to be studied. For this, the Field Output Request Manager function is used. Within the window, the edit option is

chosen and the desired variables are selected in the next open window. The output variables analysed in this project, together with their definition, are collected in the following table:

Category	Name	Definition
Stresses	S	Stresses components and invariants
	SVAVG	Volume-average stress components and invariants
Strains	PE	Plastic strain components
	PEVAVG	Volume-average plastic strain components
	PEEQ	Equivalent plastic strain
	PEEQVAVG	Volume-average equivalent Plastic strain
	LE	Logarithmic strain components
Displacement/ Velocity/ Acceleration	U	Translations and rotations
	V	Translational and rotational velocities
	A	Translational and rotational accelerations
Forces/Reactions	RF	Reaction forces and moments
Contact	CSTRESS	Contact stresses
Failure/ Fracture	PE	Plastic strain components
	DAMAGEC	Compressive damage
	DAMAGET	Tensile damage
	DAMAGESHR	Shear damage
	SDEG	Scalar stiffness degradation
	CFAILURE	Failure measure components
	DMICRT	Damage initiation criteria
State	STATUS	Status (some failure and plasticity models)

Table 6.2: Output Variables

6.6. Interaction

This section shows the process followed to create the interactions between the impactor and the profile that happen during the impact between both of them.

First, the type of contact is defined, both normal and tangential, that can appear in the model. To do this, the *Interaction Property Manager* function is used, and within it the create option. Within the *Create Interaction Property* window there are various types of interaction such as contact, film condition, cavity radiation, fluid cavity, etc. Since what we want is to define the interaction between two solid elements we will select the type Contact.

After selecting the contact option, the *Edit Contact Property* window opens. In a similar way to what was done to assign the properties to the material, in this window you can assign different mechanical, thermal and electrical properties.

To simulate this type of impact it is enough to select mechanical properties. First of all, to simulate that a solid element cannot occupy the same volume as another solid body, a *Normal Behaviour* will be defined.

Then, to simulate the existing friction between two bodies, a *Tangential Behaviour* is defined, choosing the Friction formulation option as Penalty. In this way, the friction between two solids is simulated by means of a friction coefficient multiplied by the normal force. The value chosen for the coefficient of friction is 0.2.

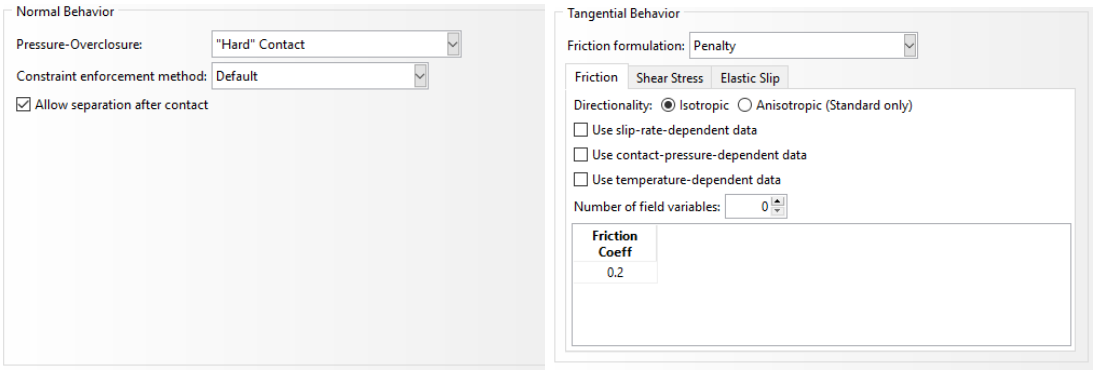

(a) Normal Behavior (b) Tangencial Behavior

Figure 6.28: Interaction: Contact

Once the types of contact have been created, it will be necessary to establish between which surfaces the impact occurs and how it affects the contact between them. To do this, an interaction will be created from the *Interaction Manager* window.

Within the *Create Interaction* window, after choosing the name of the interaction, it is important to correctly assign the interaction to the impact step, created in the previous section.

After that, you have to select the type of interaction, in this case, since what is interesting is to model the behaviour of the airfoil surface when it contacts the outer surface of the impactor, *Surface-to-surface contact (Explicit)* is chosen.

Once selected, both surfaces are chosen, firstly the entire outer surface of the impactor is chosen. For the other surface, select the leading edge of the airfoil, making sure that the impactor surface is selected as *First Surface* (red colour) and the airfoil as *Second Surface* (purple colour) and that the *Contact interaction property* chosen is the one defined previously.

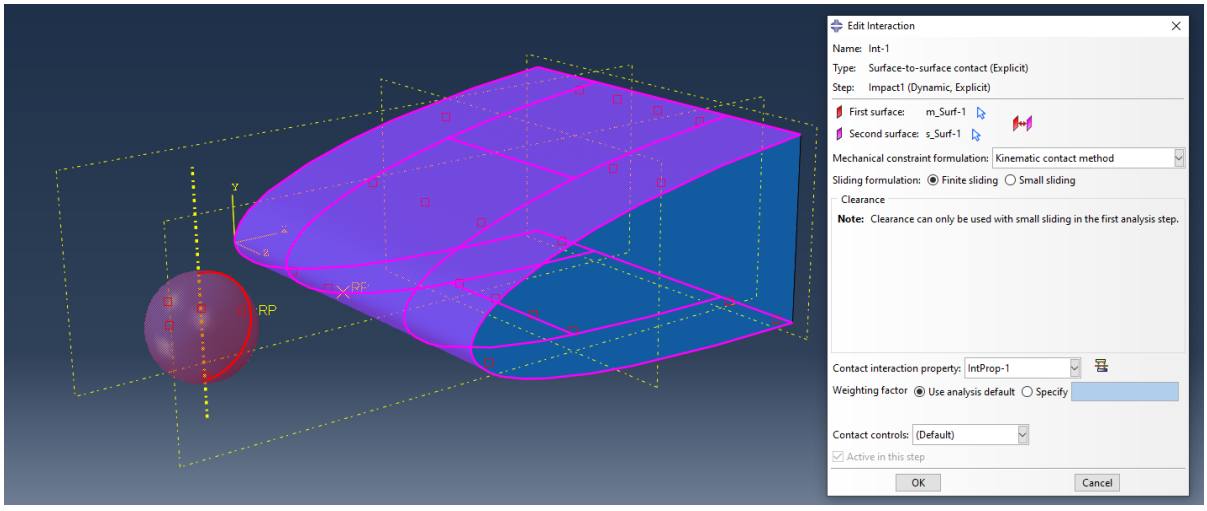

Figure 6.29: Interaction: Contact Surface Selection

As discussed in section 4.7, an analysis of the influence of self-contact in the model simulation has been carried out. To implement it, the same procedure has been followed as to create the contact between the surfaces, however, in the *Create Interaction* dialog, the Self-contact (Explicit) option is selected. After the option is chosen, the surface of the leading edge on which the condition is applied and the face on which it is applied is selected.

Since the part where it is interesting to apply the self-contact is the area where the impact occurs, the central region of the leading edge is selected as can be seen in the following image:

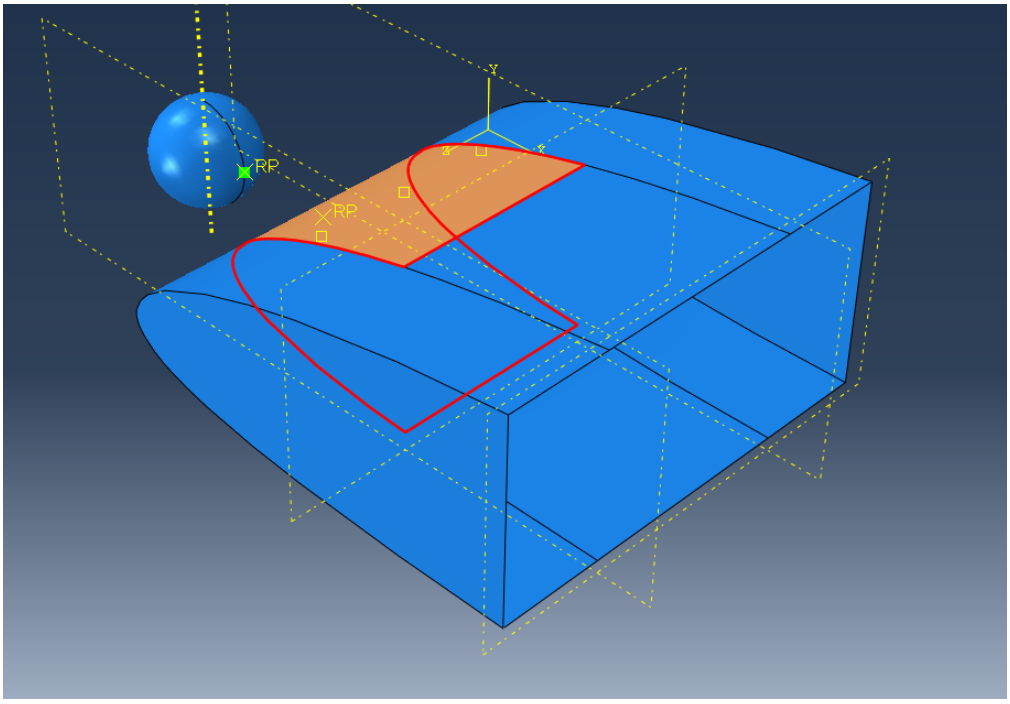

Figure 6.30: Interaction: Self-Contact Surface Selection

After selecting the inside face of the leading edge, select the Mechanical constraint formulation type as Penalty contact method and select the contact property created above for the Surface-to-surface contact.

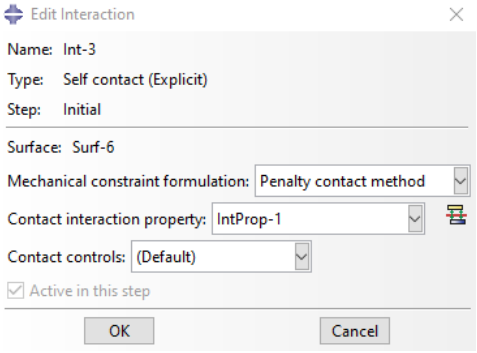

Figure 6.31: Interaction: Self-Contact Edit Interaction

As stated in section 4.6, it has been shown that the use of self-contact does not present any significant benefit compared to the model that does not use it. Therefore, the model used will not include the self-contact of the leading edge.

6.7. Load

This section shows the process followed to assign the boundary conditions in the airfoil and the impact velocity and the restricted movement and rotations in the impactor.

In order to correctly simulate the impact on the airfoil, it will be necessary to define the boundary conditions applied to it. Given that the interest when analysing the impact is focused on the front part of the leading edge and that in a real test the airfoil would be attached to a rig that would prevent it from moving or rotating when receiving an impact, these conditions are modelled by applying encastre-type boundary conditions to the sides of the airfoil.

The encastre type boundary condition consists of a restriction of the degrees of freedom corresponding to the displacement and rotation of the selected nodes.

To create the boundary condition, the *Boundary Condition Manager* window is opened and within the Create option, the mechanical category and the *Symmetry/Antisymetry/Encastre type* is selected.

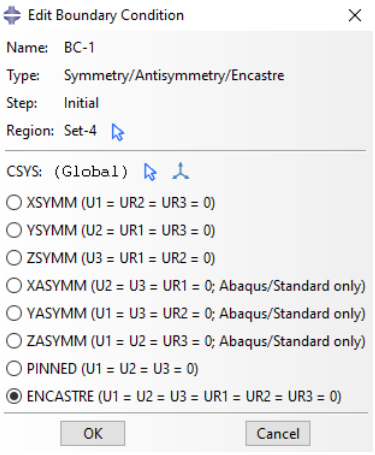

Figure 6.32: Load: Boundary Condition Selection

Once the type of boundary condition has been chosen, the application region is selected, in this case both lateral surfaces of the airfoil as can be seen in the image below.

After selecting both surfaces, within the *Edit Boundary Condition* window, select the *ENCASTRE* option (U_1=U_2=U_3=UR_1=UR_2=UR_3=0).

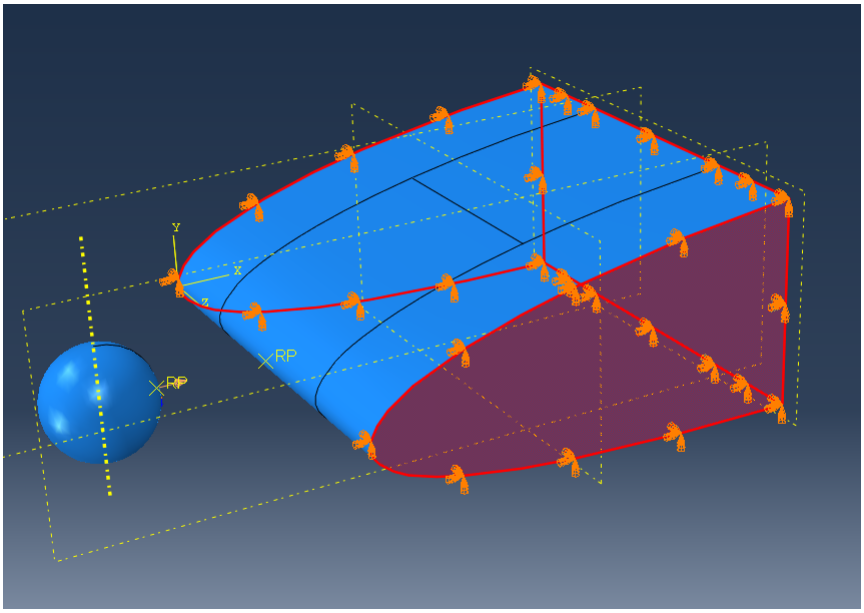

Figure 6.33: Load: Boundary Condition Surface Selection

On the other hand, to model the movement of the impactor, boundary conditions will be used to avoid movement in undesired axes as well as rotation of the impactor, combined with a *Predefined Field* where the impact velocity will be established.

The way to proceed when creating the boundary conditions in the impactor is similar to the operation carried out to assign them to the airfoil, except that in this case the *Displacement/Rotation* type is chosen and it is applied directly to the Reference Point of the impactor. Once the application point has been selected, a window called *Edit Boundary Conditions* appears where you can select the degrees of freedom that will be restricted.

As mentioned before, the rotation of the impactor will be prevented, so the degrees of freedom UR_1, UR_2 and UR_3 are selected.

Regarding the displacements, the impactor will only move on the line that joins both Reference Points that has been established in such a way that it coincides with the X axis, so the movement U_2 and U_3 will be restricted.

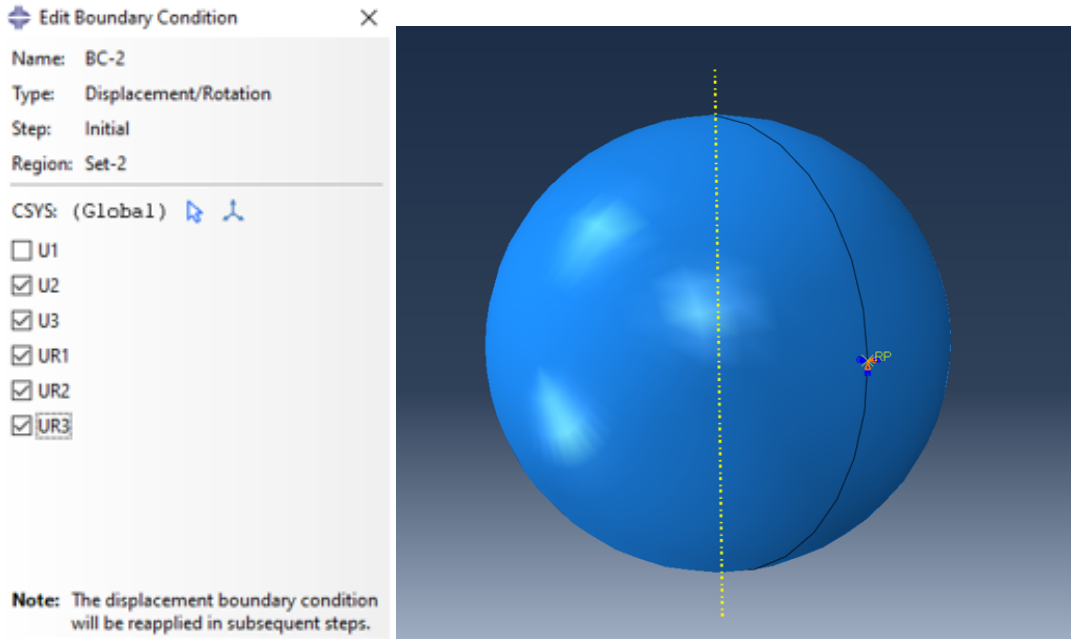

(a) Boundary Condition Definition (b) Boundary Condition Aplication

Figure 6.34: Load: Spherical Impactor Boundary Conditions

To model the impact velocity, the *Predefined Field Manager* function is used, where selecting the *Create* button opens a window similar to that of boundary conditions. Within this window the mechanical category is selected and within this, the velocity type is chosen. Just like when setting the movement restrictions on the impactor, the Velocity condition is also applied to the Reference Point.

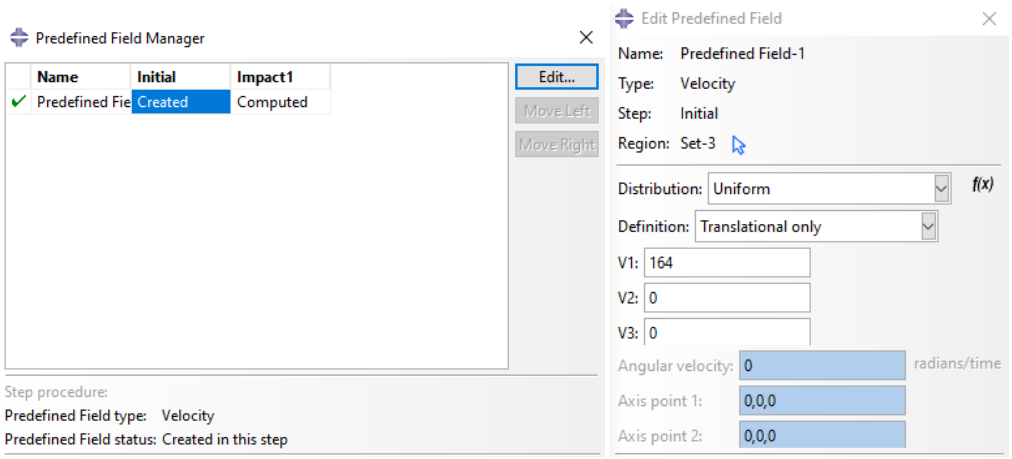

(a) Boundary Condition Definition (b) Boundary Condition Aplication

Figure 6.35: Load: Predefined Field Manager

Once the application point has been selected, the *Edit Predefined Field* window opens where the properties of the initial velocity that the model will have are defined. In the case of this simulation the velocity has a uniform distribution and has only translational components.

Finally, the impact velocity is established on the V_1 component, that is, the initial velocity is adjusted to be the closest possible to the balistic limit or the V50 speed.

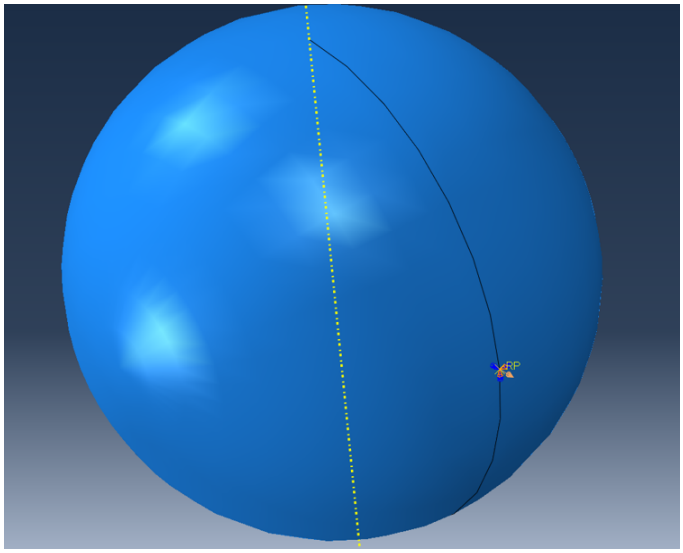

Figure 6.36: Load: Initial Velocity Aplication

6.8. Mesh

In this section, the process followed when carrying out the meshing of the simulation is exposed, given that mesh convergence has been explained in previous sections, only one example of one of the iterations carried out is exposed here.

To mesh the impactor, the option *Meshing by parts* must be selected at the top. Once the impactor is chonen, the *Seed Part* window opens and there one can assign the approximate global size of the mesh of the part. In the case of the simulation after the mesh convergence, this value has been established at 0.001.

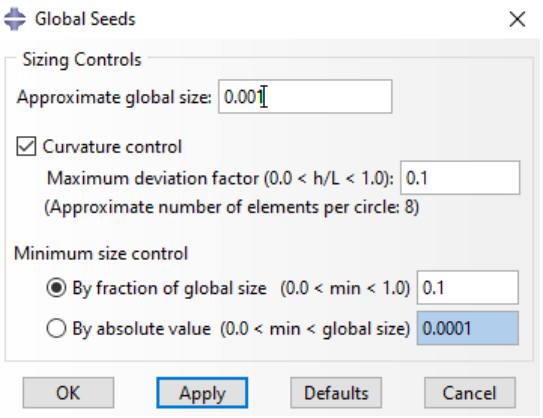

Figure 6.37: Mesh: Global Seed for Impactor

Once the size of the mesh has been selecteded, the type of element that will make the mesh is defined in the *Mesh Controls* tab. In this case Quad-dominated elements are used, and they are applied to the impactor using the *Mesh Part* function. The impactor mesh can be seen in the image below.

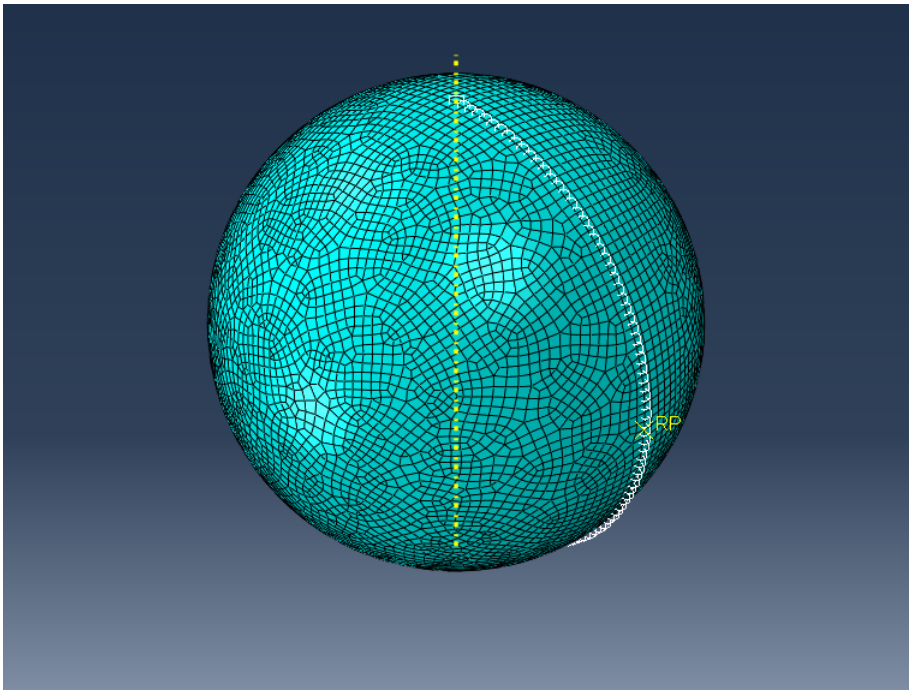

Figure 6.38: Mesh: Impactor Final Mesh

After meshing the impactor, the *Assign Element Type* function is used to select the type of element being meshed in addition to other properties of the mesh that will be seen later. In the case of the impactor, the Explicit element must be selected and in the *Family List* select Discrete Rigid Element.

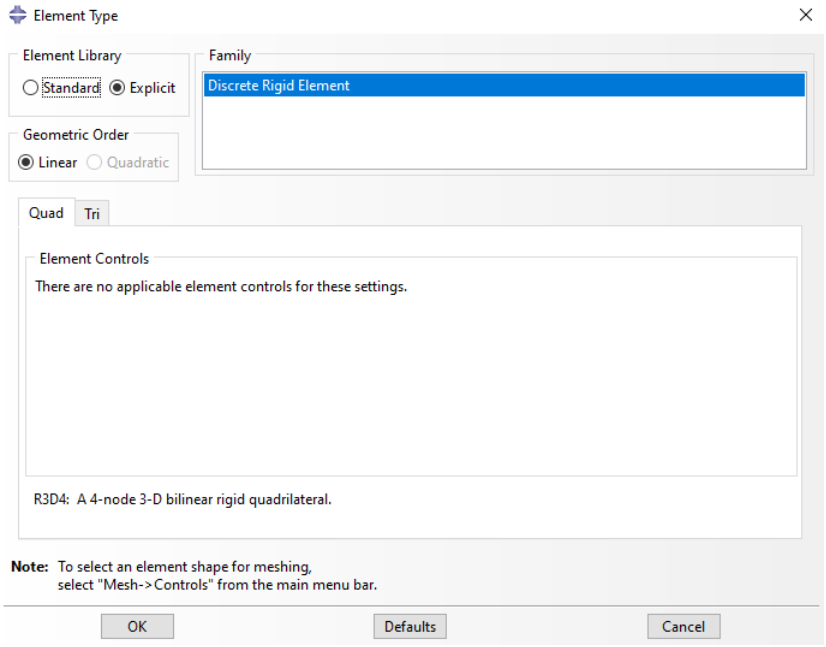

Figure 6.39: Mesh: Impactor Mesh Type

As for the meshing of the airfoil, this will be slightly more complex than that of the impactor since a different mesh will be made depending on the area of the profile.

In the same way as in the procedure followed for meshing the impactor, the first step when meshing the airfoil is to establish the approximate global size of the elements. In the case of the first simulation, the default value (established at 0.04) will be left.

Since the area of greatest interest for analysis is the leading edge of the airfoil closer to the impact zone, this section will have a finer mesh than the rest of the airfoil. To achieve this, the *Seed Edges* function will be used in the lower and upper surfaces divisions created with the help of a *Datum Plane*. The edges where the seed edges function will be used can be seen in the following illustration.

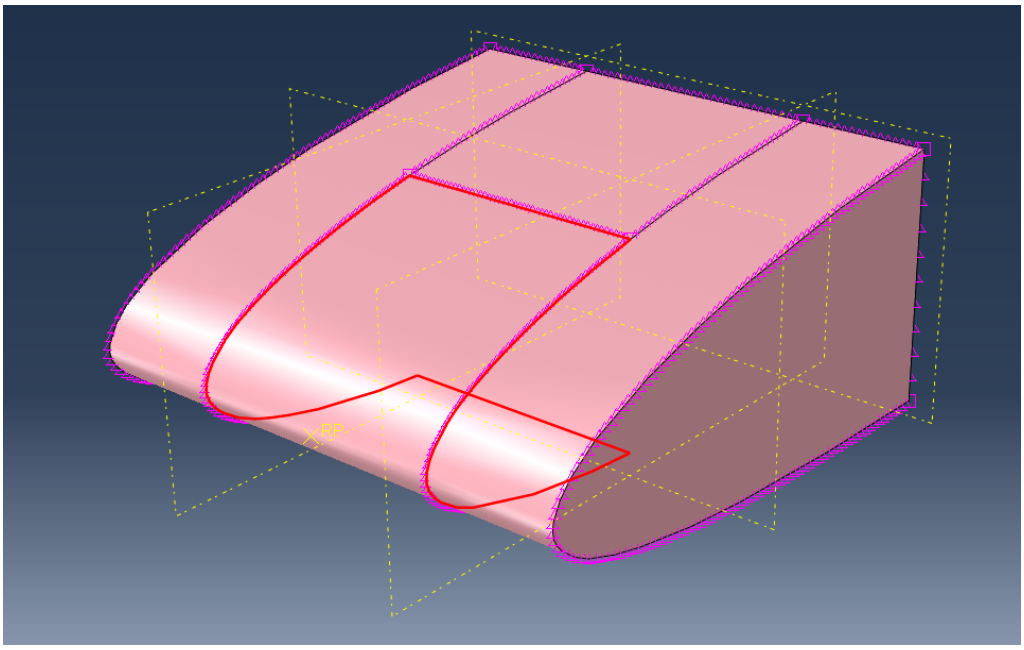

Figure 6.40: Mesh: Leading Edge Seed Edges Central Zone

Once the edges have been selected, an approximate element size smaller than that established for the rest of the model is assigned (in the case of the model used after mesh convergence, a value of 0.002 has been used).

In order to control the size of the elements outside the impact zone, an identical process to the one mentioned above is carried out, selecting the outer edges of the profile. The approximate size of these elements is 0.003.

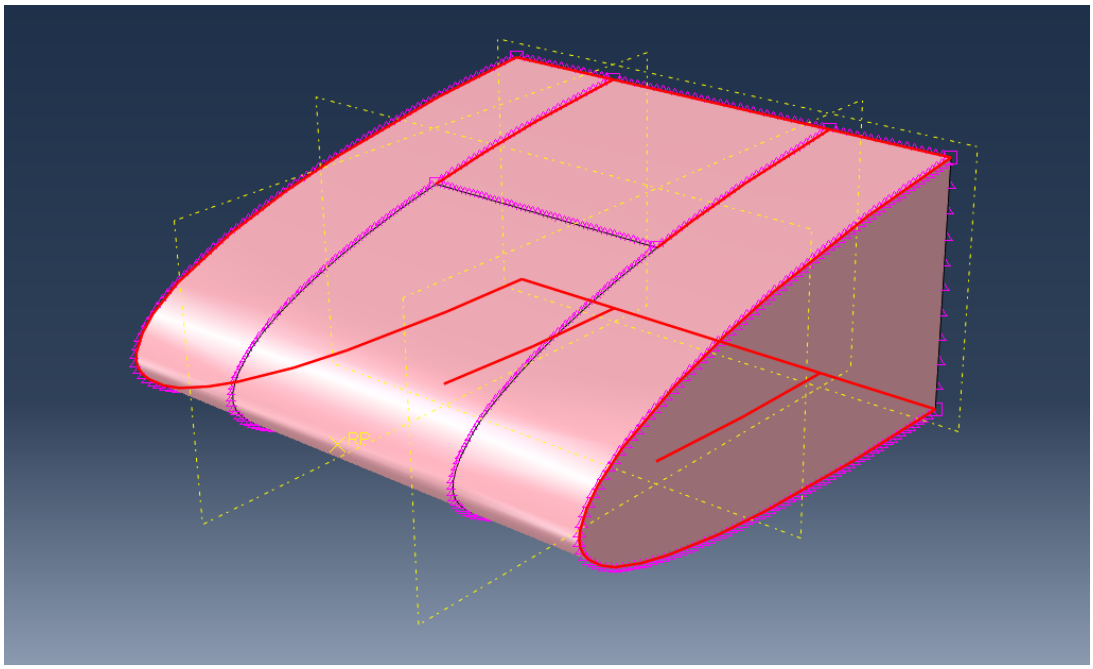

Figure 6.41: Mesh: Leading Edge Seed Edges Exterior Zone

With these values, the airfoil mesh is as follows:

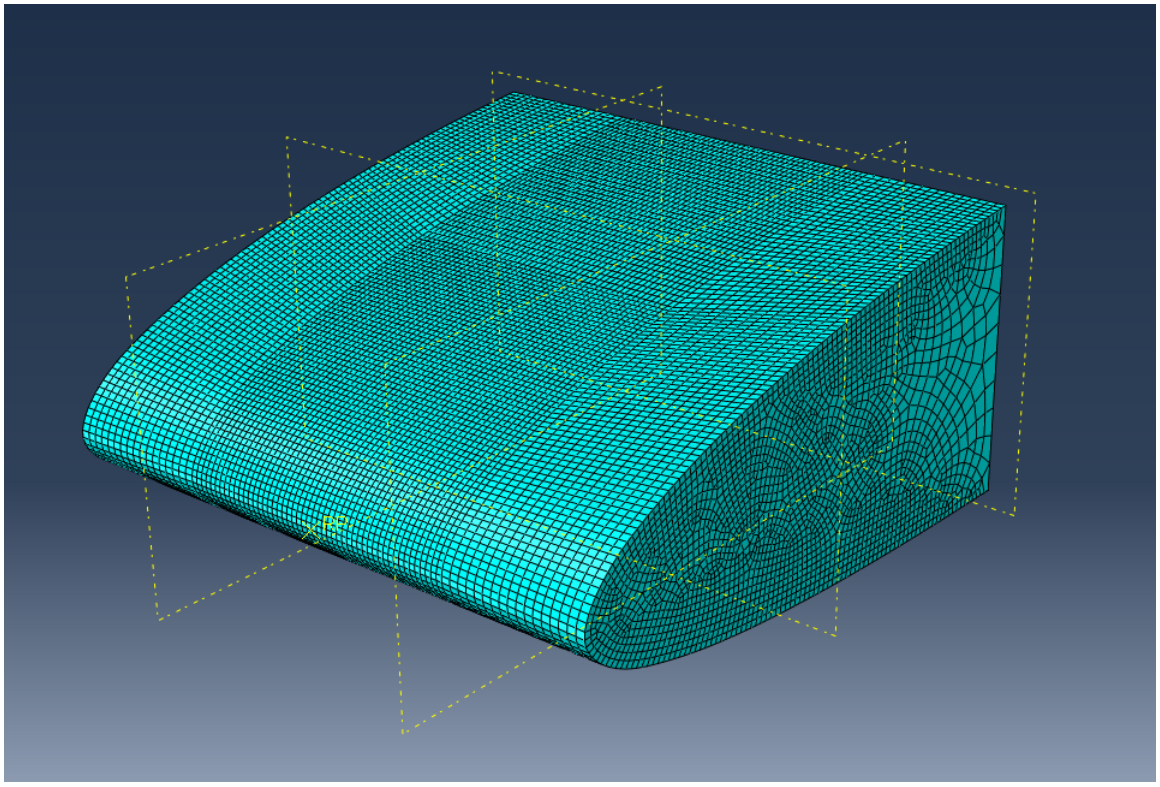

Figure 6.42: Mesh: Leading Edge Final Mesh

Lastly, in the same way as with the impactor, using the Assign Elemt Type function an explicit element is selected, but in this case it will be of the shell type and the Element Deletion option will be activated.

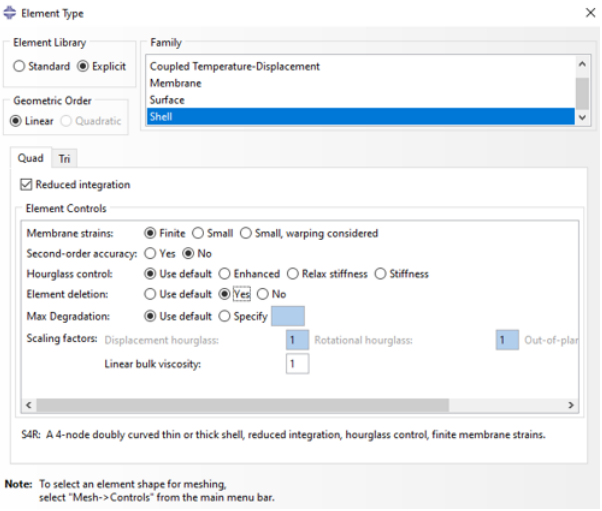

Figure 6.43: Mesh: Element Type

6.9. Job

This section shows the last step when performing the simulation, it is here where the analysis to be performed is selected.

To do this, the *Job Manager* window is opened and the create option is selected. Once the name of the Job and the model on which you are going to work have been selected, another *Edit Job* window opens

where you can adjust the analysis conditions. In the case of this study, Full analysis is selected as Job Type.

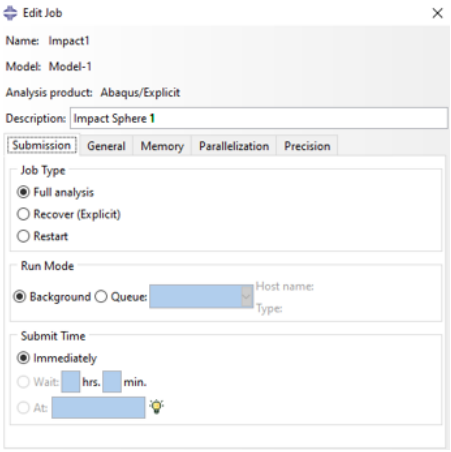

Figure 6.44: Job: Edit

Once the Job has been created, it will appear in the list of the *Job Manager* window, where, by pressing the Submit option, the analysis of the model will begin.

While the analysis is being carried out, from the *Monitor* window you can control the evolution of the analysis and if any error appears. Finally, from the *Results* window you can see a simulation of the modelled process as well as a detailed sample of how the forces, stresses and deformations evolve.

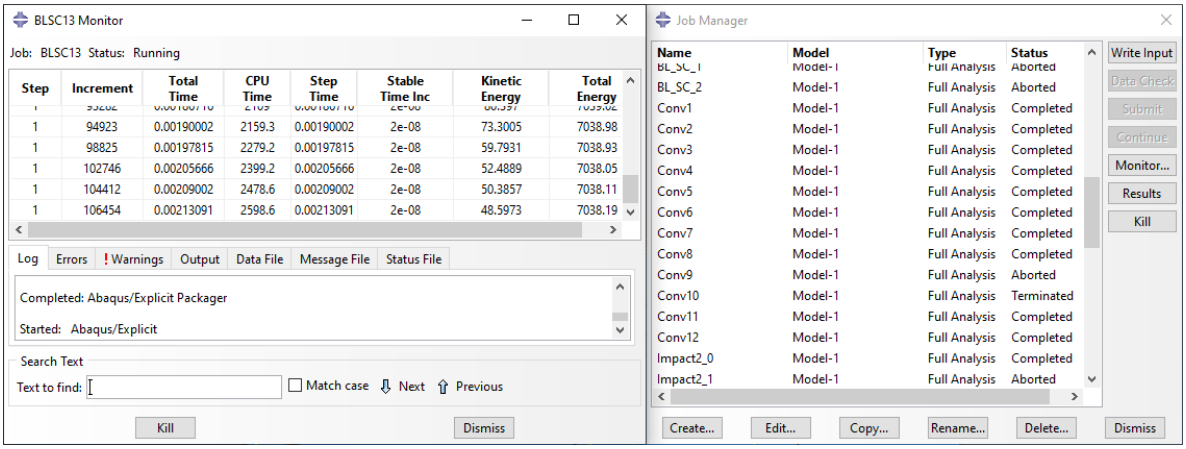

Figure 6.45: Job: Monitor and Manager

Bibliography

[1] J. Andrés and U. J. I. Relaciones tensión-deformación, 2022. URL http://www.mecapedia.uji.es/pages/relaciones_tension-deformacion.html.

[2] ANSYS. Introduction to explicit dynamics. *Introduction to ANSYS Explicit STR*, (1), 2015.

[3] Y. Capar. Implicit vs explicit approach in fem. URL https://yasincapar.com/implicit-vs-explicit-approach-in-fem/.

[4] J. Dehn. The particle dynamics of target penetration. *US Army Armament Research and Development Command*, 1979.

[5] A. A. Gorostegui. Análisis de sensibilidad de elementos finitos sobre la modelización de paneles de aluminio al2024 para estructuras aeronáuticas. -, 2020.

[6] A. Harish. Implicit vs explicit finite element method (fem): What is the difference?, 2020. URL https://www.simscale.com/blog/implicit-vs-explicit-fem/.

[7] G. Johnson and W. Cook. Fracture characteristics of three metals subjected to various strain, strain rates, temperatures and pressures. *Engineering Fracture Mechanics*, 21(1):31–48, 1985.

[8] G. Kay. Failure modeling of titanium 6al-4v and aluminum 2024-t3 with the johnson-cook material model. *DOT F1700.7*, 2003.

[9] G. I. H. Ltd. 2024 aluminum alloy: Properties. URL https://www.gabrian.com.

[10] J. Martí. Análisis de elementos finitos: esquemas implícito y explícito, 2021. URL https://principia.es/analisis-de-elementos-finitos-esquemas-implicito-y-explicito/.

[11] MatWeb. Matweb material property data. URL https://www.matweb.com/search/DataSheet.aspx?MatGUID=67d8cd7c00a04ba29b618484f7ff7524&ckck=1.

[12] G. Nilakantan. Virtual ballistic testing of kevlar soft armor: Predictive and validated modeling of the v0-v100 probabilistic penetration response using ls-dyna®. *15th International LS-DYNA® Users Conference*, Composites, 2018.

[13] J. Seidt and A. Gilat. Plastic deformation of 2024-t351 aluminum plate over a wide range of loading conditions. *International Journal of Solids and Structures*, 50:1781—-1790, 2013.

[14] A. J. Soo. What are the differences between the implicit method and the explicit method? URL https://support.functionbay.com/en/faq/single/263/differences-implicit-method-explicit-method.

[15] A. Tools. Naca 2410 (naca2410-il), . URL http://airfoiltools.com/airfoil/details?airfoil=naca2410-il.

[16] A. Tools. Naca 4 digit airfoil generator, . URL airfoiltools.com/airfoil/naca4digit.

[17] G. Villanueva and W. Cantwell. The high velocity impact response of composite and fml-reinforced sandwich structures. *Composites Science and Technology*, 64(1):35–54, 2003.

[18] Yashchuahan. Elastic behavior of materials, 2021. URL https://www.geeksforgeeks.org/elastic-behavior-of-materials/.